



HAL
open science

Non-linear mechanical behavior of strongly heterogeneous media by the mechanics of generalized continuous media and homogenization methods

Abdallah Wazne

► **To cite this version:**

Abdallah Wazne. Non-linear mechanical behavior of strongly heterogeneous media by the mechanics of generalized continuous media and homogenization methods. Mechanics of materials [physics.class-ph]. Université de Lorraine, 2023. English. NNT : 2023LORR0153 . tel-04295016

HAL Id: tel-04295016

<https://hal.univ-lorraine.fr/tel-04295016v1>

Submitted on 20 Nov 2023

HAL is a multi-disciplinary open access archive for the deposit and dissemination of scientific research documents, whether they are published or not. The documents may come from teaching and research institutions in France or abroad, or from public or private research centers.

L'archive ouverte pluridisciplinaire **HAL**, est destinée au dépôt et à la diffusion de documents scientifiques de niveau recherche, publiés ou non, émanant des établissements d'enseignement et de recherche français ou étrangers, des laboratoires publics ou privés.



**UNIVERSITÉ
DE LORRAINE**

**BIBLIOTHÈQUES
UNIVERSITAIRES**

AVERTISSEMENT

Ce document est le fruit d'un long travail approuvé par le jury de soutenance et mis à disposition de l'ensemble de la communauté universitaire élargie.

Il est soumis à la propriété intellectuelle de l'auteur. Ceci implique une obligation de citation et de référencement lors de l'utilisation de ce document.

D'autre part, toute contrefaçon, plagiat, reproduction illicite encourt une poursuite pénale.

Contact bibliothèque : ddoc-theses-contact@univ-lorraine.fr
(Cette adresse ne permet pas de contacter les auteurs)

LIENS

Code de la Propriété Intellectuelle. articles L 122. 4

Code de la Propriété Intellectuelle. articles L 335.2- L 335.10

http://www.cfcopies.com/V2/leg/leg_droi.php

<http://www.culture.gouv.fr/culture/infos-pratiques/droits/protection.htm>



C2MP



THÈSE

Pour obtenir le grade de :

DOCTEUR DE L'UNIVERSITÉ DE LORRAINE

Mention : Mécanique des Matériaux

École doctorale : C2MP

Présentée par :

Abdallah Wazne

Intitulée :

Non-linear mechanical behavior of strongly heterogeneous media by the mechanics of generalized continuous media and homogenization methods

Thèse soutenue à :

Metz, le 29/09/2023

Devant le jury composé de :

Pr. Georges Nassar	Université Polytechnique Hauts-de-France	Président-Rapporteur
Pr. Artan Sinoimeri	Université de Haute-Alsace	Rapporteur
Pr. Florence Dinzart	Université de Lorraine	Examinateur
Pr. Khaled Khalil	ECAM-Rennes	Examinateur
Dr. Hilal Reda	Lebanese University	Examinateur
Pr. Jean-François Ganghoffer	Université de Lorraine	Directeur de thèse
Pr. Hassan Lakiss	Islamic University of Lebanon	Co-directeur de thèse

Acknowledgments

I would like to acknowledge the collaborative effort between the laboratory LEM3 of Université de Lorraine and the Lebanese University, which co-directed this thesis. Firstly, I express my sincere gratitude to Pr. Georges Nassar and Pr. Artan Sinoimeri for graciously accepting the role of reviewer for my thesis. I am also thankful to Pr. Florence Dinartz and Pr. Khaled Khalil for being a part of my thesis jury as examiners. My deepest appreciation goes to my thesis supervisor, Jean-François Ganghoffer, who has been an exceptional mentor throughout this journey. Under his guidance, I have gained valuable knowledge and been inspired to think critically and creatively in my research. His dedication to my success has been truly remarkable. I am grateful to my supervisor, Hassan Lakiss, for believing in my potential and providing me with the opportunity to pursue my Ph.D. I would also like to acknowledge Hilal Reda for his invaluable guidance, support, and encouragement throughout my research journey. His contributions have greatly contributed to the successful completion of this thesis. Additionally, I express my appreciation to the members of LEM3, particularly Pr. Rachid Rahouadj, for their kindness, support, and encouragement during my thesis. I want to sincerely thank my parents, brothers, and sister for their unwavering support throughout my Ph.D. Their assistance has been invaluable, and I deeply appreciate their presence by my side. Lastly, I want to express my deepest gratitude to my incredible fiancé. Her support, love, and belief in me have been the driving force behind my accomplishments. Her constant presence and unwavering faith have provided me with strength and inspiration. I am eternally grateful to have her as my partner in both life and this journey.

Abstract/Résumé

Non-linear Mechanical Behavior of Strongly Heterogeneous Media by the Mechanics of Generalized Continuous Media and Homogenization Methods

Abstract

The objective of this thesis is to comprehensively investigate the nonlinear behavior of periodic lattice materials made of Timoshenko beams, by considering shear, extension, and bending energies, as well as their interactions. To achieve this objective, we have developed a complete set of nonlinear shape functions and derived the nonlinear dynamical equations for various architected networks. Our focus has been on incorporating the nonlinear stiffness matrix and studying the impact of the full nonlinear energy (including shear, extension and bending modes) on the dynamical response of architected materials. Furthermore, we have conducted a comparative analysis of wave propagation in different architected materials, considering the influence of nonlinear energy and the contribution of each mode (extension, flexion, and shear) to the dispersion relations. Additionally, we have performed discrete dynamical homogenization computations for different nonlinear architected materials and carried out wave propagation analyses taking into consideration the effect of second gradient terms in both 1D and 2D.

Abstract/Résumé

Comportement mécanique non-linéaires de milieux fortement hétérogènes par la mécanique des milieux continus généralisés et des méthodes d'homogénéisation

Résumé

L'objectif de cette thèse est d'étudier de manière exhaustive le comportement non linéaire des matériaux en treillis périodiques constitués de poutres de Timoshenko, en tenant compte des énergies de cisaillement, d'extension et de flexion, ainsi que de leurs interactions. Pour atteindre cet objectif, nous avons développé un ensemble complet de fonctions de forme non linéaires et dérivé les équations dynamiques non linéaires pour divers réseaux architecturés. Nous nous sommes concentrés sur l'intégration de la matrice de rigidité non linéaire et sur l'étude de l'impact de l'énergie non linéaire totale (y compris les modes de cisaillement, d'extension et de flexion) sur la réponse dynamique des matériaux architecturés. En outre, nous avons effectué une analyse comparative de la propagation des ondes dans différents matériaux architecturés, en tenant compte de l'influence de l'énergie non linéaire et de la contribution de chaque mode (extension, flexion et cisaillement) aux relations de dispersion. En outre, nous avons effectué des calculs d'homogénéisation dynamique discrète pour différents matériaux architecturés non linéaires et réalisé des analyses de propagation des ondes en tenant compte de l'effet des termes de second gradient à la fois en 1D et en 2D.

Contents

List of figures.....	6
List of tables	10
General introduction	11
1. 1 Architected Materials: A Revolutionary Paradigm in Material Science.....	11
1. 2 Nonlinearity in Architected Materials: Exploring the Interplay of Material and Geometric Nonlinearities	14
1. 3 Reduced Modeling Approach: Exploring Discrete Homogenization	16
1. 4 Wave Propagation Analysis in Periodic Networks: from band-gaps to Nonlinear Phenomena and Preexisting Deformations	18
1. 5 Limitations of works from the literature	20
1.5. 1 Kinematic Analysis of Timoshenko Beams.....	20
1.5. 2 Nonlinear Wave Propagation in Architected Materials	20
1. 6 Addressed scientific issues and methodology.....	21
1. 7 Thesis outline	21
Development and Analysis of Nonlinear Timoshenko Beams: Shape Functions, Static Solution, and Stiffness Comparison	23
2. 1 Introduction.....	24
2. 2 Kinematics of the fully Nonlinear Timoshenko beam.....	27
2.2. 1 Shape functions for the nonlinear Timoshenko beam.....	28
2. 3 Evaluation of the mass matrix and linear and nonlinear stiffness matrices for the nonlinear Timoshenko beam.....	35
2.3. 1 Assessment of the nonlinear effects on the stiffness matrix	38
2.3. 2 Case Study	40
2. 4 Conclusion	41
Appendix A: Timoshenko beam shape functions	42
Appendix B: Timoshenko beam non-linear mass, linear and non-linear stiffness matrices...	43
Appendix C: Timoshenko beam linear and non-linear mass and stiffness global matrices ...	44
Nonlinear wave propagation analysis in architected materials with consideration of extension, shear and bending effects	47
3. 1 Introduction.....	48
3. 2 Linear and non-linear wave propagation analysis	50

3.3 Nonlinear dispersion diagrams of hexagonal network materials	52
3.4 Nonlinear wave propagation analysis for different architected material	56
3.5 Discussion and conclusion	67
Propagation Analysis of Fully Nonlinear Waves in Homogenized Periodic Hexagonal and Triangular Networks in 1D and 2D	69
4.1 Introduction	70
4.2. Discrete homogenization of nonlinear architected materials	71
4.3. Wave propagation in 1D nonlinear architected materials	76
4.4. Wave propagation in 2D nonlinear architected materials	83
4.5. Discussion and Conclusion	90
Appendix D. Deformational expressions of beam the expressions of the effective moduli and second gradient of hexagonal and triangular lattices	92
General conclusion and perspectives	96
Perspectives	98
Résumé de la thèse en français	100
References	111

List of figures

Fig.1. 1: Characterizing the Strength, Modulus, and Density Interplay in Diverse Material Classes: 3D Ashby Performance Diagram for Engineering Materials [5] 12

Fig.1. 2: Illustrating various types of cellular materials: (A) closed-cell foam, (B) open-cell foam, (C) regular cellular material (body-centered cubic BCC unit cell) [6] 13

Fig.1. 3: Manipulating Poisson's ratio through 2D architectures: hexagonal, star-shaped re-entrant (a and b), rectangular, semi-entrant (c, d), diamond, kagome, triangular-shaped (e, f, g), and chiral lattices (chiral diamond h, tetrachiral i, hexachiral j)..... 14

Fig.1. 4: Example of structures prone to geometrical nonlinearities 15

Fig.1. 5: Exploring Material Nonlinearity with an Elastic-Perfectly Plastic behavior [13]..... 16

Fig.1. 6: periodicity vectors and geometrical parameters of hexagon unit cell [14]..... 17

Fig.2. 1: Timoshenko beam element with the indicated kinematic and static variables 28

Fig.2. 2: Deflection of the Timoshenko beam under a concentrated shear force 40

Fig.3. 1 :Two-dimensional hexagonal networks with its unit cell showing the node numbering, the angular variable and the periodicity vectors..... 52

Fig.3. 2: Dispersion diagram of an architected material with hexagonal shaped unit-cells showing the wave propagation mode for the two lowest eigenfrequencies for the shear and longitudinal modes with wave amplitudes a) $A=10$ mm, b) $A=5$ mm and c) $A=1$ mm. The continuous lines in green L1 and blue L2 correspond to the linear solution for shear and longitudinal respectively, while the dashed black NL1 and red NL2 lines correspond to the solution after the incorporation of the non-linear correction for shear and longitudinal modes respectively. 55

Fig.3. 3 :Two-dimensional classical hexagonal (a), re-entrant hexagonal (b), square (c) and triangular (d) periodic lattice materials with their associated unit cell [133]..... 57

Fig.3. 4: Dispersion diagram for the hexagonal (a), re-entrant hexagonal (b), square (c) and triangular (d) unit-cell designs for longitudinal mode. solid green lines correspond to the linear

solution, while black dashed lines correspond to the solution after the incorporation of the non-linear correction.....	59
Fig.3. 5 : Dispersion diagram of hexagonal (a), re-entrant hexagonal (b), square (c) and triangular (d) unit-cell designs high optical mode. Continuous green lines correspond to the linear solution, while black dashed lines correspond to the solution after the incorporation of the non-linear correction.....	62
Fig.3. 6 :Dispersion diagram of an architected material for longitudinal mode frequency with hexagonal (a), re-entrant hexagonal (b), square (c) and triangular (d) unit-cell designs. Continuous green line: linear solution. Non-linear correction for the full non-linear kinematics (Black dashed lines), for the nonlinear shear mode alone (red dashed lines), for the nonlinear extension mode (blue dashed lines), for the nonlinear bending mode (orange dashed lines).	64
Fig.3. 7 : Eigen waves of hexagonal and re-entrant hexagonal unit cells for the shear mode. The blue line corresponds to the actual shape, the green line to the linear deformation, and the dashed red line to the non-linear deformation.....	66
Fig.3. 8 : Eigen waves of hexagonal and re-entrant hexagonal unit cells at high optical mode. The blue line corresponds to the actual shape, the green line to the linear deformation, and the dashed red line to the non-linear deformation.	67
Fig.4. 1: Timoshenko beam element with the indicated of kinematic and repetitive network.	72
Fig.4. 2: 2D unit cell of the hexagonal lattice	72
Fig.4. 3: 2D unit cell of triangular lattice	72
Fig.4. 4: Homogenized Cauchy modulus in extension computed from the present discrete homogenization method and the method [14] in versus the angular variable θ for the hexagonal UC.	75
Fig.4. 5: Homogenized Cauchy modulus in extension obtained computed from the present discrete homogenization method and the method [12] in versus the length variable L for the triangular UC	75
Fig.4. 6: Homogenized Cauchy modulus o A_{11} obtained computed from the present discrete homogenization method and the method [22] in versus the angular variable θ for the hexagonal UC.	76
Fig.4. 7: Dispersion relation in the hexagonal and triangular lattice for various values of s	80

Fig.4. 8: Dispersion relation in the hexagonal (solid line) and triangular (dashed line) lattice for various values of $s = 0.2, s = 0.8, \text{ and } s = 0.95$81

Fig.4. 9: Comparison between the dispersion relation for the hexagonal lattice for different values of s , using both the full nonlinear (dashed line) and nonlinear response based on shear energy (solid line)81

Fig.4. 10: Group velocities for the hexagonal (solid line) and triangular (dashed line) lattices for various values of the nonlinearity parameter: $s = 0.2, s = 0.8, \text{ and } s = 0.95$82

Fig.4. 11: Frequency band structure as a function of the angle θ with the direction of propagation equal to $\pi/4$: (a) and (c) correspond to hexagonal and triangular lattices with a degree of nonlinearity $s = 0.1$, (b) and (d) depict the same lattice structures, but with a degree of nonlinearity $s=0.8$84

Fig.4. 12: Frequency band structure as a function of the angle θ with the direction of propagation equal to $\pi/2$: (a) and (c) correspond to hexagonal and triangular lattices with a degree of nonlinearity $s = 0.1$, (b) and (d) depict the same lattice structures, but with a degree of nonlinearity $s=0.8$85

Fig.4. 13: Frequency band structure as a function of the wave number \mathbf{k} for triangular (dashed lines) and hexagonal (solid lines) lattices: blue lines correspond to longitudinal mode while black lines correspond to shear mode at degree of nonlinearity (a) $s = 0.1$ and (c) $s = 0.8$86

Fig.4. 14 : Phase velocity for both hexagonal and triangular lattices in the nonlinear effective medium, with $\theta = 0$. (a) and (b) are hexagonal and triangular lattices with $k=1$, (b) and (d) depict the same lattice structures, but with a $k= 2$88

Fig.4. 15: Phase velocity for hexagonal lattice in the nonlinear effective medium with full nonlinear energy (red) and nonlinear based on shear energy (blue) at degree of nonlinearity $s = 0.8$ for both longitudinal (solid line) and shear (dashed line) modes, with $\theta = \pi/6$. (a) for wave number $k=0.3$ (b) for $k=1$, (c) for $k= 3$89

Fig.R. 1 : Caractérisation de l'interaction entre la résistance, le module et la densité dans diverses classes de matériaux : Diagramme de performance d'Ashby en 3D pour les matériaux d'ingénierie [5] 101

Fig.R. 2: Illustration de différents types de matériaux cellulaires : (A) mousse à cellules fermées, (B) mousse à cellules ouvertes, (C) matériau cellulaire régulier (cellule unitaire cubique centrée sur le corps BCC) [6]. 101

Fig.R. 3 : Exploration de la non-linéarité des matériaux à l'aide d'un comportement élastique et parfaitement plastique [13]..... 103

Fig.R. 4: Diagramme de dispersion d'un matériau architecturé pour la fréquence du mode longitudinal avec des cellules unitaires hexagonales (a), hexagonales rentrantes (b), carrées (c) et triangulaires (d). Ligne verte continue : solution linéaire. Correction non linéaire pour la cinématique non linéaire complète (lignes pointillées noires), pour le mode de cisaillement non linéaire seul (lignes pointillées rouges), pour le mode d'extension non linéaire (lignes pointillées bleues), pour le mode de flexion non linéaire (lignes pointillées orange). 106

Fig.R. 5: Relation de dispersion dans le réseau hexagonal (ligne continue) et triangulaire (ligne pointillée) pour différentes valeurs de $s = 0,2$, $s = 0,8$ et $s = 0,95$ 107

List of tables

Table.2. 1 Geometric and material parameters of the unit-cell structural elements.....39

Table.3. 1: Geometric and Mechanical properties of architected materials unit cells in Figure 2.1.
.....56

Table.3. 2: Percentages of difference between linear and full shear, extension and bending
nonlinear energy modes for different architected unit cells at point A of the Brillouin zone.....65

Table.3. 3: Percentages of difference between linear and full, shear, extension and bending
nonlinear energy modes for different architected unit cells at point B of the Brillouin zone65

Table.4 1 The expressions of the effective properties of 2D hexagonal lattice93

Table.4 2 The expressions of the effective properties of 2D triangular lattice93

Chapter 1

General introduction

1. 1 Architected Materials: A Revolutionary Paradigm in Material Science

Throughout history, humanity has continuously made significant discoveries in materials and manufacturing techniques, leading to notable societal impacts. This progression can be observed from the earliest periods of human existence, which are commonly referred to as the "stone age," "bronze age," and "steel age." In more recent times, particularly in the late twentieth century, revolutionary technological advancements such as additive manufacturing and atomic-level manipulation of matter have emerged. These breakthroughs have created new possibilities for designing and producing materials with exceptional mechanical and other multi-physical properties.

In response to the industry's demanding requirements, engineers in the field of materials science have shifted to a new paradigm. They now seek to enhance material properties by considering the internal architecture of the material as an additional factor, in addition to its chemical composition. This concept introduces a new degree of freedom, referred to as the "inner material's architecture," in the design and improvement of materials. The term "architected materials" was introduced in a review paper by Ashby and Bréchet [1] to establish a connection between topology optimization methods used in designing lightweight, high-performance materials and structural engineering. This approach aims to create materials that are not only functional but also visually appealing, reminiscent of the elegance found in structures like the Eiffel Tower.

An architected material, as described in the literature, refers to a material that synergistically combines multiple simpler base materials. This combination often involves a hierarchical arrangement of different scales, akin to the structure of the Eiffel Tower, as mentioned in previous works [2–4]. The inherent organization of such materials leads to the emergence of new

performance characteristics that cannot be achieved by any of the individual constituents alone, thus meeting specific requirements set by the designer. The inner architecture of architecture materials offers a vast range of possible geometries for the topologies of elementary building blocks. This abundance of design options results in a rich materials design space, allowing for the creation of materials with diverse and tailored properties. The performance attributes of these materials can be conveniently visualized and condensed into Ashby diagrams, as depicted in Fig.1.1, which illustrate properties such as modulus, strength, and density in a three-dimensional representation.

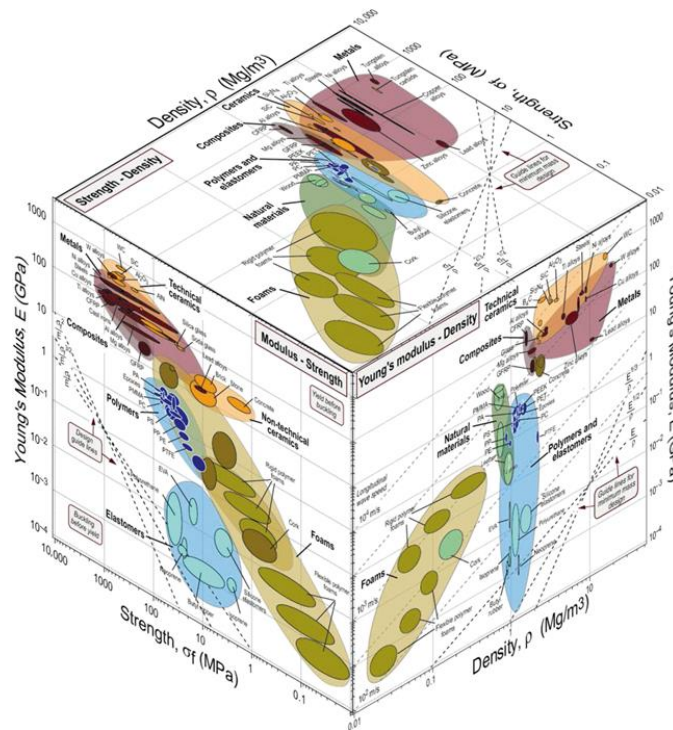


Fig.1. 1: Characterizing the Strength, Modulus, and Density Interplay in Diverse Material Classes: 3D Ashby Performance Diagram for Engineering Materials [5]

Architected materials designed for engineering applications are typically characterized by a unit cell, which serves as the fundamental building block from which the entire structure is fabricated. This unit cell exhibits a periodic arrangement, allowing for convenient fabrication and modeling. Fig.1.2 showcases a few examples of cellular materials with regular architectures, although the actual microstructure may not be perfectly periodic. Nevertheless, representing it as a periodic medium often provides a reasonable approximation.

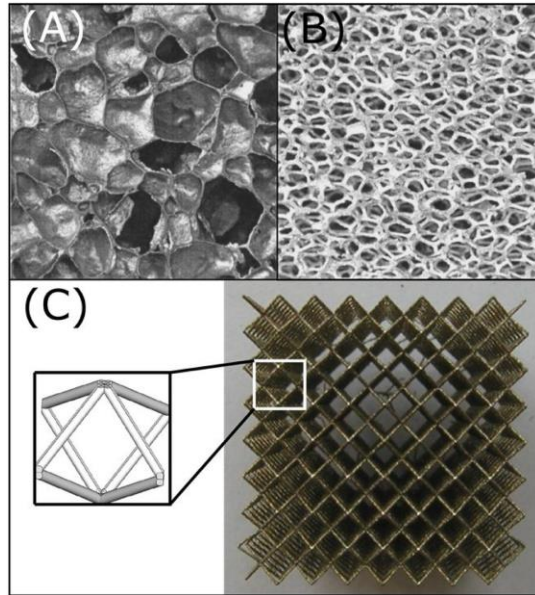


Fig.1. 2: Illustrating various types of cellular materials: (A) closed-cell foam, (B) open-cell foam, (C) regular cellular material (body-centered cubic BCC unit cell) [6]

The architecture of these materials can span from the atomic or molecular level to macroscopic dimensions. In contemporary practice, materials design is commonly integrated into structural mechanics right from the beginning. However, this methodology heavily relies on heuristics, experience, and designer intuition. It lacks a more rigorous and systematic approach to define suitable or even optimal topologies for specific applications or mechanical requirements. The term "metamaterials" has been coined to describe a distinct class of materials among architected materials that have emerged in recent decades [7]. Metamaterials possess mechanical attributes, whether static or dynamic, that are not typically found in natural materials. This terminology emphasizes the ability to adjust the effective material properties at the unit cell level by modifying the internal topology, rather than relying solely on changes in chemical composition to alter the base material properties. The progress in this technological advancement has been made possible primarily due to rapid developments and advancements in additive manufacturing techniques. Among various mechanical properties, Poisson's ratio holds a significant role and is sometimes considered a metric of material properties. Materials with a negative Poisson's ratio, known as auxetic materials, exhibit exceptional static and dynamic characteristics, such as high resistance to shock and impact, vibration mitigation, and sound wave manipulation.

Fig.1.3 presents a collection of periodic architected materials with both positive and negative (auxetic) Poisson's ratios.

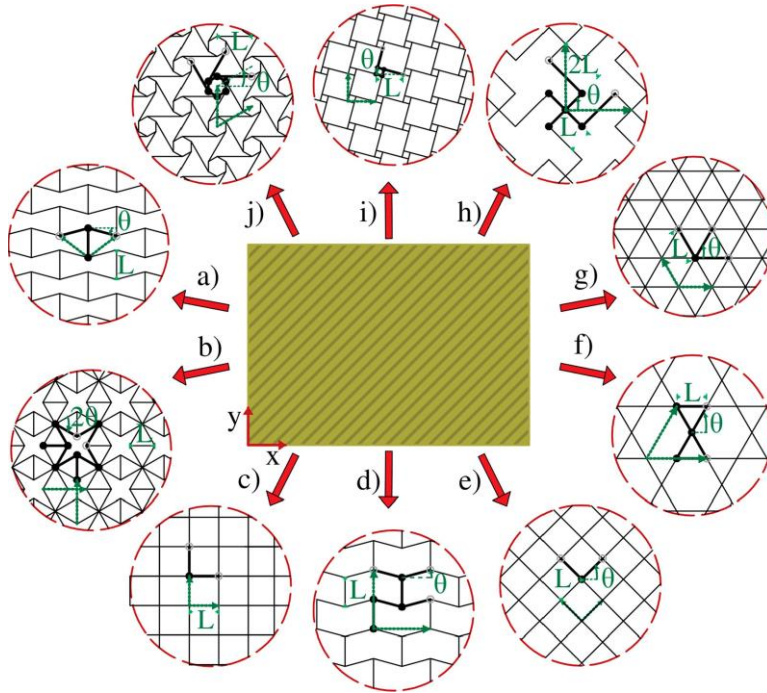


Fig.1. 3: Manipulating Poisson's ratio through 2D architectures: hexagonal, star-shaped re-entrant (a and b), rectangular, semi-entrant (c, d), diamond, kagome, triangular-shaped (e, f, g), and chiral lattices (chiral diamond h, tetrachiral i, hexachiral j)

1. 2 Nonlinearity in Architected Materials: Exploring the Interplay of Material and Geometric Nonlinearities

The link between architected materials and nonlinearity concerns how the loading conditions affect the architected structure's mechanical response. The overall stiffness and strength of architected materials, in particular, have an important role in determining their nonlinear response. Large deformations, material nonlinearity in the elastic regime or involving irreversible phenomena like plasticity or viscoelasticity, geometric nonlinearities, and specific types of boundary conditions are simply a few factors that lead to a possible nonlinear behavior. These factors can cause architected materials to deviate from a linear elastic behavior and exhibit nonlinear characteristics.

In structural analysis, one makes a distinction between two important types of nonlinearity, namely material nonlinearity and geometrical nonlinearity [8], [9]. Geometric nonlinearity may occur when the deformation of a structure is sufficiently large that it causes significant changes in its geometry, like a metallic bridge submitted to strong wind or to a heavy weight, or a metallic pylon under lateral wind. In architected material, the high internal porosity associated to the presence of slender elements (like beams with low aspect ratio) leads to internal large rotations and displacements that are not necessarily associated to large strains or bending moments.

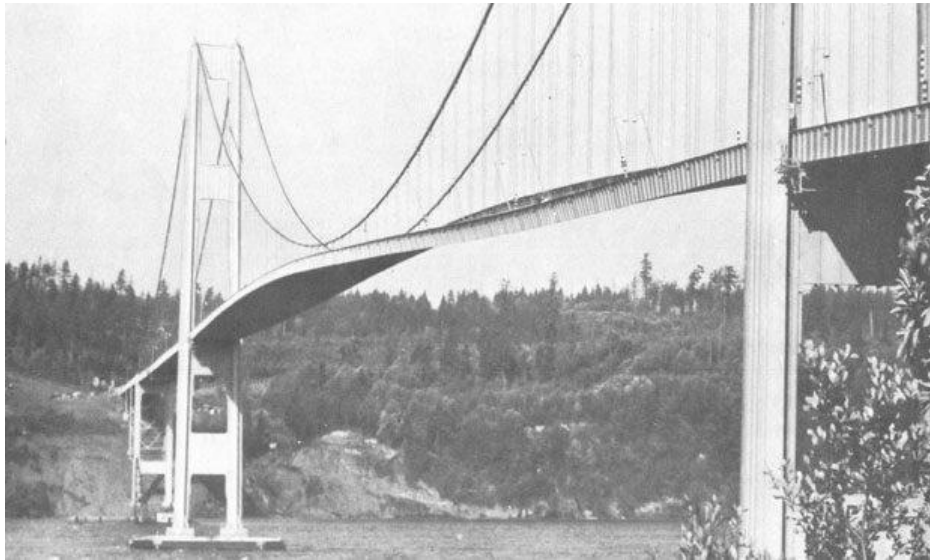


Fig.1. 4: Example of structures prone to geometrical nonlinearities

Structures under heavy loads, where strain is greater than the standard threshold of 5%, might go through this. When the deformation is severe enough, the stiffness and density of the structure may vary locally (at the level of individual structural members) or at the global macroscopic level [10]. In other words, such nonlinearities traduce the existence of large displacements, large rotations, large strains and possible interactions of these.

A second kind of nonlinearities is called material nonlinearities, with the meaning that the force-displacement or the strain-strain relation is essentially nonlinear; a typical example being contact problems. The assumption that stress and strain are directly proportional, as in the simple linear elastic situation, is then no longer valid [11]. It is essential to recognize that no material exhibits an entirely linear elastic response, since this is merely an approximation that adequately describe

most scenarios. Various material models can be employed to describe such a behavior, such as nonlinear elastic, elastoplastic, viscoelastic, or visco-plastic models [12]. The ideal behavior of an elastic, fully plastic material is shown in Fig.1.5, where the elastic region's initial slope sharply decreases to zero, allowing the material to strain indefinitely without experiencing further increase in stress. Nevertheless, this represents an idealized situation, since up to the material's maximum stress, almost all of the real materials show some strain-hardening [13].

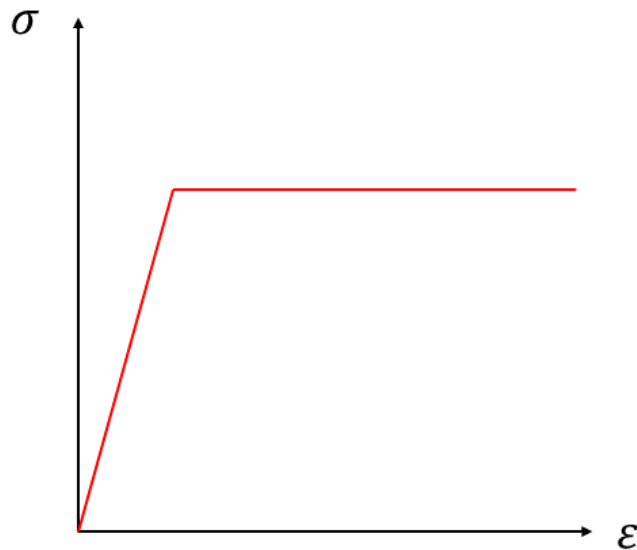


Fig.1. 5: Exploring Material Nonlinearity with an Elastic-Perfectly Plastic behavior [13]

Similar to how geometric nonlinearity may result in instabilities (bifurcation buckling, snap-through, snap-back), material nonlinearity can similarly result in instability mechanism within structures, like necking, plastic hinges, or shear bands [13].

In summary, while geometric nonlinearity is linked to large deformations or changes in the geometry of the structure, material nonlinearity is tied to the response of the material itself. For a thorough and realistic examination of structures and materials, it is necessary to consider both types of nonlinearities.

1. 3 Reduced Modeling Approach: Exploring Discrete Homogenization

Homogenization methods aim to replace a heterogeneous structure by an equivalent substitution medium at a higher scale of description, endowed with so-called effective properties. This

procedure avoids a high numerical cost that would result from modeling all microstructural detailed characteristics of the structure. For periodic media, a unit cell can be identified (Fig.1.6), which by translation generates the entire structure; homogenization is then carried out at the level of a reference unit cell enclosing the microstructure, which is replaced by a homogeneous medium with homogenized properties.

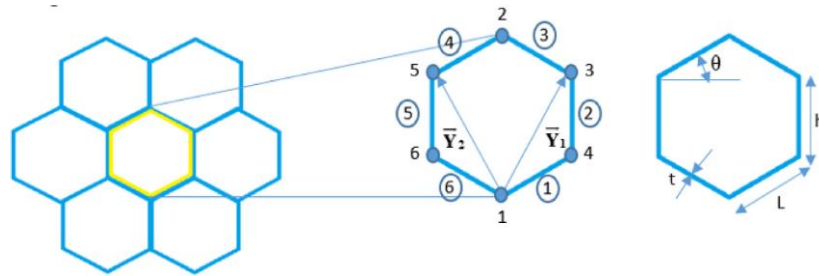


Fig.1. 6: periodicity vectors and geometrical parameters of hexagon unit cell [14]

There are essentially two different types of homogenization methods: continuous homogenization ones, which are traditionally used for composites, and continualization or discrete homogenization techniques that utilize condensed, discrete models for the structural elements that characterize the unit cell, such as rods, bars or beams [15]. While the of departure of the modeling relies on discrete equations at the microscopic level of individual structural members, continualization methods, based e.g. on Taylor series expansion of finite differences of the fields (typically across the end nodes of a beam within the lattice) to reach a continuum model.

Discrete homogenization (DH in short) is an appropriate technique for modelling low-density lattice materials since their internal structural components can be represented as a group of beams or rods. This method is advantageous in terms of computational efficiency compared to continuous homogenization approaches. These DH methods specifically consider a finite number of degrees of freedom (abbreviated as DOF) and can offer straightforward mathematical formulas to determine homogenized moduli [7,16]. The continualization methods, introduced in [17], have gained significant interest in the field of discrete homogenization. These methods involve replacing the discrete equations of motion with continuum differential equations to determine the static and dynamic effective properties of periodic lattices at a continuous level [18]. These approaches are based on two essential steps: (i) substituting discrete kinematics degrees of freedom (DOF) with

continuously varying field variables in both time and space, and (ii) representing the microscopic DOF within neighboring unit cells (UCs) through a Taylor series expansion relative to the selected continuous DOF. Approximately two decades ago, the Lagrangian formulation arose as a technique in the field, providing an alternative approach to describe the statics or dynamics of lattices [19–21]. By limiting the Taylor series to the first order, it becomes possible to derive an effective Cauchy continuum, where only the first displacement gradient holds importance.

The development of efficient computational methods for incorporating both material nonlinearity and geometric nonlinearity within the context of discrete homogenization has been a subject of significant interest in recent research [22–24]. In a broad sense, the basic goal of homogenization techniques is to substitute a real heterogeneous structure with an equivalent homogeneous one that shows the same average macroscopic behavior.

1. 4 Wave Propagation Analysis in Periodic Networks: from band-gaps to Nonlinear Phenomena and Preexisting Deformations

A lot of research activities has been devoted in the last two decades to wave propagation analysis in periodic networks [25], and especially wave attenuation due to physical damping or geometrical effects, and occurrence of full or partial bandgaps. The wave propagation properties within periodic networks depend on the characteristics of their internal architecture, including both geometric and material properties [26,27]. Extensive research has been conducted to investigate the features of elastic wave propagation in two-dimensional media [28,29]. Specific configurations of unit cells have the ability to restrict wave propagation across a specific frequency range [4], resulting in the creation of band-gaps [30]. Furthermore, these unit-cell designs can also manipulate the characteristics of particular modes through alterations in their internal topology alone [31]. By applying Bloch's theorem [32], the wave propagation characteristics of periodic structures can be determined. This theorem takes advantage of the periodic nature of the structure, allowing the study of wave propagation within a single unit cell by considering the Brillouin zone of that cell [33]. The wave propagation characteristics of the effective medium are found to be affected by changes in the internal lattice design [34]. Consequently, conducting high-parametric sensitivity studies becomes crucial in order to gain a better understanding of the band structure of architecture materials [35]. Optimal design of the band structure remains an ongoing engineering challenge [36].

While a considerable amount of research has been conducted on the propagation of elastic waves within linear frameworks, only a limited number of authors have delved into wave propagation in nonlinear media. The inclusion of nonlinear characteristics in the analysis of wave propagation becomes essential when significant deformations are present [37–41], but it continues to pose significant challenges in the field nowadays. When nonlinear waves propagate through periodic structures, several new phenomena arise that are distinct from those observed in linear media. The presence of a nonlinearity in periodic structures leads to a dependence of wave propagation, phase velocity, and group velocity on the wave's amplitude. This phenomenon is known as amplitude-dependent dispersion relation. It opens up new possibilities for passive tuning of the dispersion band structure by exploiting the amplitude-dependency of propagating waves, going beyond simply controlling the dynamic and acoustic properties of repetitive structures through design [42] or external stimuli. Consequently, solutions to wave propagation equations in nonlinear periodic structures are significantly more intricate in comparison to the harmonic plane solutions of linear wave equations. Nonlinear periodic structures exhibit a range of wave solutions that depend on factors such as wave amplitude, wave interactions, and the specific type of nonlinearity present. Notable examples include solitary wave solutions for Boussinesq-type equations and shallow water waves for Burger's equation [43–49].

Furthermore, the impact of an existing pre-stress or pre-strain on wave propagation in homogeneous anisotropic media has garnered attention from numerous researchers. However, studying the influence of preexisting finite elastic deformations on wave propagation remains a significant challenge. The initial deformation must be substantial enough to induce changes in the medium's geometry, as infinitesimal initial deformations do not affect the material properties according to the superposition principle applicable to the small deformation's framework. In previous studies [23,50–54], the incremental effective properties of pre-stressed homogeneous media undergoing large deformation were analyzed. The authors in previous cited works impose certain restrictions on the strain energy to ensure that elastic waves can propagate within the material.

1.5 Limitations of works from the literature

Despite significant advancements in understanding the mechanical behavior of architected materials in the nonlinear regime, researchers still face challenges in accurately predicting their mechanical response.

1.5.1 Kinematic Analysis of Timoshenko Beams

Many researchers have studied the kinematic analysis of Timoshenko beams with a specific focus on the development of their shape function [55–57]. However, most of these studies have neglected the impact of the complete nonlinear energy and have not considered the effects of shear and bending modes. This omission prevents from obtaining accurate results and leads to an incorrect expression of the beam's stiffness matrices.

The shear and bending modes are important factors in understanding how Timoshenko beams behave, but they are often ignored in literature [58,59]. Additionally, the coupling between these modes is also disregarded, further diminishing the accuracy of the analysis and hindering the prediction of the beam's behavior under various loading conditions.

To improve the analysis, it is crucial to consider the full nonlinear energy and consider both shear and bending modes, along with their interaction. By doing so, we can obtain more reliable results and create a more accurate stiffness matrix, leading to a better understanding of how Timoshenko beams behave under different loading conditions.

1.5.2 Nonlinear Wave Propagation in Architected Materials

The impact of a nonlinear kinematics on wave propagation in architected materials was studied in Timoshenko beam elements in recent works [38,60]. However, the focus in these works was mainly on the effect of extension energy [40,41], overlooking other important modes of nonlinear contributions such as extension and bending.

It is essential to consider that nonlinear effects in Timoshenko beams involve not only extension but also shear and bending, which have significant influences on wave propagation. Neglecting these additional modes of the nonlinear energy can result in an incomplete understanding of how the material responds to wave propagation.

Therefore, it is crucial to investigate how the inner architecture material responds when exposed to wave propagation, considering different modes of nonlinear energy. By considering these various modes, researchers can gain a better understanding of the material's response and accurately characterize its wave propagation features. Such developments will contribute to enhancing our knowledge of the complex relationship between the nonlinear kinematics and wave propagation in architected materials.

1. 6 Addressed scientific issues and methodology

The main challenge of this thesis is to develop a model of the nonlinear behavior of periodic lattice materials made of Timoshenko beams, by considering shear, extension, and bending energies, as well as their interactions. To address these scientific issues, this thesis introduces several novel aspects, which are outlined below:

- Develop a complete set of nonlinear shape functions.
- Identify the full nonlinear stiffness matrix and study the impact of the (full) nonlinear energy (including shear, extension, and bending modes) on the dynamical response of architected materials.
- Conduct a comparative analysis of wave propagation in different architected materials, considering the influence of nonlinear energy and the contribution of each mode (extension, flexion, and shear).
- Perform a discrete dynamical homogenization to evaluate the nonlinear continuum response of different nonlinear architected materials.
- Develop wave propagation analyses taking into consideration the effect of second gradient terms, extending the previously developed nonlinear Cauchy type effective models.

1. 7 Thesis outline

This document is organized as follows: a full nonlinear Timoshenko beam model employing nonlinear shape functions is developed in Chapter 2. The extended Hamilton principle is employed for deriving the linear and nonlinear mass and stiffness matrices of the Timoshenko beam element. The nonlinear dispersion diagram incorporating the non-linear corrections is obtained using the Linstedt-Poincaré perturbation method. An analysis of the effect of internal transverse shear, and bending on the nonlinear dispersion characteristics of wave propagation in two-dimensional

periodic network materials made of nonlinear Timoshenko beams is done. In Chapter 3, we analyze wave dispersion features due to nonlinear material effects, recursing to the Linstedt-Poincaré method. We examine how the shear, extension, and bending deformation modes influence the internal material deformation within square, triangular, hexagonal, and re-entrant hexagonal unit cells. We quantify the relative contribution of each non-linear energy mode to the attributes of nonlinear wave dispersion. In Chapter 4, we use discrete homogenization to derive the nonlinear response of hexagonal and triangular planar lattice materials, to study their dynamical response. The obtained nonlinear constitutive law includes strain gradient effects, the influence of which on the acoustic response is studied in addition to the impact of the degree of nonlinearity. Especially, the occurrence of so-called subsonic and supersonic modes is shown to occur, depending on the degree of nonlinearity. Finally, we summarize chapter 5 as a general conclusion of the thesis the employed methodology, and the main obtained results, and provide directions for continued research in the light of the achieved work.

Chapter 2

Development and Analysis of Nonlinear Timoshenko Beams: Shape Functions, Static Solution, and Stiffness Comparison

Summary:

In this chapter, a full nonlinear Timoshenko beam employing nonlinear shape functions is developed. The extended Hamilton principle is employed for deriving the differential equations of motion and the associated boundary conditions. The general form of the boundary conditions is then utilized to determine the static solution of the beam motion. Using this solution for the deformation and rotation of the beam, the nonlinear shape functions of the beam are identified, which leads to the linear and nonlinear mass and stiffness matrices of the Timoshenko beam element. Comparing both matrices of the linear and non-linear regimes shows that the non-linear stiffness matrix has larger values compared to the linear one, underlining that the non-linear effects make the structure overall stiffer. The examination of mode effects on the behavior of linear and nonlinear Timoshenko beams under a concentrated force reveals a stiffer response of the nonlinear Timoshenko beam compared to the linearized beam model, owing to the contribution of nonlinear stiffness terms.

2. 1 Introduction

Many research activities have been devoted to the effective mechanical properties of periodic networks due to the ability of tuning static and dynamic properties, with a wide range of applications in civil engineering, construction mechanics, or biomechanics [61–64]. Several techniques have been developed to compute the effective mechanical properties of heterogeneous periodic structures, and especially network materials, thereby by passing the need to resolve the smallest spatial scale [65]. Homogenization methods aim at describing the overall response of heterogeneous structures, including periodic structural lattices and composites in terms of their effective properties, as presented in the recent contributions [66,67]. More recently, [68] extended the linear model developed in [69,70] to formulate the nonlinear constitutive law for hyperplastic network materials with arbitrary symmetry. An alternative approach was proposed in [71,72] using a computational homogenization method to derive a nonlinear constitutive model for network materials. Many research works have been done in the last two decades devoted to the dynamical behavior of periodic networks, particularly since non-destructive techniques are used as a mean to access mechanical properties of the investigated material [73].

According to classical continuum mechanics theories, a material's response to the displacement of its points is defined by a symmetric stress tensor and material continua are points with three degrees of freedom in translation [74]. Using the classical continuum mechanics theory, Friedman and Kosmatka [15] constructed the stiffness, mass, and consistent force matrices of a simple two-node Timoshenko beam element. For the transversal and rotational displacements, respectively, the cubic and Lagrangian polynomials were used to formulate the shape functions of the exact solution. Extended continuum theories containing the material length scale parameters are required because the classical beam models lack an internal material length scale parameter. Many continuum-based theories have been elaborated to account for size effects by incorporating several parameters having the physical meaning of a material length scale. The couple stress theory (CST), micropolar elasticity, strain gradient theory, and nonlocal elasticity theory are the most important representative of these theories [76]. The CST and micropolar theories were introduced in the 1960s by well-known researchers, including Mindlin-Tiersten [77], Koiter [78], and Eringen [79]. Two sets of degrees of freedom, the displacement and rotation fields, are present in micropolar theory [64]. The constitutive equations of the micropolar theory involves four additional constants in addition to the two Lamé constants for linear isotropic elastic materials. Dos Reis and

Ganghoffer [64] used an asymptotic homogenization technique to replace periodic beam lattices with an equivalent micropolar continuum. A close agreement was established between the homogenized moduli of the hexagonal and square lattices and the moduli discovered from finite element simulations.

In several applications of beams employed as structural elements, such as biosensors [80] or open foam cellular structures, size effects have been observed [81,82], which cannot be correctly captured by classical beam theories. For this reason, enriched continuum theories incorporating material length scales have been proposed, the most prominent of which being the couple stress theory (CST), micropolar elasticity, strain gradient theory, and the nonlocal elasticity theory [76]. CST theory is a special case of the micropolar theory, in which the rotation vector of the microstructure is identified with the macro-rotation vector [83]; it involves two additional length scale parameters. Homogenized models replacing the periodic beam lattices with an effective generalized continuum were developed, like Dos Reis and Ganghoffer [64], who replaced periodic beam lattices by an equivalent micropolar continuum using an asymptotic homogenization method. Size effects in Timoshenko beams were investigated by various authors Asghari [84]; Alotta [85]; Dehrouyeh-Semnani and Bahrami [86], relying on the couple stress theory. The stiffness matrix was computed accounting for the axial deformation, bending deflection, and beam cross-section rotation. The so-called modified couple stress theory was developed by Yang et al.[87], including a single higher-order material length scale parameter, followed by diverse authors (Ma [88]; Kahrobaiyan [89]; Goncalves [90]; Karttunen [91]; Goncalves [92]).

Structural geometric nonlinear analysis of beam elements relies on the kinematic description, the stress-strain relation and the shape functions interpolating the kinematic variables. In situations of moderate slenderness ratio, the Timoshenko beam theory is more adapted than Euler-Bernoulli beam theory. Several higher-order bending theories have been developed in the literature[40,60,93–98]. The geometrical nonlinearity can be incorporated relying on either a full Lagrangian, updated Lagrangian or a co-rotational approach [99–104].

Since computing the dynamical response of periodic networks with many structural elements (and thus including a huge number of degrees of freedom) is prohibitively expensive, it is more cost-effective to portray network materials on the macroscale based on a homogeneous substitution material obtained by some suitable homogenization method.

Extensive research activities have been devoted to the wave propagation and bandgaps concept in periodic networks [105]; within some frequency range, waves cannot propagate through the network, since they are attenuated due to damping effects or geometrical attenuation [105]. The width and the location of the bandgaps depend on the network topology shapes and on the direction of wave propagation. While the propagation of elastic waves in a linear framework has been well studied [28,33,106–109], only a few works deal so far with wave propagation in nonlinear media. The incorporation of nonlinear aspects of wave propagation in periodic structures is however necessary whenever large deformations occur [38,41,110,111], but it remains a considerable challenge due to the complexity of solving the nonlinear wave motion equations, considering that its solution by far differs from its linearized version. To our knowledge, the literature misses the full nonlinear stiffness matrix based on nonlinear shape functions. Two types of nonlinearities may arise in a broad sense: material nonlinearities [112,113] and geometrical nonlinearities [42]. A number of new phenomena that differ accompanies the propagation of nonlinear waves in periodic networks from the linear wave propagation situation: this includes the dependency of the frequency, phase and group velocities of wave propagation upon the wave amplitude. This dependency of the dispersion relation on the amplitude of waves opens new possibilities for a passive tuning of the bandgap structure, thereby going beyond a mere control of the dynamic and acoustic properties of network periodic structures by the design [113]. This has the consequence that the solutions of the wave propagation equations are more complex and differ from the harmonic planar wave solutions (of the linear wave equations): nonlinear periodic structures support indeed a variety of wave solutions depending on wave amplitude, wave interactions, and the type of nonlinearity. Such specific solutions include for instance solitary wave solutions for Boussinesq type equation, and shallow water waves for Burger's equation [22,47,48,114–120].

Network or architected materials under consideration in the present contribution consist of an assembly of beam elements connected at nodes; in Timoshenko beam, each material point has three degrees of freedom in a planar situation, namely the two components of the displacement vector and one out-of-plane rotation [121]. Friedman and Kosmatka [122] developed the stiffness, mass, and consistent force matrices of a simple two-node Timoshenko beam element based on the classical continuum mechanics theory. Alavi and Ganghoffer [57] considered a Timoshenko beam element with two nodes and set two degrees of freedom (vertical displacement and the rotation). The same authors considered bending deflection (rotation) and axial deformation (displacement)

and cross-section angle in the static case. From the computation of the shape functions using Lagrangian and extended Hamilton's principle [57], these last authors obtained the stiffness matrix using the strain energy and the mass matrix using the kinetic energy. The impact of the nonlinear kinematics of Timoshenko beam elements on wave propagation features of architected materials (that will be studied in Chapter 3) was studied in [40,41]; the authors however did not consider all of the nonlinear contributions to the beam kinematics, restricting to the mere effect of the nonlinear extension mode.

The aim of this chapter is to:

- Derive nonlinear shape functions considering the full nonlinear kinematics of the network beam elements,
- Formulate a nonlinear dynamical equation for hexagonal networks incorporating the nonlinear stiffness matrix,
- Study the difference between linear and nonlinear effects,

The present chapter is organized as follows: in order to set the stage, the shape functions for the nonlinear Timoshenko beams are evaluated in section 2.2, based on Hamilton principle for the formulation of equilibrium. Based on this knowledge, the mass matrix and the linear and nonlinear stiffness matrices are constructed at the local beam level and global unit cell level and study the effect of nonlinear stiffness matrix in section 2.3, section 2.4 provides the conclusion.

2. 2 Kinematics of the fully Nonlinear Timoshenko beam

We aim to develop a nonlinear Timoshenko theory for periodic network materials of Cauchy type, based on a beam mechanics description of the network at the lattice level. To this aim, the nonlinear and linear stiffness matrix for a Timoshenko beam will be calculated as a first step. The extended Hamilton's principle is utilized to obtain the governing differential equations and boundary conditions. The general form of boundary conditions resulting from the Euler-Lagrange equations is employed to determine the static solution of the beam. Using this differential equation and boundary condition for the beam's deformation and rotation, we will extract the shape functions, leading to the mass, linear stiffness, and nonlinear stiffness matrices.

2.2. 1 Shape functions for the nonlinear Timoshenko beam

Fig.2.1 shows the Timoshenko beam element coordinates, displacements, shear deformation, and rotation fields. The displacement functions u_z and u describe the translation of the beam's neutral axis, in the z direction and x direction respectively, while the function ϕ denotes the rotation of the cross-section at the mid-plane, and $\theta(x)$ is the slope of the central axis of the beam, as illustrated in Fig.2.1. The displacement field in Timoshenko beam theory is assumed to take the form Eq.(2.1)

$$u_x = u(x) - z\phi(x); u_y = 0; u_z = u_z(x) \quad (2.1)$$

in which the slope of the central axis of the beam is given by

$$\theta = \frac{du_z}{dx} \quad (2.2)$$

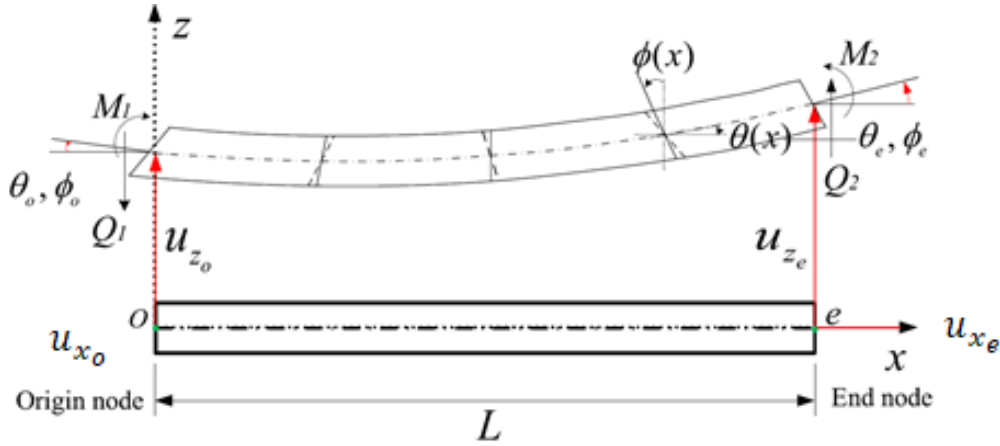


Fig.2. 1: Timoshenko beam element with the indicated kinematic and static variables

The displacement gradient is then given from previous kinematic relations by:

$$u_{x,x} = \frac{du_x(x)}{dx} - z \frac{d\phi(x)}{dx}; u_{x,z} = -\phi(x); u_{z,x} = \frac{du_z(x)}{dx}; u_{z,z} = 0 \quad (2.3)$$

The expression of strain energy expressed as the contraction of the Cauchy stress \mathbf{S} and Lagrangian strain tensor \mathbf{E} is given as follows:

$$U = \frac{1}{2} S_{ij} E_{ij} \quad (2.4)$$

The general expression of the Lagrangian strain components for the non-linear kinematics is given as the sum of the linearized strain tensor and a term quadratic in the displacement gradient:

$$E_{ij} = \varepsilon_{ij} + \frac{1}{2} u_{k,i} u_{k,j} \quad (2.5)$$

The non-zero strain components follow from previous Eq.(2.5) of the displacement components

$$E_{xx} = \frac{du_x(x)}{dx} - z \frac{d\phi(x)}{dx} + \frac{1}{2} (\varepsilon_{xx})^2 + \frac{1}{2} \left(\frac{du_z}{dx} \right)^2 \quad (2.6)$$

$$E_{zz} = \frac{1}{2} \phi(x)^2 \quad (2.7)$$

$$E_{xz} = E_{zx} = \frac{1}{2} \left(\frac{du_z}{dx} - \phi \right) - \frac{1}{2} \phi \left(\frac{du_x}{dx} - z\phi_{,x} \right) \quad (2.8)$$

The non-zero stress components follow from the adopted linear isotropic constitutive law for the base material of the beam

$$S_{xx} = \lambda(E_{xx} + E_{zz}) + 2\mu E_{xx} \quad (2.9)$$

$$S_{xz} = 2\mu E_{xz} = \mu \gamma_{xz} \quad (2.10)$$

$$S_{zz} = \lambda(E_{xx} + E_{zz}) + 2\mu E_{zz} \quad (2.11)$$

where λ and μ are the lame coefficients. The expression of the nonlinear strain energy results from the integration of the strain energy density over the beam length, evaluated as follows (we use the same notation for the energy density expressed in Eq.(2.4) and its integrated form over the beam length in Eq.(2.12)):

$$U = \int_0^L \underbrace{\left[\frac{1}{2} k_s GA (u_{z,x} - \phi)^2 + \frac{(\lambda + 2G)}{2} (u_{x,x})^2 A + \frac{EI}{2} (\phi_{,x})^2 \right]}_{\text{linear}} dx + \underbrace{\int_0^L \frac{EA}{8} \phi^2 dx}_{\text{linear term related to non-linear theory}} \quad (2.12)$$

$$+ \int_0^L \underbrace{\left[\frac{G}{2} \left(\phi^2 (u_{x,x})^2 - 2\phi u_{x,x} u_{z,x} + 2\phi^2 u_{x,x} \right) A (k_k k_s) + \frac{1}{8} EA (u_{x,x})^4 + \frac{1}{8} k_s EA (u_{z,x})^4 \right.}_{\text{non-linear}} \\ \left. + \frac{EA}{4} k_s (u_{z,x})^2 u_{x,x}^2 + \frac{EA}{2} (u_{x,x})^3 + \frac{EA}{2} k_s u_{x,x} (u_{z,x})^2 + \frac{\lambda A}{2} u_{x,x} \phi^2 + \frac{\lambda A}{4} u_{x,x}^2 \phi^2 \right. \\ \left. + \frac{\lambda A}{4} (u_{z,x})^2 \phi^2 \right] dx \quad (2.13)$$

wherein k_s and k_k are the beam correction factors. The previous expression of the internal strain energy of the beam splits overall into a linear first contribution and a second nonlinear contribution. Then we derive the equation of motion using the extended Hamilton's principle, viz.

$$\delta \int_0^t \mathcal{L} dt = 0 \quad (2.14)$$

$$\mathcal{L} = T - U + W_e$$

wherein \mathcal{L} , T , U and W_e are the Lagrangian, kinetic energy (here no kinetic energy term is considered $T=0$), strain energy, and work of external loads, respectively. The strain energy is given by

$$U = \frac{1}{2} \int_{\Omega} S_{ij} E_{ij} d\Omega \quad (2.15)$$

Finally, we obtain the variations of the work of external forces:

$$W_e = \int_0^L \begin{Bmatrix} u_z \\ \phi \end{Bmatrix}^T \begin{Bmatrix} q \\ m \end{Bmatrix} dx \quad (2.16)$$

where ‘ \mathbf{q} ’ is external distributed force and ‘ \mathbf{m} ’ is the moment. After substituting the Lagrangian function in the extended Hamilton’s principle, and a few derivations, we obtain Eq. (A.1), which is provided in detailed form in the **Appendix A**. Based on Eq.(2.12), Eq.(2.13), and Eq.(A.1) from the **Appendix A**, the balance equations for shear, extension and bending are successively obtained as:

For the shear deformation mode, it holds the differential equation:

$$\begin{aligned} & k_s GA \left(\frac{d^2 u_z}{dx^2} - \frac{d\phi}{dx} \right) - GA(k_k k_s) \left(\frac{d^2 u_x}{dx^2} \phi + \frac{d\phi}{dx} \frac{du_x}{dx} \right) + k_s GA \left(\frac{du_z}{dx} - \phi \right) - GA(k_k k_s) \phi \left(\frac{du_x}{dx} \right)^2 \\ & + GA(k_k k_s) \frac{du_x}{dx} \frac{du_z}{dx} - 2GA(k_k k_s) \left(\phi \frac{du_x}{dx} \right) + GA(k_k k_s) \left(\frac{d^2 u_x}{dx^2} \phi^2 + 2\phi \frac{du_x}{dx} \frac{d\phi}{dx} \right) \\ & - GA(k_k k_s) \left(\frac{d^2 u_z}{dx^2} \phi + \frac{d\phi}{dx} \frac{du_z}{dx} \right) + 2GA(k_k k_s) \left(\phi \frac{d\phi}{dx} \right) = 0 \end{aligned} \quad (2.17)$$

For the extension mode, the following differential equation is obtained:

$$\begin{aligned}
& \frac{3}{2}k_s EA \left(\frac{du_z}{dx} \right)^2 \frac{d^2 u_z}{dx^2} + \frac{1}{2}k_s EA \left(\frac{d^2 u_z}{dx^2} \left(\frac{du_x}{dx} \right)^2 + 2 \frac{du_x}{dx} \frac{d^2 u_x}{dx^2} \frac{du_z}{dx} \right) + EA \left(\frac{d^2 u_z}{dx^2} \frac{du_x}{dx} + \frac{d^2 u_x}{dx^2} \frac{du_z}{dx} \right) \\
& + \frac{(\lambda + 2G)}{2} A \frac{du_x^2}{dx^2} + \frac{3}{2} EA \left(\frac{du_x}{dx} \right)^2 \frac{d^2 u_x}{dx^2} + \frac{1}{2} k_s EA \left(\frac{d^2 u_x}{dx^2} \left(\frac{du_z}{dx} \right)^2 + 2 \frac{du_z}{dx} \frac{d^2 u_z}{dx^2} \frac{du_x}{dx} \right) + 3EA \frac{du_x}{dx} \frac{d^2 u_x}{dx^2} \\
& + k_s EA \frac{du_z}{dx} \frac{d^2 u_z}{dx^2} = 0
\end{aligned} \tag{2.18}$$

Lastly, for bending, the following differential equation is obtained:

$$\begin{aligned}
& \frac{1}{2} \lambda A \left(\frac{d^2 u_z}{dx^2} \phi^2 + 2\phi \frac{d\phi}{dx} \frac{du_z}{dx} \right) + EI \frac{d^2 \phi}{dx^2} - \frac{1}{4} EA \phi - \lambda A \frac{du_x}{dx} \phi - \frac{1}{2} \lambda A \phi \left(\frac{du_x}{dx} \right)^2 - \frac{1}{2} \lambda A \left(\frac{du_z}{dx} \right)^2 \phi \\
& + \lambda A \phi \frac{d\phi}{dx} + \frac{1}{2} \lambda A \left(\frac{d^2 u_x}{dx^2} \phi^2 + 2\phi \frac{d\phi}{dx} \frac{du_x}{dx} \right) = 0
\end{aligned} \tag{2.19}$$

For the classical Timoshenko beam theory, the functions $u_z(x)$, $\phi(x)$ and $u_x(x)$ are the kinematic primary variables. Additionally, the displacement degree of freedom u_z and u_x are energetically conjugated to the transverse forces τ and P , respectively, while the slope $\phi(x)$ is a primary variable with the conjugate bending moment M_ϕ , where M_ϕ, τ, P are the bending moment, shear force and axial force respectively. The corresponding natural and essential boundary conditions write:

$$\begin{aligned}
\tau &= 0 \text{ or } \delta u_z = 0 \\
M_\phi &= 0 \text{ or } \delta \phi = 0 \\
P &= 0 \text{ or } \delta u = 0
\end{aligned} \tag{2.20}$$

The moments and transverse force are identified from Hamilton's principle as explained into the **Appendix A** as:

$$\begin{aligned}
\tau &= k_s GA \left(\frac{du_z}{dx} - \phi \right) - GA(k_k k_s) \frac{du_x}{dx} \phi + \frac{1}{2} k_s EA \left(\frac{du_z}{dx} \right)^3 + \frac{1}{2} k_s EA \left(\frac{du_z}{dx} \right) \left(\frac{du_x}{dx} \right)^2 + EA \frac{du_z}{dx} \frac{du_x}{dx} \\
& + \frac{1}{2} \lambda A \frac{du_z}{dx} \phi^2
\end{aligned} \tag{2.21}$$

$$M_\phi = EI \left(\frac{d\phi}{dx} \right) \tag{2.22}$$

$$\begin{aligned}
P = & \frac{(\lambda + 2G)}{2} A \left(\frac{du_x}{dx} \right) + GA(k_k k_s) \frac{du_x}{dx} \phi^2 - GA(k_k k_s) \frac{du_z}{dx} \phi + GA(k_k k_s) \phi^2 + \frac{1}{2} EA \left(\frac{du_x}{dx} \right)^3 \\
& + \frac{1}{2} k_s EA \frac{du_x}{dx} \left(\frac{du_z}{dx} \right)^2 + \frac{3}{2} k_s EA \left(\frac{du_x}{dx} \right)^2 + \frac{1}{2} k_s EA \left(\frac{du_z}{dx} \right)^2 + \frac{1}{2} \lambda A \phi^2 + \frac{1}{2} \lambda A \frac{du_x}{dx} \phi^2
\end{aligned} \tag{2.23}$$

It is known from the classical Timoshenko beam theory that the equilibrium equations are satisfied by taking functions $u_z(x)$, $u_x(x)$ and $\phi(x)$ as cubic and quadratic polynomials, respectively. Accordingly, it is assumed that the kinematic fields $u_z(x)$, $\phi(x)$ and $u_x(x)$ receive the following forms

$$u_z(x) = C_1 + C_2 x + C_3 x^2 + C_4 x^3 \tag{2.24}$$

$$\phi(x) = C_5 + C_6 x + C_7 x^2 \tag{2.25}$$

$$u_x(x) = C_8 + C_9 x + C_{10} x^2 \tag{2.26}$$

wherein $C_i = (i=1, \dots, 10)$ are unknown constants determined from the following boundary conditions

$$x = 0: u_z = u_{z_0}, \phi = \phi_0, u_x = u_{x_0} \tag{2.27}$$

$$x = L: u_z = u_{z_e}, \phi = \phi_e, u_x = u_{x_e}$$

By substituting Eq.(2.24), Eq.(2.25) and Eq.(2.26) in the shear balance equation of Eq.(2.17) and taking into consideration only the single terms, the unknown coefficients can be evaluated from the polynomial relation:

$$k_s GA \left[(2C_3 + 6C_4 x) - (C_6 + 2C_7 x) \right] + k_s GA \left[(C_2 + 2C_3 + 3C_4 x) - (C_5 + C_6 x + C_7 x^2) \right] = 0$$

By setting the coefficients of x^i ($i=1, 2$) equal to zero, we obtain:

$$\begin{cases} x^2: k_s GA(3C_4 - C_7) = 0 \rightarrow C_7 = 3C_4 \\ x^1: k_s GA(2C_3 - C_6) = 0 \rightarrow C_6 = 2C_3 \end{cases}$$

After calculations and using boundary conditions from Eqs.(2.27), the functions $u_z(x)$, $\phi(x)$ and $u(x)$ take the following polynomial forms:

$$u_z(x) = u_{z_0} + C_2 x + C_3 x^2 + C_4 x^3 \tag{2.28}$$

$$\phi(x) = \phi_0 + 2C_3 x + 3C_4 x^2 \tag{2.29}$$

$$u_x(x) = u_{x_0} + C_9x + C_{10}x^2 \quad (2.30)$$

The expressions of functions $u_z(x)$, $\phi(x)$ and $u_x(x)$ at the beam extremity $x=L$ take the following forms:

$$u_{z_e} = u_{z_0} + C_2L + C_3L^2 + C_4L^3 \quad (2.31)$$

$$\phi_e = \phi_0 + 2C_3L + 3C_4L^2 \quad (2.32)$$

$$u_{x_e} = u_{x_0} + C_9L + C_{10}L^2 \quad (2.33)$$

Using the balance equation of the non-linear expression energy from Eq. (2.17) and Eq.(2.19) and the expression of the kinematic variables $u_z(x)$, $\phi(x)$ and $u_x(x)$ from Eq.(2.28), Eq.(2.29), and Eq.(2.30) lead to the following coefficients [123,124]:

$$C_2 = (\phi_e - \phi_0) \frac{15(-30Gk_k k_s + 15\lambda)}{2(675Gk_k k_s - 338\lambda)} + (u_{z_e} - u_{z_0}) \frac{15(90Gk_k k_s - 45\lambda)}{2L(675Gk_k k_s - 338\lambda)} + (u_{x_e} - u_{x_0}) \frac{15(2Gk_k k_s - \lambda)}{2L(675Gk_k k_s - 338\lambda)}$$

$$C_3 = (\phi_e - \phi_0) \frac{\lambda}{1350GLk_k k_s - 676L\lambda} + (u_{z_e} - u_{z_0}) \frac{-3\lambda}{1350GL^2k_k k_s - 676L^2\lambda} + (u_{x_e} - u_{x_0}) \frac{45\lambda - 90Gk_k k_s}{1350GL^2k_k k_s - 676L^2\lambda}$$

$$C_4 = (\phi_e - \phi_0) \frac{225Gk_k k_s - 113\lambda}{L^2(675Gk_k k_s - 338\lambda)} + (u_{z_e} - u_{z_0}) \frac{\lambda}{L^3(675Gk_k k_s - 338\lambda)} + (u_{x_e} - u_{x_0}) \frac{30Gk_k k_s - 15\lambda}{L^3(675Gk_k k_s - 338\lambda)}$$

$$C_9 = (\phi_e - \phi_0) \frac{15\lambda}{2L(675Gk_k k_s - 338\lambda)} + (u_{z_e} - u_{z_0}) \frac{-45\lambda}{2L(675Gk_k k_s - 338\lambda)} + (u_{x_e} - u_{x_0}) \frac{-\lambda}{2L(675Gk_k k_s - 338\lambda)}$$

$$C_{10} = (\phi_e - \phi_0) \frac{-15\lambda}{2L(675Gk_k k_s - 338\lambda)} + (u_{z_e} - u_{z_0}) \frac{45\lambda}{2L^2(675Gk_k k_s - 338\lambda)} + (u_{x_e} - u_{x_0}) \frac{1350Gk_k k_s - 675\lambda}{2L^2(675Gk_k k_s - 338\lambda)}$$

After substituting the expressions of constant $C_i (i=1, \dots, 10)$ in Eq.(2.28), the vertical displacement $u_z(x)$ is given in closed form by

$$u_z(x) = (\phi_e - \phi_0)(ax + dx^2 + gx^3) + u_{z_e}(bx + ex^2 + hx^3) - u_{z_0}(bx + ex^2 + hx^3 - 1) + (u_{x_e} - u_{x_0})(cx + fx^2 + ix^3) \quad (2.34)$$

Similarly, after substituting expressions of the parameters C_3, C_4 into Eq.(2.29), the analytical solution for the rotation of the normal to the mid line of the beam, function $\phi(x)$, takes the following form:

$$\phi(x) = \phi_e(2dx + 3gx^2) - \phi_o(2dx + 3gx^2 - 1) + (u_{z_e} - u_{z_o})(2ex + 3hx^2) + (u_{x_e} - u_{x_o})(2fx + 3ix^2) \quad (2.35)$$

in which the coefficients therein express as:

$$a = \frac{15(-30Gk_k k_s + 15\lambda)}{2(675Gk_k k_s - 338\lambda)}; b = \frac{15(90Gk_k k_s - 45\lambda)}{2L(675Gk_k k_s - 338\lambda)}; c = \frac{15(2Gk_k k_s - \lambda)}{2L(675Gk_k k_s - 338\lambda)}$$

$$d = \frac{\lambda}{1350GLk_k k_s - 676L\lambda}; e = \frac{-3\lambda}{1350GL^2k_k k_s - 676L^2\lambda}; f = \frac{45\lambda - 90Gk_k k_s}{1350GL^2k_k k_s - 676L^2\lambda}$$

$$g = \frac{225Gk_k k_s - 113\lambda}{L^2(675Gk_k k_s - 338\lambda)}; h = \frac{\lambda}{L^3(675Gk_k k_s - 338\lambda)}; i = \frac{30Gk_k k_s - 15\lambda}{L^3(675Gk_k k_s - 338\lambda)}$$

Similarly, after substituting expressions of constant C_9, C_{10} into Eq. (2.30) leads to the analytical solution for the displacement field $u(x)$:

$$u_x(x) = (\phi_e - \phi_o)(jx + mx^2) + (u_{z_e} - u_{z_o})(kx + nx^2) + u_{x_e}(lx + ox^2) - u_{x_o}(lx + ox^2 - 1) \quad (2.36)$$

wherein the following constants have been introduced:

$$j = \frac{15\lambda}{2L(675Gk_k k_s - 338\lambda)}; k = \frac{-45\lambda}{2L(675Gk_k k_s - 338\lambda)}; l = \frac{-\lambda}{2L(675Gk_k k_s - 338\lambda)}$$

$$m = \frac{-15L\lambda}{2L^2(675Gk_k k_s - 338\lambda)}; n = \frac{45\lambda}{2L^2(675Gk_k k_s - 338\lambda)}; o = \frac{1350Gk_k k_s - 675\lambda}{2L^2(675Gk_k k_s - 338\lambda)}$$

From Eqs.(2.34),(2.35), and (2.36), we obtain the expression of the non-linear Timoshenko beam shape functions allowing to express the continuous kinematic fields versus their nodal counterparts:

$$\begin{pmatrix} u_x(x) \\ u_z(x) \\ \phi(x) \end{pmatrix} = \begin{pmatrix} -lx - ox^2 + 1 & -kx - nx^2 & -jx - mx^2 & lx + ox^2 & kx + nx^2 & jx + mx^2 \\ -cx - fx^2 - ix^3 & -bx - ex^2 - hx^3 + 1 & -ax - dx^2 - gx^3 & cx + fx^2 + ix^3 & bx + ex^2 + hx^3 & ax + dx^2 + gx^3 \\ -2fx - 3ix^2 & -2ex - 3hx^2 & -2dx - 3gx^2 + 1 & 2fx + 3ix^2 & 2ex + 3hx^2 & 2dx + 3gx^2 \end{pmatrix} \begin{pmatrix} u_{x_o} \\ u_{z_o} \\ \phi_o \\ u_{x_e} \\ u_{z_e} \\ \phi_e \end{pmatrix} \quad (2.37)$$

2. 3 Evaluation of the mass matrix and linear and nonlinear stiffness matrices for the nonlinear Timoshenko beam

We consider network materials in a 2D context consisting of Timoshenko beam elements as structural elements within a repetitive unit cell; each beam element is assigned two end nodes n_1 and n_2 , with a total of three degrees of freedom per node, namely two translations and one rotation. The expression of the first node $n_1 : \mathbf{q}_1 = (q_1, q_2, q_3) = (u_{x_o}, u_{z_o}, \phi_o)$, and for the second node $n_2 : \mathbf{q}_2 = (q_4, q_5, q_6) = (u_{x_e}, u_{z_e}, \phi_e)$. The beam longitudinal, vertical displacements and slope $u_x(x, t)$, $u_z(x, t)$ and $\phi(x, t)$ (where is the x curvilinear local beam coordinates) are expressed for each inner structural beam element as a function of its end node displacements using the shape functions in Eq.(2.37) as follows:

$$\begin{aligned} u_x(x, t) &= \sum_{n=1}^6 a_n(x) q_n(t) \Rightarrow u_x(x, t) = a_1(x)q_1 + a_2(x)q_2 + a_3(x)q_3 + a_4(x)q_4 + a_5(x)q_5 \\ &\quad + a_6(x)q_6 \\ u_z(x, t) &= \sum_{n=1}^6 b_n(x) q_n(t) \Rightarrow u_z(x, t) = b_1(x)q_1 + b_2(x)q_2 + b_3(x)q_3 + b_4(x)q_4 + b_5(x)q_5 \\ &\quad + b_6(x)q_6 \\ \phi(x, t) &= \sum_{n=1}^6 c_n(x) q_n(t) \Rightarrow \phi(x, t) = c_1(x)q_1 + c_2(x)q_2 + c_3(x)q_3 + c_4(x)q_4 + c_5(x)q_5 \\ &\quad + c_6(x)q_6 \end{aligned} \quad (2.38)$$

wherein $a_n(x)$, $b_n(x)$, $c_n(x)$ are the expression of shape function detailed in the **Appendix A**. Based on the kinematic definitions of Eq.(2.38), the kinetic and potential energy of each beam element

can be computed. Upon the use of Eq.(2.38), the beam kinetic energy T is computed for each inner element neglecting inertia effects as follows:

$$T = \frac{1}{2} \int_0^L \rho S \left(\frac{\partial \mathbf{u}}{\partial t} \right)^2 dx + \frac{1}{2} \int_0^L \rho S \left(\frac{\partial \mathbf{v}}{\partial t} \right)^2 dx = \frac{1}{2} \rho S \sum_{r=1}^6 \sum_{s=1}^6 \dot{q}_r \dot{q}_s \int_0^L ((a_r a_s + b_r b_s)) dx \quad (2.39)$$

In Eq.(2.39), ρ stands for the beam element density and S for the element area, while L stands for the beam length. The total potential energy U is elaborated making use of the full nonlinear Green-Lagrange strain of Eq.(2.6), Eq.(2.7), and Eq.(2.8) and the expansions of the displacement in Eq.(2.38), leading to:

$$U = \frac{1}{2} (S_{xx} E_{xx} + S_{zz} E_{zz} + \underbrace{S_{xz} E_{xz} + S_{zx} E_{zx}}_{S_{xz} \gamma_{xz}}) = U_1 + U_2 + U_3 + U_4 \quad (2.40)$$

where U_1 is the linear part of the non-linear energy, and the quadratic energy U_2 represents the linear part of the non-linear energy defined by

$$U_1 = \frac{1}{2} \sum_{o=1}^6 \sum_{j=1}^6 q_o q_j \int_0^L \left[k_s GA \left(\frac{\partial b_o}{\partial x} - c_o \right) \left(\frac{\partial b_j}{\partial x} - c_j \right) + \frac{(\lambda + 2G)}{2} \frac{\partial a_o}{\partial x} \frac{\partial a_j}{\partial x} A + \frac{EI}{2} \left(\frac{\partial c_o}{\partial x} \frac{\partial c_j}{\partial x} \right) \right] dx \quad (2.41)$$

$$U_2 = \frac{1}{8} \sum_{o=1}^6 \sum_{j=1}^6 q_o q_j \int_0^L EA c_o c_j dx \quad (2.42)$$

The non-linear energies U_3 and U_4 are defined as cubic and quartic contributions to the total energy, respectively given by the expressions:

$$\begin{aligned} U_3 = & - \sum_{o=1}^6 \sum_{j=1}^6 \sum_{n=1}^6 q_o q_j q_n \int_0^L \left(GA(k_k k_s) c_o \frac{\partial a_j}{\partial x} \frac{\partial b_n}{\partial x} \right) dx + \sum_{o=1}^6 \sum_{j=1}^6 \sum_{n=1}^6 q_o q_j q_n \int_0^L \left(GA(k_k k_s) c_o c_j \frac{\partial a_n}{\partial x} \right) dx \\ & + \frac{1}{2} \sum_{o=1}^6 \sum_{j=1}^6 \sum_{n=1}^6 q_o q_j q_n \int_0^L \left(EA \frac{\partial a_o}{\partial x} \frac{\partial a_j}{\partial x} \frac{\partial a_n}{\partial x} \right) dx + \frac{1}{2} \sum_{o=1}^6 \sum_{j=1}^6 \sum_{n=1}^6 q_o q_j q_n \int_0^L \left(EAK_s \frac{\partial a_o}{\partial x} \frac{\partial b_j}{\partial x} \frac{\partial b_n}{\partial x} \right) dx \\ & + \frac{1}{2} \sum_{o=1}^6 \sum_{j=1}^6 \sum_{n=1}^6 q_o q_j q_n \int_0^L \left(\lambda A \frac{\partial a_o}{\partial x} c_j c_n \right) dx \end{aligned} \quad (2.43)$$

$$\begin{aligned}
U_4 = & \frac{1}{2} \sum_{o=1}^6 \sum_{j=1}^6 \sum_{n=1}^6 \sum_{t=1}^6 q_o q_j q_n q_t \int_0^L \left(GA(k_k k_s) c_o c_j \frac{\partial a_n}{\partial x} \frac{\partial a_t}{\partial x} \right) dx \\
& + \frac{1}{8} \sum_{o=1}^6 \sum_{j=1}^6 \sum_{n=1}^6 \sum_{t=1}^6 q_o q_j q_n q_t \int_0^L \left(EA \frac{\partial a_o}{\partial x} \frac{\partial a_j}{\partial x} \frac{\partial a_n}{\partial x} \frac{\partial a_t}{\partial x} \right) dx \\
& + \frac{1}{8} \sum_{o=1}^6 \sum_{j=1}^6 \sum_{n=1}^6 \sum_{t=1}^6 q_o q_j q_n q_t \int_0^L \left(k_s EA \frac{\partial b_o}{\partial x} \frac{\partial b_j}{\partial x} \frac{\partial b_n}{\partial x} \frac{\partial b_t}{\partial x} \right) dx \\
& + \frac{1}{4} \sum_{o=1}^6 \sum_{j=1}^6 \sum_{n=1}^6 \sum_{t=1}^6 q_o q_j q_n q_t \int_0^L \left(k_s EA \frac{\partial b_o}{\partial x} \frac{\partial b_j}{\partial x} \frac{\partial a_n}{\partial x} \frac{\partial a_t}{\partial x} \right) dx \\
& + \frac{1}{4} \sum_{o=1}^6 \sum_{j=1}^6 \sum_{n=1}^6 \sum_{t=1}^6 q_o q_j q_n q_t \int_0^L \left(\lambda A \frac{\partial a_o}{\partial x} \frac{\partial a_j}{\partial x} c_n c_t \right) dx + \frac{1}{4} \sum_{o=1}^6 \sum_{j=1}^6 \sum_{n=1}^6 \sum_{t=1}^6 q_o q_j q_n q_t \int_0^L \left(\lambda A \frac{\partial b_o}{\partial x} \frac{\partial b_j}{\partial x} c_n c_t \right) dx
\end{aligned} \tag{2.44}$$

Based on the quartic energies in Eq.(2.39), the non-linear stiffness matrix will be used for the subsequent analysis of wave propagation as will be explained in the next section.

Combining Eqs.(2.39) and (2.40), the Euler-Lagrange equations of motion write in generic format as follows:

$$\frac{\partial}{\partial t} \left(\frac{\partial T}{\partial \dot{q}} \right) - \frac{\partial U}{\partial q} = f_r \tag{2.45}$$

f_r can be defined as the force corresponding to the degree of freedom q , with the equilibrium conditions $f_r = 0$. Using the definitions introduced in Eqs. (2.39) and (2.40) along with Eq.(2.45), the local mass matrix \mathbf{M} can be obtained from the kinetic energy; the linear stiffness matrix \mathbf{K} can be extracted from U_1 and U_2 , and the nonlinear stiffness matrix \mathbf{K}'' can be derived from the quartic contribution, U_4 to the non-linear energy. The expression of the matrices \mathbf{K} and \mathbf{K}'' are provided in the **Appendix B**, and the mass matrix \mathbf{M} is given by:

$$\mathbf{M} = \begin{pmatrix} \frac{\rho SL}{3} & 0 & 0 & \frac{\rho SL}{6} & 0 & 0 \\ 0 & \frac{13\rho SL}{35(1+\beta)^2} & \frac{\rho SL^2(22+49\beta)}{420(1+\beta)^2} & 0 & \frac{9\rho SL}{70(1+\beta)^2} & \frac{\rho SL^2(-13+14\beta)}{420(1+\beta)^2} \\ 0 & \frac{\rho SL^2(22+49\beta)}{420(1+\beta)^2} & \frac{\rho SL^3(56\beta^2+21\beta+4)}{420(1+\beta)^2} & 0 & \frac{13\rho SL^2(1+7\beta)}{420(1+\beta)^2} & \frac{\rho SL^3(21\beta^2-7\beta-2)}{280(1+\beta)^2} \\ \frac{\rho SL}{6} & 0 & 0 & \frac{\rho SL}{3} & 0 & 0 \\ 0 & \frac{9\rho SL}{70(1+\beta)^2} & \frac{13\rho SL^2(1+7\beta)}{420(1+\beta)^2} & 0 & \frac{13\rho SL}{35(1+\beta)^2} & \frac{\rho SL^2(-11+28\beta)}{210(1+\beta)^2} \\ 0 & \frac{\rho SL^2(-13+14\beta)}{420(1+\beta)^2} & \frac{\rho SL^3(21\beta^2-7\beta-2)}{280(1+\beta)^2} & 0 & \frac{\rho SL^2(-11+28\beta)}{210(1+\beta)^2} & \frac{\rho SL^3(21\beta^2-14\beta+4)}{420(1+\beta)^2} \end{pmatrix} \quad (2.46)$$

From the obtained mass and stiffness matrices \mathbf{M} , \mathbf{K} and \mathbf{K}'' , we compute the mass and global stiffness matrices characterizing the equilibrium equation of the lattice unit cell, using the usual finite element assembly procedure. Using the local to global coordinate system transformation matrix \mathbf{R} , the local beam element contributions is transformed and assembled to the global coordinate system to build the global mass and stiffness matrices for the lattice unit cell, as explained into the **Appendix C**. The global equilibrium of the structural system is expressed by the following differential equation:

$$\mathbf{M}\ddot{\mathbf{q}} + \mathbf{K}\mathbf{q} + \mathbf{K}''\mathbf{q}^3 = 0 \quad (2.47)$$

Eq.(2.47) represents the non-linear differential equation of motion, with the presence of terms relating to the cubic order contributions of the nodal displacements of the structural system in the absence of external forces.

2.3. 1 Assessment of the nonlinear effects on the stiffness matrix

In order to study the mechanical properties of the non-linear Timoshenko beam structure and to study the difference between the linear and non-linear stiffness matrix, we consider a beam of length L and thickness t as shown in Fig.2.1. We also assume that the beam is made of steel with the geometrical and material properties of Table 2.1, with correction factors $k_s = 0.83 = k_k$, based on [41].

Geometric parameters of the beam	Mechanical properties
$L = 15\text{mm}$	$E = 210\text{GPa}, \nu = 0.3, G = 81\text{GPa}$

Table.2. 1 Geometric and material parameters of the unit-cell structural elements.

Using Eq.(2.44), the linear part of the strain energy U_1 , the linear Timoshenko beam shape function from [42] and the parameters from Table 2.1 associated to the linear stiffness matrix for a steel material, we obtain the local linear stiffness matrix in numerical form:

$$K = \begin{pmatrix} 14000 & 0 & 0 & -14000 & 0 & 0 \\ 0 & 61.37326462 & 4.602994846 & 0 & -61.37326462 & 4.602994846 \\ 0 & 4.602994846 & 0.4618912800 & 0 & -4.602994846 & 0.2285579469 \\ -14000 & 0 & 0 & 14000 & 0 & 0 \\ 0 & -61.37326462 & -4.602994846 & 0 & 61.37326462 & -4.602994846 \\ 0 & 4.602994846 & 0.2285579469 & 0 & -4.602994846 & 0.4618912800 \end{pmatrix} \text{N/m}$$

Using Eq.(2.40) providing the fourth order expression of the non-linear energy U_4 and relying on the non-linear Timoshenko beam shape function in Eq.(2.37), while substituting the parameters from Table.2.1, we get the nonlinear stiffness matrix K^* over a single Timoshenko beam element:

$$K^* = \begin{pmatrix} 950333.4854 & -281670.3302 & -18508.44254 & -950333.4854 & 281670.3302 & 18446.58700 \\ -503336.6384 & 837457.1301 & -4073.384160 & 503336.6384 & -837457.1301 & 2286.316611 \\ -214416.1431 & -292.8051450 & 10149.98024 & 214416.1431 & 292.8051450 & -8669.396672 \\ -950333.4854 & 281670.3302 & 18508.44254 & 950333.4854 & -281670.3302 & -18446.58700 \\ 503336.6384 & -837457.1301 & 4073.384160 & -503336.6384 & 837457.1301 & -2286.316611 \\ 215724.2813 & -1169.402805 & -9240.349080 & -215724.2813 & 1169.402805 & 9008.075414 \end{pmatrix} \text{N/m}^3$$

Comparing the matrices of the linear and non-linear regimes shows that the non-linear stiffness matrix has larger values compared to the linear one, underlining that the non-linear effects make the structure overall stiffer. This can be attributed to the existence of couplings between shear, bending, and extension. On the other hand, comparing the modes of the nonlinear stiffness matrix shows that the extension-extension mode has higher energy in comparison to the shear-shear and bending-bending modes. Similarly, the coupling of shear-extension and bending-extension has a higher energy compared to the coupling between shear and bending.

2.3. 2 Case Study

To compare the behavior of linear and nonlinear Timoshenko beams under a concentrated force P , a numerical experiment is done using the Timoshenko beam element and subjected to a concentrated transverse force P on its free end where $x=L$ and the beam is assumed to be made of material with properties mentioned in Table 2.1. Using the linear and the nonlinear stiffness matrix the stiffness equation for the nonlinear static response obeys the following nonlinear equilibrium equation:

$$\mathbf{K} \begin{bmatrix} u_{z_e} \\ \phi_e \end{bmatrix} + \mathbf{K}'' \begin{bmatrix} u_{z_e} \\ \phi_e \end{bmatrix}^3 = \begin{bmatrix} P \\ 0 \end{bmatrix} \quad (2.48)$$

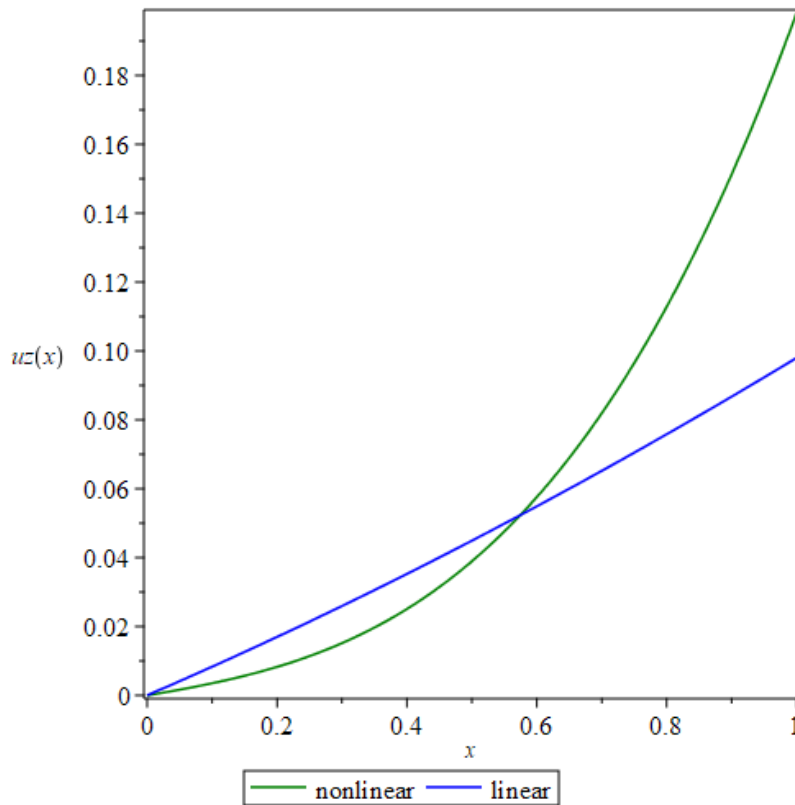


Fig.2. 2: Deflection of the Timoshenko beam under a concentrated shear force

Substituting u_{z_0} into Eq.(2.31), the solution of $u_z(x)$ can be determined. Fig.2.2 shows a comparison of the Timoshenko beam free end under a concentrated shear force based on linear and nonlinear solutions respectively. Fig.2.2 shows a stiffer response of the nonlinear Timoshenko beam in comparison to the linearized beam model, due to the contribution of nonlinear stiffness terms. In the sequel, the formulated nonlinear Timoshenko beam element theory is utilized in the context of wave propagation to compute the dispersion characteristics for hexagonal unit cells comprising Timoshenko beam elements endowed with a full nonlinear kinematics.

2. 4 Conclusion

In this chapter, we have analyzed the nonlinear kinematics effect of Timoshenko beams element with the presence of shear, bending, and extension energies and coupling between them. Application of the Hamilton principle has led to the determination of the nonlinear beam shape functions, allowing the determination of the mass matrix and nonlinear stiffness matrices firstly for a single beam element and subsequently for the reference lattice unit cell. Overall, consideration of the full non-linear kinematics for the Timoshenko beam elements has evidenced that the nonlinear stiffness matrix plays an important role by making the material stiffer due to the consideration of the couplings between shear, bending, and extension. In the forthcoming chapter, we will study the impact of the nonlinear kinematics of Timoshenko beam elements on wave propagation features of architected materials.

Appendix A: Timoshenko beam shape functions

After substituting the Lagrangian function in the extended Hamilton's principle, and after a few derivations, we obtain the following expression of the variation of the action integral built from the Lagrangian:

$$\begin{aligned}
\delta \int_0^L \mathcal{L} dt = & \int_0^L \left[-EI \left(\frac{d\phi}{dx} \right) \delta\phi \right]_0^L + \int_0^L EI \frac{d^2\phi}{dx^2} \delta\phi dx + \int_0^L k_s GA \left(\frac{du_z}{dx} - \phi \right) \delta\phi dx - k_s GA \left(\frac{du_z}{dx} - \phi \right) \delta u_z \Big|_0^L \\
& + \int_0^L k_s GA \left(\frac{d^2u_x}{dx^2} - \frac{d\phi}{dx} \right) \delta u_x dx - \frac{(\lambda + 2G)}{2} A \left(\frac{du_x}{dx} \right) \delta u_x \Big|_0^L + \int_0^L \frac{(\lambda + 2G)}{2} A \frac{du_x^2}{dx^2} \delta u_x dx dt \\
& - GA(k_k k_s) \int_0^L \left(\int_0^L \phi \left(\frac{du_x}{dx} \right)^2 \delta\phi dx + \frac{du_x}{dx} \phi^2 \delta u_x \Big|_0^L - \int_0^L \left(\frac{d^2u_x}{dx^2} \phi^2 + 2\phi \frac{du_x}{dx} \frac{d\phi}{dx} \right) \delta u_x dx \right) dt - \int_0^L \frac{1}{4} EA \phi \delta\phi dx dt \\
& + GA(k_k k_s) \int_0^L \left(\int_0^L \frac{du_x}{dx} \frac{du_z}{dx} \delta\phi dx - \int_0^L \left(\frac{d^2u_x}{dx^2} \phi + \frac{d\phi}{dx} \frac{du_x}{dx} \right) \delta u_x dx + \frac{du_x}{dx} \phi \delta u_x \Big|_0^L - \int_0^L \left(\frac{d^2u_x}{dx^2} \phi + \frac{d\phi}{dx} \frac{du_x}{dx} \right) \delta u_z dx + \frac{du_x}{dx} \phi \delta u_z \Big|_0^L \right) dt \\
& - \int_0^L \int_0^L 2GA(k_k k_s) \left(\phi \frac{du_x}{dx} \right) \delta\phi dx dt - \int_0^L GA(k_k k_s) \phi^2 \delta u_x \Big|_0^L dt + \int_0^L \int_0^L 2GA(k_k k_s) \left(\phi \frac{d\phi}{dx} \delta u_x \right) dx dt - \int_0^L \frac{1}{2} EA \left(\frac{du_x}{dx} \right)^3 \delta u_x \Big|_0^L dt \\
& + \int_0^L \int_0^L \frac{3}{2} EA \left(\frac{du_x}{dx} \right)^2 \frac{d^2u_x}{dx^2} \delta u_x dx dt - \int_0^L \frac{1}{2} k_s EA \left(\frac{du_z}{dx} \right)^3 \delta u_z \Big|_0^L dt + \int_0^L \int_0^L \frac{3}{2} k_s EA \left(\frac{du_z}{dx} \right)^2 \frac{d^2u_z}{dx^2} \delta u_z dx dt - \int_0^L \frac{1}{2} k_s EA \left(\frac{du_z}{dx} \right) \left(\frac{du_x}{dx} \right)^2 \delta u_z \Big|_0^L dt \\
& + \int_0^L \int_0^L \frac{1}{2} k_s EA \left(\frac{d^2u_x}{dx^2} \left(\frac{du_x}{dx} \right)^2 + 2 \frac{du_x}{dx} \frac{d^2u_x}{dx^2} \frac{du_x}{dx} \right) \delta u_x dx dt - \int_0^L \frac{1}{2} k_s EA \frac{du_x}{dx} \left(\frac{du_z}{dx} \right)^2 \delta u_x \Big|_0^L dt + \int_0^L \int_0^L \frac{1}{2} k_s EA \left(\frac{d^2u_x}{dx^2} \left(\frac{du_z}{dx} \right)^2 + 2 \frac{du_z}{dx} \frac{d^2u_x}{dx^2} \frac{du_x}{dx} \right) \delta u_x dx dt \\
& - \int_0^L \frac{3}{2} k_s EA \left(\frac{du_x}{dx} \right)^2 \delta u_x \Big|_0^L dt + \int_0^L \int_0^L 3EA \frac{du_x}{dx} \frac{d^2u_x}{dx^2} \delta u_x dx dt - \int_0^L \frac{1}{2} k_s EA \left(\frac{du_z}{dx} \right)^2 \delta u_x \Big|_0^L dt + \int_0^L \int_0^L k_s EA \frac{du_z}{dx} \frac{d^2u_z}{dx^2} \delta u_z dx dt - \int_0^L EA \frac{du_z}{dx} \frac{du_x}{dx} \delta u_z \Big|_0^L dt \\
& + \int_0^L \int_0^L EA \left(\frac{d^2u_x}{dx^2} \frac{du_x}{dx} + \frac{d^2u_x}{dx^2} \frac{du_z}{dx} \right) \delta u_z dx dt - \int_0^L \int_0^L \lambda A \frac{du_x}{dx} \phi \delta\phi dx dt - \int_0^L \frac{1}{2} \lambda A \phi^2 \delta u_x \Big|_0^L dt + \int_0^L \int_0^L \lambda A \phi \frac{d\phi}{dx} \delta u_x dx dt - \int_0^L \int_0^L \frac{1}{2} \lambda A \phi \left(\frac{du_x}{dx} \right)^2 \delta\phi dx dt \\
& - \int_0^L \frac{1}{2} \lambda A \frac{du_x}{dx} \phi^2 \delta u_x \Big|_0^L dt + \int_0^L \int_0^L \frac{1}{2} \lambda A \left(\frac{d^2u_x}{dx^2} \phi^2 + 2\phi \frac{d\phi}{dx} \frac{du_x}{dx} \right) \delta u_x dx dt - \int_0^L \frac{1}{2} \lambda A \frac{du_z}{dx} \phi^2 \delta u_z \Big|_0^L dt + \int_0^L \int_0^L \frac{1}{2} \lambda A \left(\frac{d^2u_z}{dx^2} \phi^2 + 2\phi \frac{d\phi}{dx} \frac{du_z}{dx} \right) \delta u_z dx dt \\
& - \int_0^L \int_0^L \frac{1}{2} \lambda A \left(\frac{du_z}{dx} \right)^2 \phi \delta\phi dx dt + \int_0^L \left(\int_0^L q \delta u_z dx + \int_0^L m \delta\phi dx \right) dt = 0
\end{aligned} \tag{A.1}$$

where λ is Lamé coefficient, k_s and k_k are the beam correction factors.

The expression of the nonlinear Timoshenko beam shape functions is:

$$\begin{aligned}
a_1(x) &= -lx - ox^2 + 1; & a_2(x) &= -kx - nx^2; & a_3(x) &= -jx - mx^2; & a_4(x) &= lx + ox^2; & a_5(x) &= kx + nx^2; & a_6(x) &= jx + mx^2; \\
b_1(x) &= -cx - fx^2 - ix^3; & b_2(x) &= -bx - ex^2 - hx^3 + 1; & b_3(x) &= -ax - dx^2 - gx^3; & b_4(x) &= cx + fx^2 + ix^3; & b_5(x) &= bx + ex^2 + hx^3; \\
b_6(x) &= ax + dx^2 + gx^3; & c_1(x) &= -2fx - 3ix^2; & c_2(x) &= -2ex - 3hx^2; & c_3(x) &= -2dx - 3gx^2 + 1; & c_4(x) &= 2fx + 3ix^2; \\
c_5(x) &= 2ex + 3hx^2; & c_6(x) &= 2dx + 3gx^2
\end{aligned} \tag{A.2}$$

Appendix B: Timoshenko beam non-linear mass, linear and non-linear stiffness matrices

The elements related to coefficients of the 6x6 symmetric linear stiffness matrix of the Timoshenko beam (B.1) are:

$$\mathbf{K} = \begin{pmatrix} \frac{EA}{L} & 0 & 0 & -\frac{EA}{L} & 0 & 0 \\ \frac{GAk_s \beta^2 L^2 + 12EI}{(1+\beta)^2 L^3} & \frac{GAk_s \beta^2 L^2 + 12EI}{2L^2(1+\beta)^2} & 0 & -\frac{GAk_s \beta^2 L^2 + 12EI}{L^3(1+\beta)^2} & \frac{GAk_s \beta^2 L^2 + 12EI}{2L^2(1+\beta)^2} & 0 \\ \frac{GAk_s L^2 \beta^2 + 4EI \beta^2 + 8EI \beta + 16EI}{4(1+\beta)^2 L} & 0 & 0 & -\frac{GAk_s \beta^2 L^2 + 12EI}{2L^2(1+\beta)^2} & -\frac{GAk_s L^2 \beta^2 + 4EI \beta^2 + 8EI \beta - 8EI}{4(1+\beta)^2 L} & 0 \\ \text{sym} & & & \frac{EA}{L} & 0 & 0 \\ & & & \frac{GAk_s \beta^2 L^2 + 12EI}{L^3(1+\beta)^2} & \frac{GAk_s \beta^2 L^2 + 12EI}{2L^2(1+\beta)^2} & 0 \\ & & & & \frac{GAk_s L^2 \beta^2 + 4EI \beta^2 + 8EI \beta + 16EI}{4(1+\beta)^2 L} & 0 \end{pmatrix}$$

Due to the large size of the non-linear stiffness matrix, it will not be displayed in this contribution you can view it throw the following GitHub link. <https://github.com/AbdallahWazne/NLmatrix.git>

Appendix C: Timoshenko beam linear and non-linear mass and stiffness global matrices

The elements related to coefficients of the 12x12 symmetric global mass matrix of the Timoshenko beam (C.1) are:

$$M_{G_{11}} = \frac{13\rho SL}{35(1+\beta)^2} ; M_{G_{13}} = -\frac{\rho SL^2(22+49\beta)}{420(1+\beta)^2} ; M_{G_{14}} = \frac{9\rho SL}{70(1+\beta)^2} ; M_{G_{16}} = -\frac{\rho SL^2(-13+14\beta)}{420(1+\beta)^2}$$

$$M_{G_{22}} = \frac{\rho SL}{3} ; M_{G_{25}} = \frac{\rho SL}{6} ; M_{G_{33}} = \frac{\rho SL^3(56\beta^2+21\beta+4)}{420(1+\beta)^2} ; M_{G_{34}} = -\frac{13\rho SL^2(1+7\beta)}{420(1+\beta)^2}$$

$$M_{G_{36}} = \frac{\rho SL^3(21\beta^2-7\beta-2)}{280(1+\beta)^2} ; M_{G_{44}} = \frac{39\rho SL}{70(1+\beta)^2} + \frac{\rho SL}{2} ; M_{G_{46}} = \frac{9\rho SL}{280(1+\beta)^2} + \frac{\rho SL}{8}$$

$$M_{G_{47}} = \frac{\sqrt{3}\rho SL}{24} - \frac{9\sqrt{3}\rho SL}{280(1+\beta)^2} ; M_{G_{48}} = -\frac{\rho SL^2(-13+14\beta)}{840(1+\beta)^2} ; M_{G_{57}} = \frac{\rho SL}{24} + \frac{27\rho SL}{280(1+\beta)^2}$$

$$M_{G_{58}} = \frac{\sqrt{3}\rho SL^2(-13+14\beta)}{840(1+\beta)^2} ; M_{G_{59}} = -\frac{\sqrt{3}\rho SL}{24} + \frac{9\sqrt{3}\rho SL}{280(1+\beta)^2} ; M_{G_{66}} = \frac{\rho SL}{4} + \frac{13\rho SL}{140(1+\beta)^2} ;$$

$$M_{G_{67}} = -\frac{\sqrt{3}\rho SL}{12} - \frac{13\sqrt{3}\rho SL}{140(1+\beta)^2} ; M_{G_{68}} = -\frac{\rho SL^2(-11+28\beta)}{420(1+\beta)^2} ; M_{G_{69}} = -\frac{13\rho SL^2(1+7\beta)}{840(1+\beta)^2} ;$$

$$M_{G_{6,10}} = -\frac{13\sqrt{3}\rho SL^2(1+7\beta)}{840(1+\beta)^2} ; M_{G_{77}} = \frac{\rho SL}{12} + \frac{39\rho SL}{140(1+\beta)^2} ; M_{G_{78}} = \frac{\sqrt{3}\rho SL^2(-11+28\beta)}{420(1+\beta)^2} ;$$

$$M_{G_{88}} = \frac{\rho SL^3(21\beta^2-14\beta+4)}{420(1+\beta)^2}$$

$$M_{G_{4,10}} = -M_{G_{47}} , M_{G_{49}} = M_{G_{46}} , M_{G_{56}} = M_{G_{47}} , M_{G_{55}} = M_{G_{44}} , M_{G_{5,10}} = M_{G_{57}} , M_{G_{5,11}} = -M_{G_{58}} ,$$

$$M_{G_{6,11}} = M_{G_{36}} , M_{G_{74}} = M_{G_{47}} , M_{G_{76}} = M_{G_{67}} , M_{G_{86}} = M_{G_{68}} , M_{G_{87}} = M_{G_{78}} , M_{G_{95}} = -M_{G_{47}} ,$$

$$M_{G_{99}} = M_{G_{66}} , M_{G_{9,10}} = -M_{G_{67}} , M_{G_{9,11}} = M_{G_{68}} , M_{G_{10,4}} = -M_{G_{47}} , M_{G_{10,5}} = M_{G_{57}} , M_{G_{10,10}} = M_{G_{77}} ,$$

$$M_{G_{10,11}} = -M_{G_{78}} , M_{G_{11,4}} = M_{G_{48}} , M_{G_{11,6}} = M_{G_{36}} , M_{G_{11,11}} = M_{G_{88}} ,$$

$$\begin{aligned}
M_{G_{12}} &= M_{G_{15}} = M_{G_{17}} = M_{G_{18}} = M_{G_{19}} = M_{G_{1,10}} = M_{G_{1,11}} = M_{G_{1,12}} = M_{G_{23}} = M_{G_{24}} = M_{G_{26}} = M_{G_{27}} \\
&= M_{G_{28}} = M_{G_{29}} = M_{G_{2,10}} = M_{G_{2,11}} = M_{G_{2,12}} = M_{G_{35}} = M_{G_{37}} = M_{G_{38}} = M_{G_{39}} = M_{G_{3,10}} = M_{G_{3,11}} = M_{G_{3,12}} \\
&= M_{G_{45}} = M_{G_{4,12}} = M_{G_{5,12}} = M_{G_{6,12}} = M_{G_{79}} = M_{G_{7,10}} = M_{G_{7,11}} = M_{G_{7,12}} = M_{G_{89}} = M_{G_{8,10}} = M_{G_{8,11}} = M_{G_{8,12}} \\
&= M_{G_{9,12}} = M_{G_{10,12}} = M_{G_{11,1}} = M_{G_{11,2}} = M_{G_{11,3}} = M_{G_{11,7}} = M_{G_{11,8}} = M_{G_{11,12}} = M_{G_{12,12}} = 0
\end{aligned}$$

The elements related to coefficients of the 12x12 symmetric linear global stiffness matrix of the Timoshenko beam (C.2) are:

$$\begin{aligned}
K_{G_{11}} &= \frac{AGL^2\beta^2k_s + 12EI}{(1+\beta)^2L^3} ; \quad K_{G_{13}} = -\frac{AGL^2\beta^2k_s + 12EI}{2L^2(1+\beta)^2} ; \quad K_{G_{22}} = \frac{EA}{L} \\
K_{G_{33}} &= \frac{GAK_sL^2\beta^2 + 4EI\beta^2 + 8EI\beta + 16EI}{4(1+\beta)^2L} ; \quad K_{G_{36}} = -\frac{-GAK_sL^2\beta^2 + 4EI\beta^2 + 8EI\beta - 8EI}{4(1+\beta)^2L} \\
K_{G_{44}} &= \frac{AGL^2\beta^2k_s + 12EI}{(1+\beta)^2L^3} + \frac{3EA}{2L} + \frac{AGL^2\beta^2k_s + 12EI}{2(1+\beta)^2L^3} ; \quad K_{G_{47}} = -\frac{3EA}{4L} - \frac{AGL^2\beta^2k_s + 12EI}{4(1+\beta)^2L^3} \\
K_{G_{48}} &= -\frac{\sqrt{3}EA}{4L} + \frac{\sqrt{3}(AGL^2\beta^2k_s + 12EI)}{4(1+\beta)^2L^3} ; \quad K_{G_{49}} = -\frac{AGL^2\beta^2k_s + 12EI}{4L^2(1+\beta)^2} \\
K_{G_{55}} &= \frac{EA}{L} + \frac{EA}{2L} + \frac{3(AGL^2\beta^2k_s + 12EI)}{2(1+\beta)^2L^3} ; \quad K_{G_{58}} = -\frac{EA}{4L} - \frac{3(AGL^2\beta^2k_s + 12EI)}{4(1+\beta)^2L^3} \quad K_{G_{59}} = \frac{\sqrt{3}(AGL^2\beta^2k_s + 12EI)}{4(1+\beta)^2L^2} \\
K_{G_{66}} &= \frac{3(AGL^2\beta^2k_s + 4EI\beta^2 + 8EI\beta + 16EI)}{(1+\beta)^24L} \\
K_{G_{77}} &= \frac{3EA}{4L} + \frac{AG\beta^2L^2k_s + 12EI}{4(1+\beta)^2L^3} ; \quad K_{G_{99}} = \frac{GAK_sL^2\beta^2 + 4EI\beta^2 + 8EI\beta + 16EI}{4(1+\beta)^2L} \\
K_{G_{10,10}} &= \frac{3EA}{4L} + \frac{AGL^2\beta^2k_s + 12EI}{4(1+\beta)^2L^3}
\end{aligned}$$

$$\begin{aligned}
K_{G_{14}} &= -K_{G_{11}}, \quad K_{G_{16}} = K_{G_{13}}, \quad K_{G_{25}} = -K_{G_{22}}, \quad K_{G_{34}} = -K_{G_{13}}, \quad K_{G_{4,10}} = K_{G_{47}}, \quad K_{G_{4,11}} = -K_{G_{48}}, \quad K_{G_{4,12}} = K_{G_{49}}, \\
K_{G_{57}} &= K_{G_{48}}, \quad K_{G_{5,10}} = -K_{G_{57}}, \quad K_{G_{5,11}} = K_{G_{58}}, \quad K_{G_{5,12}} = -K_{G_{59}}, \quad K_{G_{67}} = -K_{G_{49}}, \quad K_{G_{68}} = -K_{G_{59}}, \\
K_{G_{69}} &= K_{G_{36}}, \quad K_{G_{78}} = -K_{G_{48}}, \quad K_{G_{88}} = -K_{G_{58}}, \quad K_{G_{89}} = -K_{G_{59}}, \quad K_{G_{10,11}} = -K_{G_{78}}, \quad K_{G_{10,12}} = K_{G_{79}}, \\
K_{G_{11,11}} &= K_{G_{88}}, \quad K_{G_{11,11}} = -K_{G_{89}}, \quad K_{G_{12,12}} = K_{G_{99}}
\end{aligned}$$

$$\begin{aligned}
& K_{G_{12}} = K_{G_{15}} = K_{G_{17}} = K_{G_{18}} = K_{G_{19}} = K_{G_{1,10}} = K_{G_{1,11}} = K_{G_{1,12}} = K_{G_{21}} = K_{G_{23}} = K_{G_{24}} = K_{G_{26}} = K_{G_{27}} = K_{G_{28}} \\
& = K_{G_{29}} = K_{G_{2,10}} = K_{G_{2,11}} = K_{G_{2,12}} = K_{G_{35}} = K_{G_{37}} = K_{G_{38}} = K_{G_{39}} = K_{G_{3,10}} = K_{G_{3,11}} = K_{G_{3,12}} = K_{G_{45}} = K_{G_{46}} \\
& = K_{G_{56}} = K_{G_{6,10}} = K_{G_{6,11}} = K_{G_{6,12}} = K_{G_{7,10}} = K_{G_{7,11}} = K_{G_{7,12}} = K_{G_{8,10}} = K_{G_{8,11}} = K_{G_{8,12}} = K_{G_{9,10}} = K_{G_{9,11}} = K_{G_{9,12}} = 0
\end{aligned}$$

Due to the large size of the non-linear Global stiffness matrix, it will not be displayed in this contribution you can view it throw the following GitHub link.
<https://github.com/AbdallahWazne/matrix1.git>

Chapter 3

Nonlinear wave propagation analysis in architected materials with consideration of extension, shear and bending effects

Summary:

The current chapter focuses on analyzing the wave dispersion features in two-dimensional architected materials, considering both linear and nonlinear regimes. We examine how the shear, extension, and bending deformation modes within the square, triangular, hexagonal, and re-entrant hexagonal unit cells influence the internal material deformation. Our study involves a dynamical analysis conducted at high and low frequencies, as well as for two different wave amplitudes. By employing the Linstedt-Poincare perturbation method, we assess the non-linear correction to the dispersion diagram. We quantify the relative contribution of each non-linear energy mode to the attributes of nonlinear wave dispersion. The results we obtain indicate that the wavenumber and lattice design significantly affect the nonlinear wave corrections in the dispersion characteristics. Among all considered architected materials, the shear mode demonstrates the highest impact on the non-linear correction, while the flexural mode contributes the least amount of energy. To compare the deformation of hexagonal and re-entrant hexagonal unit cells across the entire Brillouin zone, we employ eigenwave vectors. Overall, this research provides valuable guidance for selecting appropriate inner designs of architected materials that are prone to strong nonlinear dynamical effects.

3. 1 Introduction

Extensive research efforts over the past twenty years have been focused on investigating wave propagation analysis in periodic networks [125]. These studies primarily examine wave attenuation resulting from physical damping or due to geometric factors, as well as the emergence of bandgap phenomena. The topology of the network significantly influences the width and position of the bandgap, as well as the direction of wave propagation. However, incorporating nonlinear effects arising from geometric or material nonlinearities into wave propagation analyses within periodic network materials [126,127] presents substantial challenges due to the complexity associated with solving nonlinear wave motion equations.

The behavior of nonlinear waves in periodic networks deviates from linear wave propagation, primarily due to the influence of wave amplitude, nonlinearity type, and lattice deformation modes on the frequency, phase, and group velocities of wave propagation. Additionally, investigating various inner designs offers greater flexibility in manipulating the dynamic characteristics of architected materials, such as fine-tuning the structure of the bandgap [128].

Wave propagation attributes in presence of material and geometrical nonlinearities differ from the linear case. One of the wave propagation models is the Boussinesq-type wave model which builds on the traditional second-order wave operator while adding new effects.; more precisely, it shows the following attributes [129]: i) wave bi-direction caused by the second-order wave operator; (ii) nonlinearity, and (iii) dispersion.

Likewise, it is widely known that Burgers' equation describes the behavior of weakly nonlinear and viscoelastic waves in the far field when employing the Maxwell-Voigt or Voigt model. This equation strikes a balance between the opposing effects of dissipation caused by viscoelasticity and wave steepening due to nonlinearity. A straightforward example of Burgers' equation reveals shock and pulse solutions that illustrate the exponential nature of relaxation. Wave profiles in these solutions are described by exponential functions, known as relaxation functions, derived from spring-dashpot models such as the Maxwell-Voigt or Voigt model. These models exhibit a discrete relaxation spectrum [130].

On the other hand, supersonic shock waves have the potential to induce irreversible plastic deformations in structures. Despite extensive experimental and theoretical research on shock-

induced plasticity, the connection between high-strain-rate plastic deformations and the initial atomic-scale elastic compression remains unclear [131].

The perturbation method has garnered significant attention among researchers studying wave propagation, offering valuable insights into the field. Within this framework, there are two prominent perturbation-based analysis methods applicable to both discrete and continuous systems. The first method, specifically designed for monochromatic excitations, has proven instrumental in showcasing novel wave-beaming phenomena. Moreover, its applications have extended to the domain of topology optimization, where it has demonstrated great utility [132]. The second method is more comprehensive, allowing for the study of wave-wave interactions using multi-frequency excitations. This broader approach enables a deeper exploration of the complex dynamics and interactions occurring within the system [132]. As a result, these perturbation-based analysis methods have opened up new avenues for understanding and manipulating wave propagation characteristics in a variety of contexts.

The focus of this chapter is to analyze the impact of non-linear corrections on the inner structural response of various architected materials, which are modeled as assemblies of beam-like structural elements. To achieve this objective, we begin by employing a non-linear wave propagation method to compute the linear and non-linear dispersion diagrams in Section 3.2. Moving forward, in Section 3.3, we delve into the study of wave amplitude (A) and its role in the nonlinear correction frequency using hexagonal-shaped unit cells. In Section 3.4, we proceed to calculate the linear and non-linear dispersion diagrams for different architected materials. These materials encompass unit cells with hexagonal, re-entrant hexagonal, square, and triangular shapes. The analysis is conducted at both low and high frequencies, taking into consideration various deformation modes such as extension, shear, and bending. Additionally, we discuss the effects of wave amplitude, inner unit-cell design, and the mode of deformation on the contribution of non-linear energy. Furthermore, we compare the eigenvectors associated with the hexagonal and re-entrant hexagonal unit cells across various stages of deformation, including the initial, linear, and non-linear modes.

Concluding in Section 3.5, we provide a summary of the key findings and contributions of our work. This chapter serves as a valuable resource for understanding the intricacies of non-linear corrections in architected materials. It sheds light on the significance of wave amplitude, unit-cell design, and deformation modes in shaping the overall response of these materials.

3. 2 Linear and non-linear wave propagation analysis

Using Eq. (2.49) from chapter 2, the characteristics of wave propagation within nonlinear network materials will be calculated. The stiffness matrix related to the cubic energy terms of Eq.(2.40) from chapter 2 has been shown to not contribute to the dispersion characteristics of the structure according to the first order perturbation method developed in [113,133]. Only the stiffness matrix \mathbf{K}'' related to the fourth order terms displacements in the **Appendix B** above will be considered. The dynamical response of the nonlinear system will be computed based on the Linstedt-Poincaré perturbation method, asymptotically expanding Eq.(2.45) from chapter 2 using the small perturbation parameter ν , where $|\nu| \ll 1$. For the expansion we use the dimensionless time form $\tau = \omega t$, defined in terms of the wave frequency ω . The higher order term related stiffness matrix \mathbf{K}'' contributes to the perturbed response of the structural system. The contribution $\mathbf{K}'' = \nu \bar{\mathbf{K}}''$ is the nonlinear stiffness matrix arising from the nonlinear stress-strain relationship wherein ν is a small parameter used to quantify the degree of nonlinearity. The frequency and displacement components for the perturbed system are defined as follows:

$$\begin{aligned} \omega &= \omega_0 + \nu \omega_1, \\ \mathbf{q} &= \mathbf{q}_0 + \nu \mathbf{q}_1, \end{aligned} \quad (3.1)$$

with \mathbf{q}_0 the zero-order solution, and \mathbf{q}_1 its first order perturbation.

Inserting Eq. (3.1) into Eq.(2.47) from the above chapter, the following expression of the perturbed structural system we will obtain:

$$\mathbf{M}(\omega_0 + \nu \omega_1)^2 (\ddot{\mathbf{q}}_0 + \nu \ddot{\mathbf{q}}_1) + \mathbf{K}(\mathbf{q}_0 + \nu \mathbf{q}_1) + \nu \bar{\mathbf{K}}''(\mathbf{q}_0 + \nu \mathbf{q}_1)^3 = 0 \quad (3.2)$$

After expanding Eq. (3.2) and separating the linear term at first order $O(0)$ from the first order perturbed $O(\nu)$ contributions, we retrieve the following system of equations:

$$\begin{aligned} O(0): \quad \mathbf{M}(\omega_0)^2 \frac{\partial^2 \mathbf{q}_0}{\partial \tau^2} + \mathbf{K} \mathbf{q}_0 &= 0 \\ O(\nu): \quad \mathbf{M}(\omega_0)^2 \frac{\partial^2 \mathbf{q}_1}{\partial \tau^2} + \mathbf{K} \mathbf{q}_1 &= -2\omega_0 \omega_1 \mathbf{M} \frac{\partial^2 \mathbf{q}_0}{\partial \tau^2} - \bar{\mathbf{K}}''(\mathbf{q}_0)^3 \end{aligned} \quad (3.3)$$

From Eq. (3.3), the $O(0)$ term shows the linear dispersion relation of the unperturbed medium; however, its higher order correction term $O(v)$ shows the first order perturbation induced dispersion characteristics. For the wave propagation characteristics of the medium to be obtained, a planar harmonic wave Ansatz is used for the displacement components \mathbf{q}_0 , as follows:

$$\mathbf{q}_0 = A \phi_j \exp(i\tau) = A \phi_j \cos(\tau) \quad (3.4)$$

In Eq.(3.4), the scalar parameter A represent the amplitude vector of the harmonic wave; then the $O(0)$ terms yields a standard eigenvalue problem $(w_0)^2$ with eigenvectors $\phi_j(\mathbf{k})$, which depend on the wave vector \mathbf{k} . We obtain the nonlinear effects on the band diagram structures by substituting the linear solution into the first order perturbation equation. In particular, the nonlinear correction is considered to be a wave with amplitude (A) dependent correction for each waveform, whose influence on the wave modes is to be determined. Eliminating the secular terms (the terms in factor of $\cos(\tau)$) by setting the left-hand side of the first order perturbation $O(v)$ in Eq. (3.3) to vanish, we obtain the following system of equations for the perturbed structural system:

$$O(v): -2w_0w_1\mathbf{M}\frac{\partial^2\mathbf{q}_0}{\partial\tau^2} - \bar{\mathbf{K}}''(\mathbf{q}_0)^3 = 0 \Rightarrow \left(2w_0w_1A\mathbf{M} + \frac{3}{4}A^2\right)\bar{\mathbf{K}}''\phi_j + O(3\tau - 3\mathbf{k}\mathbf{x}) = 0 \quad (3.5)$$

In Eq. (3.4), we have linearized the cubic order term related to perturbed system of Eq. (3.3), expanding the cubic power cosine terms as $\cos^3(\tau) \approx \frac{3}{4}\cos(\tau)$. The higher order terms (involving $\cos(3\tau)$) neglected upon the linearization process are denoted in Eq. (3.5) as $O(3\tau - 3\mathbf{k}\mathbf{x})$. For each eigenvalue w_0 , a secondary, first order $O(v)$ eigenvalue problem needs to be solved, defining the correction frequency w_1 of the linear zero-order eigenvalue problem of the system perturbation. For each linear eigenvalue, a correction arising from the perturbation is computed, making use of the eigenvalues $\lambda_i = \left(2w_n^0w_n^1 / (3/4)(A)^2\right)$ of the perturbed system. The latter depend on the wave amplitude A of the propagating modes ϕ_i . Each frequency w^i is then given as a summation of the linear zero order frequency and the perturbed system solution from [41,134], as follows:

$$w^i = (w_0)^i + \frac{\frac{3}{4} \phi_i^T \left(\frac{3}{4} (A)^2 (K^n)_{ij} \right) \phi_i}{2(w_0)^i \phi_i^T (M_{ij}) \phi_i} \quad (3.6)$$

The frequency expression of Eq. (3.6) represents an amplitude-dependent dispersion relation and the values of the corrected eigenfrequencies w^i change depending on the specific considered inner architectural design.

In the next section, we analyze the nonlinear wave propagation within hexagonal network materials, based on the obtained amplitude-dependent dispersion relation.

3. 3 Nonlinear dispersion diagrams of hexagonal network materials

Although past literature works focus on the role of extension in the internal beam elements [41, 42], in this section, we analyze the role of both shear, extension, and bending of the internal lattice beam elements on the nonlinear wave propagation characteristics of periodic network materials. As a matter of illustration of the proposed analysis, we consider hexagonal lattice materials.

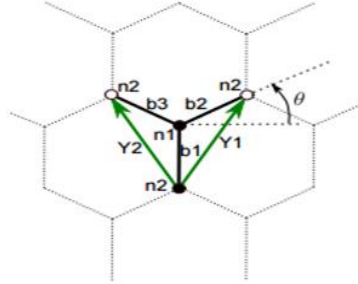


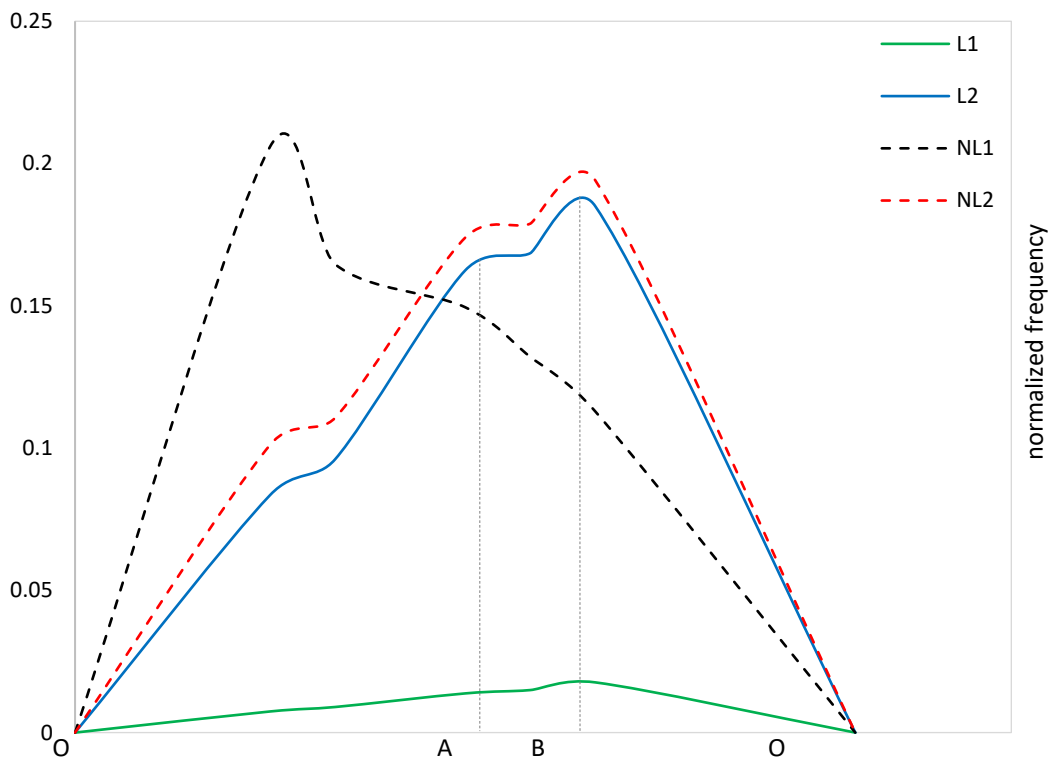
Fig.3. 1 :Two-dimensional hexagonal networks with its unit cell showing the node numbering, the angular variable and the periodicity vectors.

The hexagonal unit cell is characterized by a total of two truly independent nodes n_1 and n_2 in Fig.3.1, with each node having three degrees of freedom, namely two in-plane displacement components u_z, u and a rotation ϕ . Each beam element is assigned a length $L = 15mm$, density $\rho = 7850 \text{ kg/m}^3$ and Young modulus $E = 210GPa$, while the beam thickness is set to $t = 1mm$.

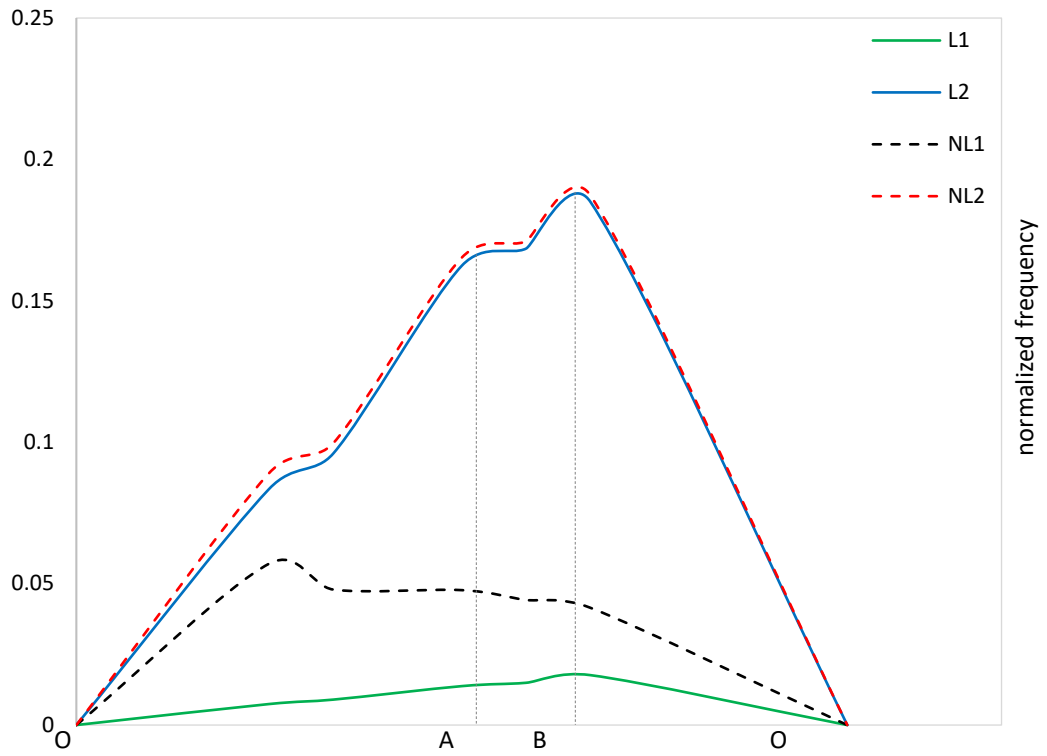
We first carry out the linear eigenfrequency analysis making use of the zero-order relation of Eq. (3.3). For this purpose, we make use of the wavenumber reduced Bloch transformed mass and

stiffness matrix. The eigenfrequencies are computed for the first Brillouin zone of the hexagonal unit cell for an angular variable $\theta = 30^\circ$.

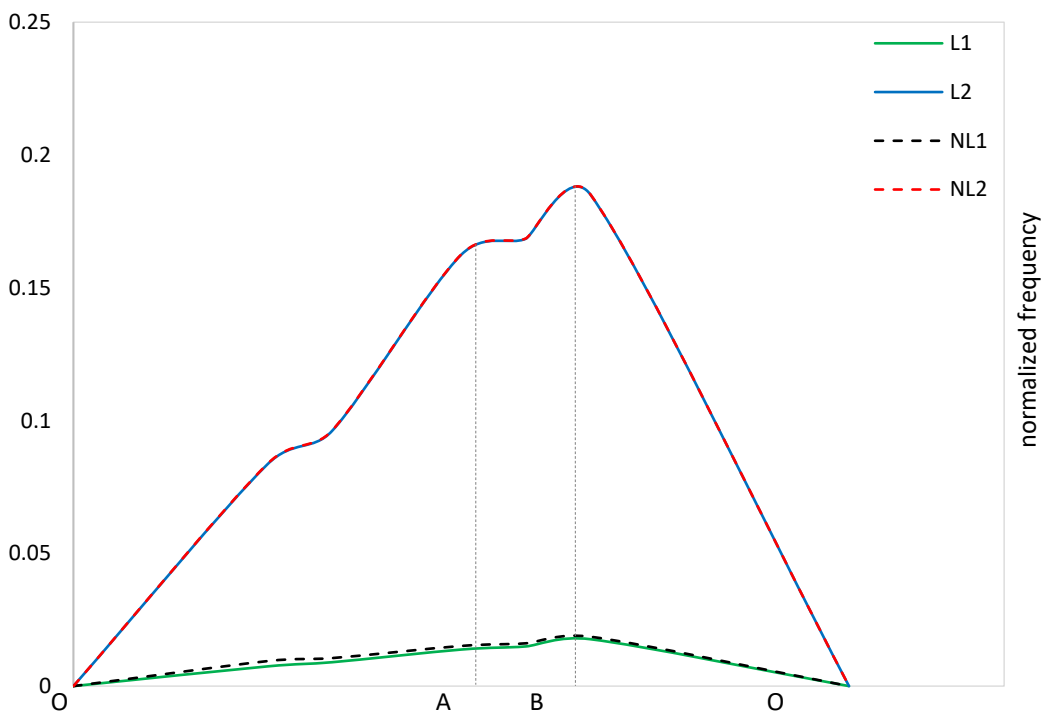
We compute the dispersion curves of the periodic structure of Fig.3.1, as a function of the wave vector $\mathbf{k}(\mathbf{k}_1, \mathbf{k}_2)$, with all frequencies being normalized by the beam eigenfrequency $\omega = \sqrt{E / \rho} / L$, wherein E , ρ , and L are the elastic modulus, density, and length of inner structural members respectively. We adopt the correction factors $k_s = 0.83$ and $k_k = 0.83$ based on [42].



a)



b)



c)

Fig.3. 2: Dispersion diagram of an architected material with hexagonal shaped unit-cells showing the wave propagation mode for the two lowest eigenfrequencies for the shear and longitudinal modes with wave amplitudes a) $A=1$ mm, b) $A=0.5$ mm and c) $A=0.1$ mm. The continuous lines in green L_1 and blue L_2 correspond to the linear solution for shear and longitudinal respectively, while the dashed black NL_1 and red NL_2 lines correspond to the solution after the incorporation of the non-linear correction for shear and longitudinal modes respectively.

Fig.3.2 shows the dispersion diagram of a material architected with the hexagonal shaped unit-cell for a fully nonlinear kinematics incorporating a nonlinear correction factor for the lowest eigenfrequencies of the shear and longitudinal modes. The dispersion diagram is shown in Fig.3.2 for three different waves amplitude $\mathbf{A}=1$ mm, $\mathbf{A}=0.5$ mm, and $\mathbf{A}=0.1$ mm, over the entire range of the Brillouin zone (O, A, B), determined based on the procedure elaborated in [33]. The continuous lines green L_1 and blue L_2 lines correspond to the linear solution for the shear and longitudinal modes respectively, while the dashed black lines NL_0 and the red lines NL_1 correspond to the solution after the incorporation of the non-linear correction for the shear and longitudinal modes respectively. As the eigenvalues increase, the nonlinear correction percentage substantially decreases for all wavenumbers, from 96.3 % to 17.4 % , 86.9 % to 6.2 % , and 21.1 % to 0.2 % for Fig.3.2 (a), (b) and (c) cases respectively. More specifically, it is the lowest eigenmode that undergoes the more significant nonlinear corrections, while upon increasing the eigenmode number, the effect of the correction diminishes to practically vanish for the highest eigenmodes. The corresponding band gap accordingly decreases as mentioned [132].

Fig.3.2 shows a direct proportional relation between the wave amplitude and the band gap between the linear and nonlinear corrections, namely 96.3 % for $\mathbf{A}=1$ mm, decreasing to 86.9 % for $A=0.5$ mm until it reaches 21.1 % for the lowest amplitude $\mathbf{A}=0.1$ mm for the shear mode. Fig.3.2 shows the that the frequency upshifts are greatest near the edge of the Brillouin zone where the group velocity vanishes, as mentioned in [40,41,132]. Fig.3.2 above shows a similar variation as in [40,41], with the dispersion curve starting from a nil value and reaching a similar highest frequency, also closed in the upshifts near the edge of the Brillouin zone, with the group velocity becoming negative. Fig.3.2 -a shows a very similar shape of the dispersion diagram for the linear and nonlinear shear and longitudinal modes to those obtained in [40] for the hexagonal-shaped unit cell. The slight difference between the following results and the previous ones can be attributed to

using a different material for linear waves; moreover, different values of the wave amplitude \mathbf{A} are adopted, with the presence of bending and shear energy in addition to extension energy in the nonlinear correction unlike works in [21,41] considering only extension energy in the nonlinear correction.

In the upcoming section, we shall study the role of the geometry of the unit cell in the magnitude of the nonlinear frequency across various architected materials.

3. 4 Nonlinear wave propagation analysis for different architected material

Following that, we examine the effects of linear and full nonlinear wave propagation for different architected materials, and comparing the classical hexagonal with re-entrant-hexagonal, square and triangular-shaped lattices. Two basic nodes n_1 and n_2 for the unit cell of the classical and reentrant hexagonal lattice and one basic node n_1 for the square and triangular-shaped unit cells are introduced, as represented in Fig.3.3 with the geometric and mechanical properties mentioned in the Table 3.1.

Beam Geometric Parameters	Beam Mechanical Properties
$L = 15\text{ mm}, t = 1\text{ mm}$	$G = 81\text{ GPa}, E = 210\text{ GPa}, \nu = 0.3,$

Table.3. 1: Geometric and Mechanical properties of architected materials unit cells in Figure 2.1.

Notice that the hexagonal lattice (its regular and auxetic versions) are bending dominated, whereas the square and triangular lattices are tension dominated.

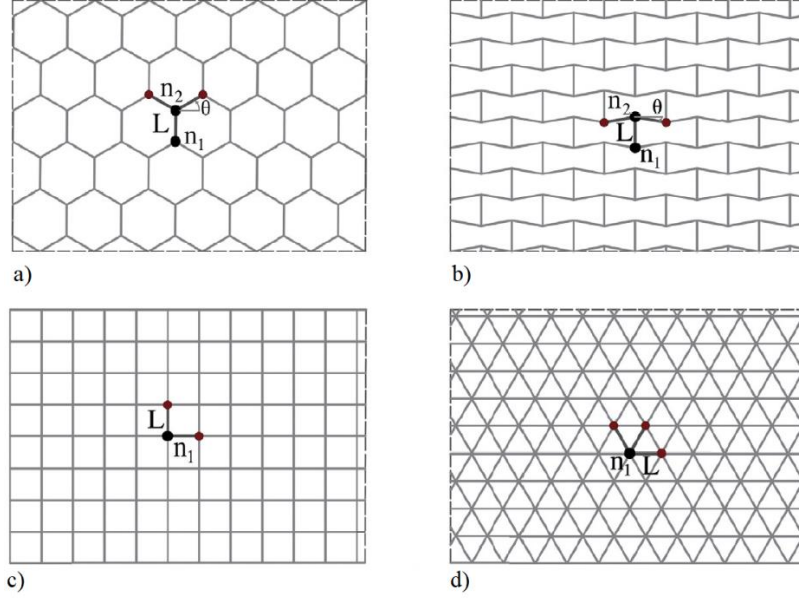
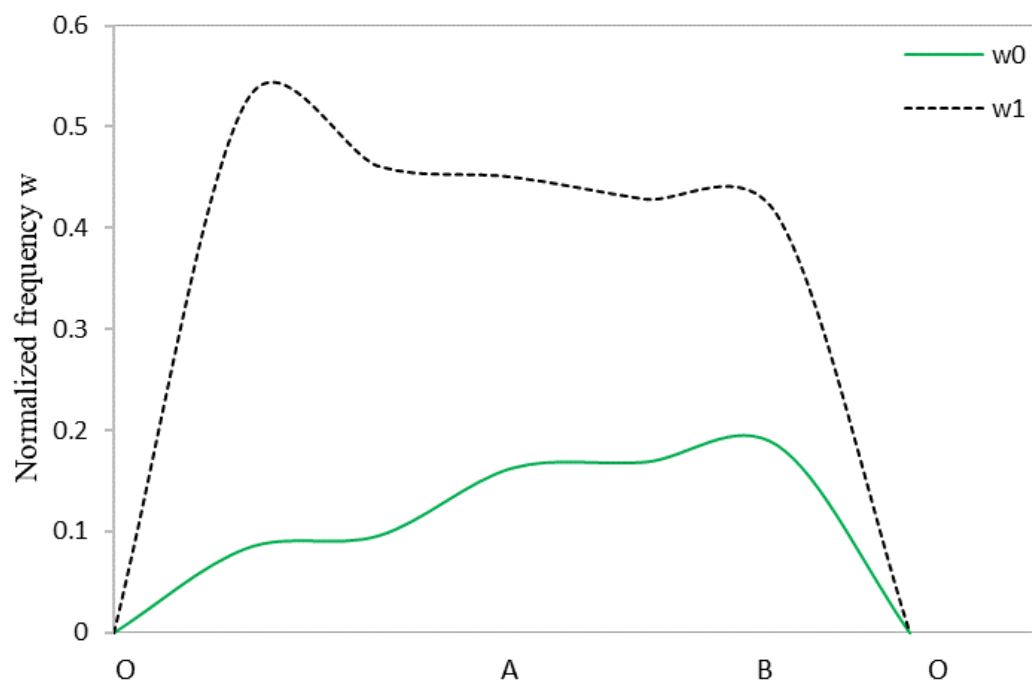
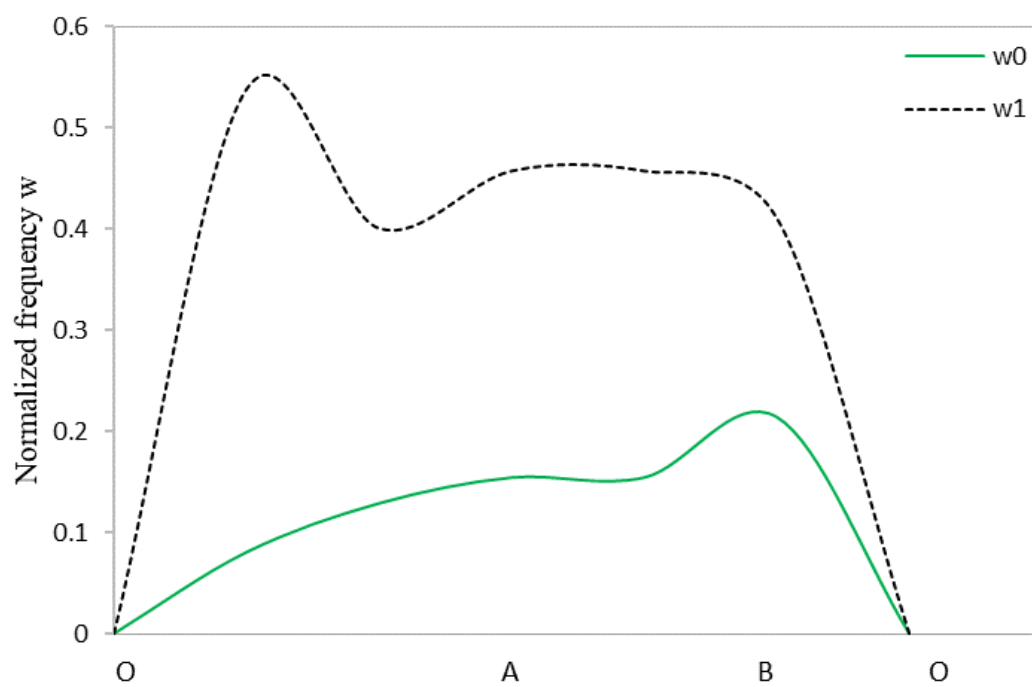


Fig.3. 3 :Two-dimensional classical hexagonal (a), re-entrant hexagonal (b), square (c) and triangular (d) periodic lattice materials with their associated unit cell [135]

The configuration parameter, namely the angle θ for the hexagonal and re-entrant-hexagonal lattices is set to be $\theta = 60$ and $\theta = -15$ respectively in the numerical examples to follow. The dispersion curves for each lattice are computed within the first Brillouin zone (OAB) determined using the method described in [33] for the different architected materials illustrated in Fig.3.3 , as a function of the wave vector $\mathbf{k}(k_1, k_2)$ in a 2D situation. All frequencies have been normalized by the beam eigenfrequency $w = \sqrt{E / \rho} / L$, wherein E , ρ , and L are the elastic modulus, density, and length of inner structural members respectively as mentioned above. Two wave amplitude values are considered, $A_1 = 5 \times 10^{-3} m$ and $A_2 = 10 \times 10^{-3} m = 2A_1$, chosen to be smaller than the Length L , and adopting the shear correction factors $k_s = 0.83$ and $k_k = 0.83$ [75].



(a)



(b)

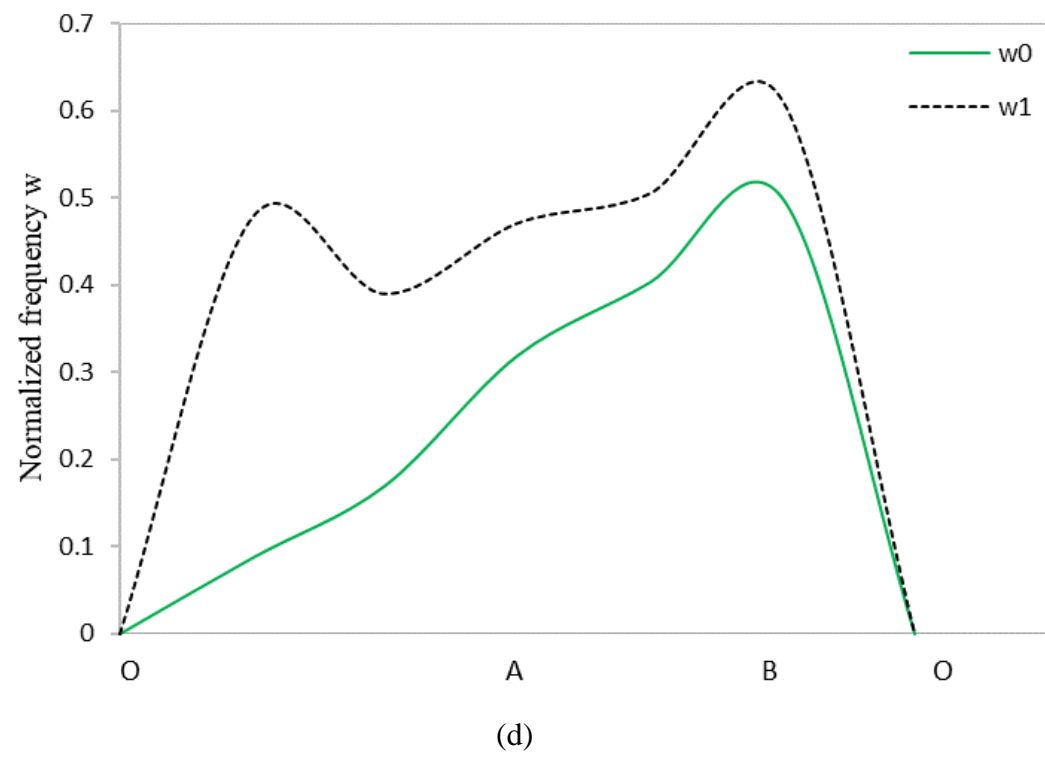
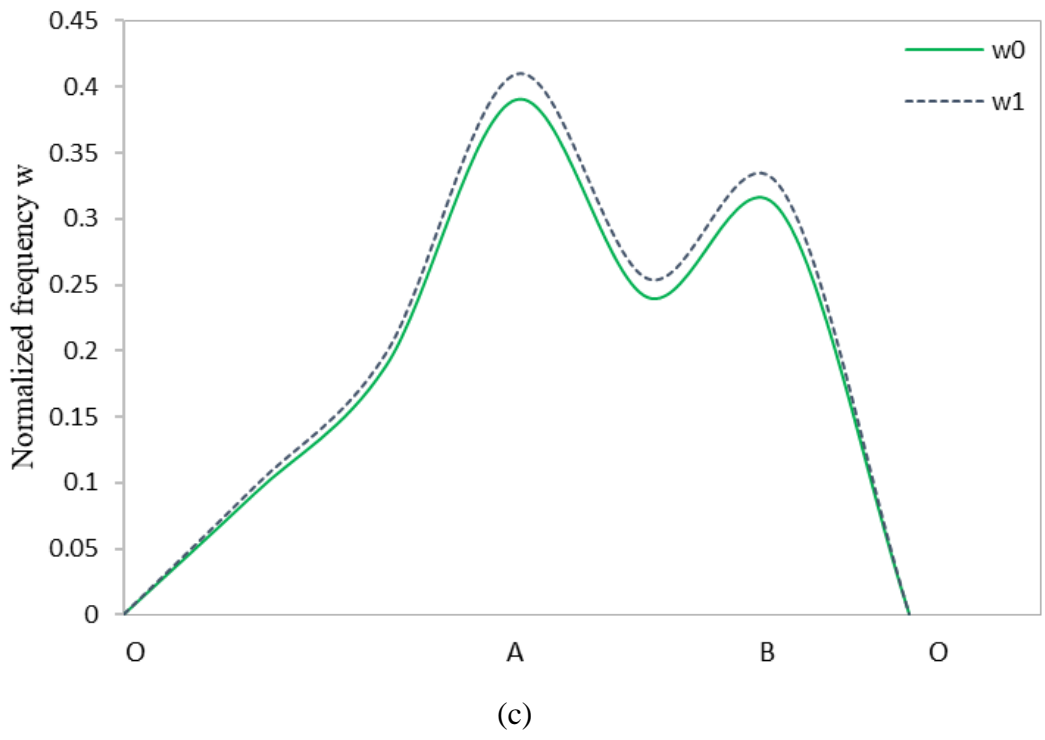
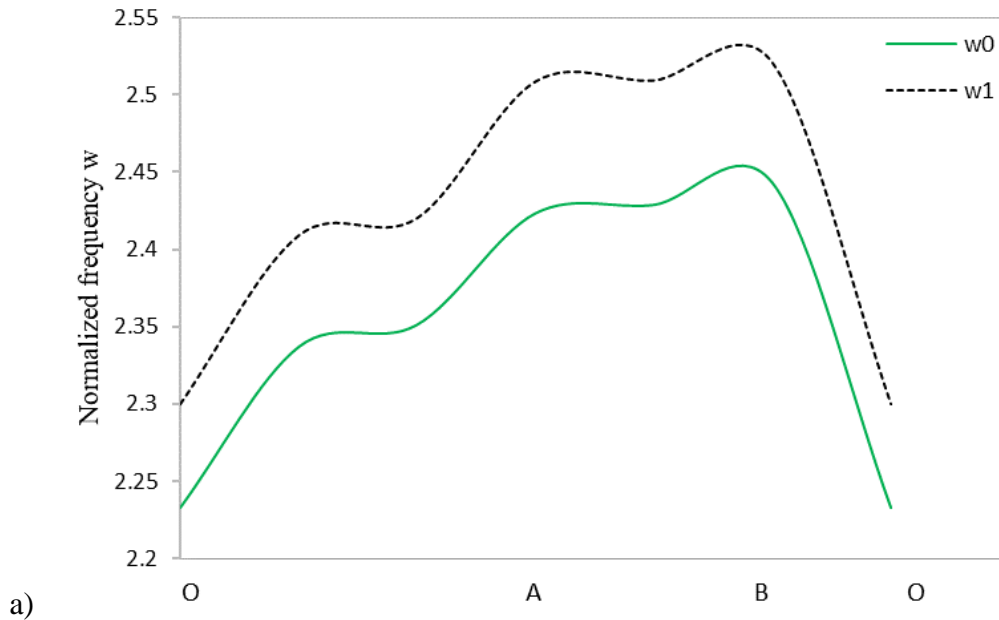
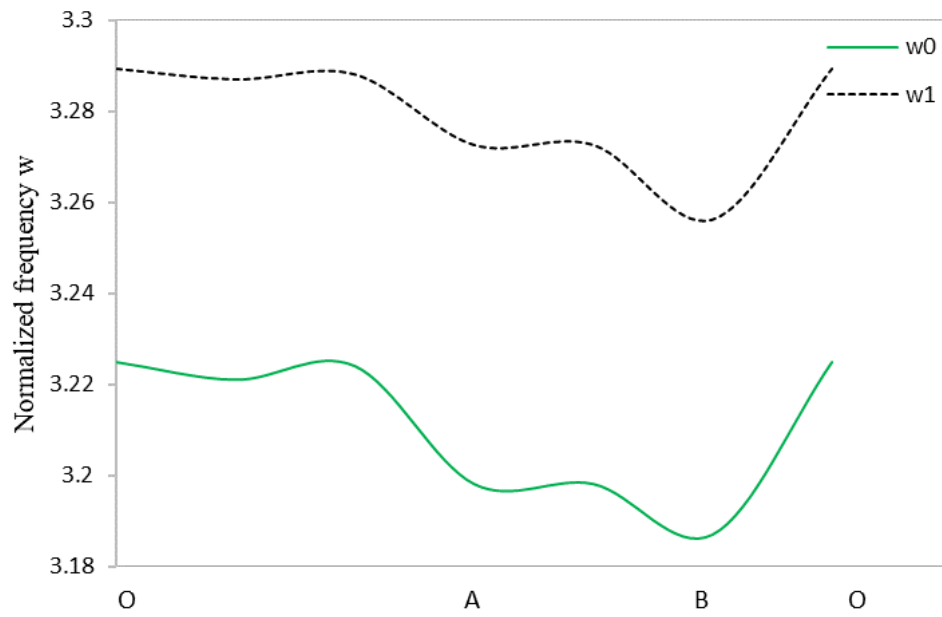


Fig.3. 4: Dispersion diagram for the hexagonal (a), re-entrant hexagonal (b), square (c) and triangular (d) unit-cell designs for longitudinal mode. solid green lines correspond to the linear solution, while black dashed lines correspond to the solution after the incorporation of the non-linear correction.

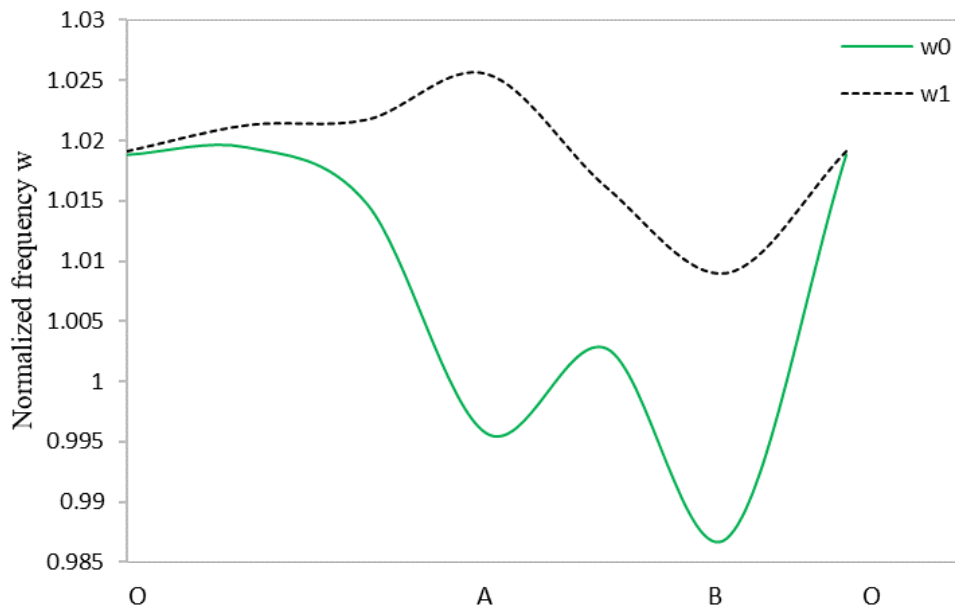
Fig.3.4 shows the effect of the inner architected design on the nonlinear correction of the dispersion diagram for the longitudinal mode of the hexagonal (a), re-entrant hexagonal (b), square (c) and triangular (d) unit-cell designs in the framework of a fully nonlinear dynamical analysis. The nonlinear correction factors over the entire range of the Brillouin zone (O, A, B) are computed based on the methodology described above. Continuous green lines correspond to the linear solution w_0 , while dashed lines refer to the solution after incorporation of the non-linear correction w_1 .

From Fig.3.4, we observe that hexagonal unit cell shows the highest non-linear correction, followed by the re-entrant hexagonal unit cell, and the triangular unit cell, while the non-linear energy shows a low effect for the square unit cell. In terms of numerical comparison, we study the effect of the non-linear energy stored within the selected architected materials on two different frequency scales of high and low frequency respectively. For the longitudinal mode and for wave amplitudes A_1 smaller than the Length L , the nonlinear correction percentage amounts to 55.1%, 47.7%, 5.4%, and 18.4% for the classical hexagonal, re-entrant hexagonal, square and triangular lattices respectively. For the high optical mode, the percentage contribution of the different unit-cells decreases to 0.78%, 0.97%, 0.55% and 6.5% for the regular hexagonal, re-entrant hexagonal, square and triangular lattices respectively.





b)



c)

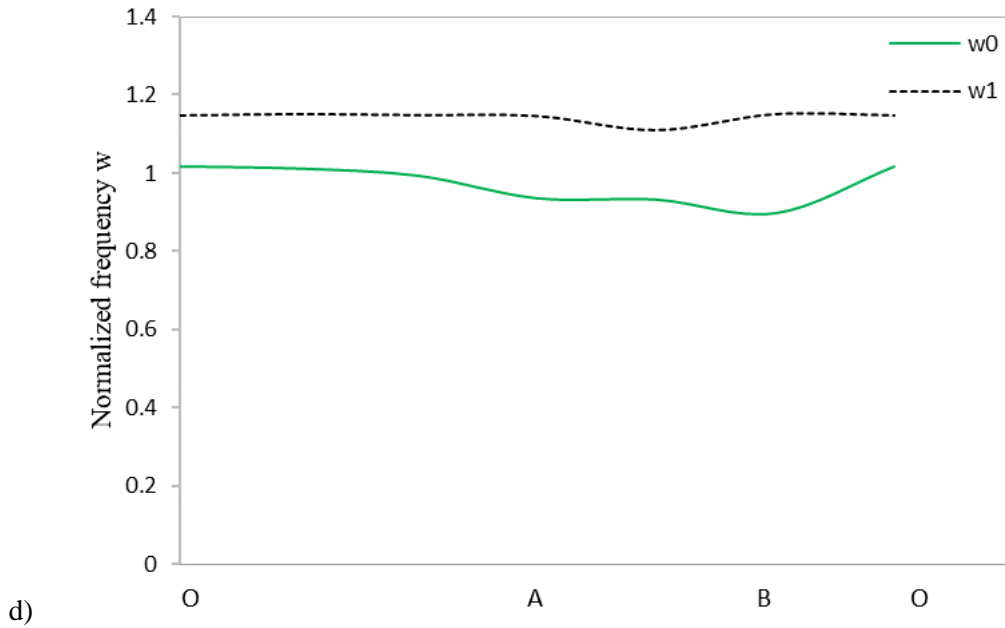
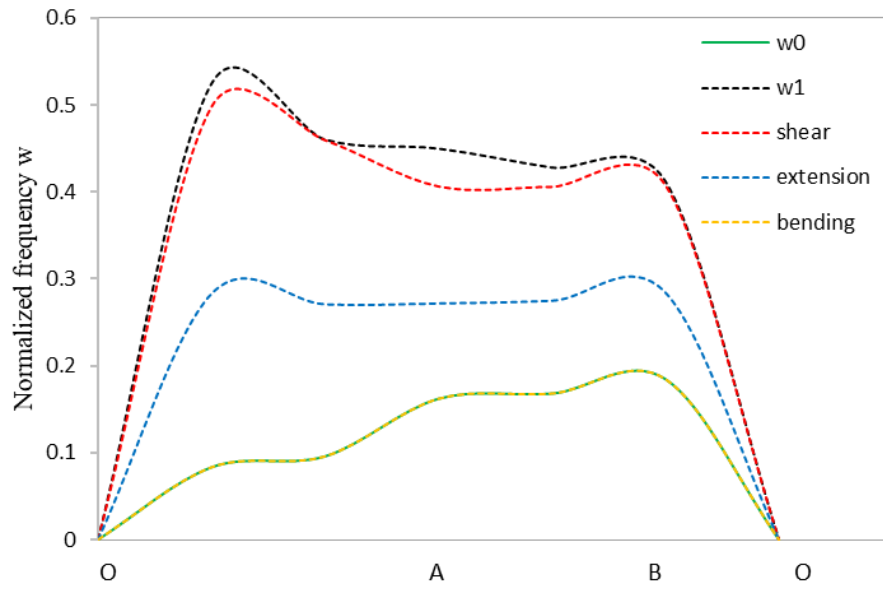
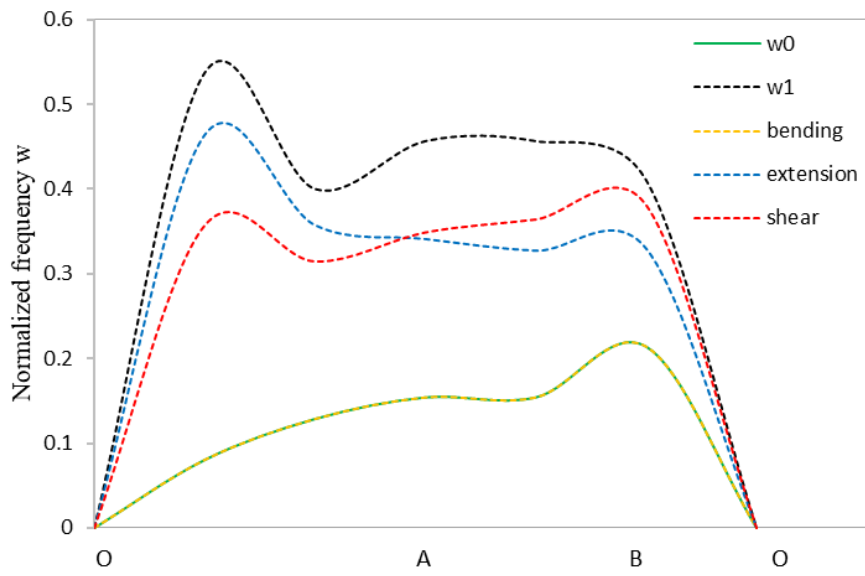


Fig.3. 5 : Dispersion diagram of hexagonal (a), re-entrant hexagonal (b), square (c) and triangular (d) unit-cell designs high optical mode. Continuous green lines correspond to the linear solution, while black dashed lines correspond to the solution after the incorporation of the non-linear correction.

Similarly, Fig.3.5 underlines the contribution of the non-linear energy for different architected unit cells at high optical mode and for the second wave amplitude $A_2 = 10 \times 10^{-3} m$. The dispersion diagram shows the highest effect of non-linear energy occurring in triangular unit cells, whereas it is of much lower importance for the three other lattices. The results obtained in Fig.3.4 and Fig.3.5 show an inversely proportional relation between the eigenfrequency and its correction term and we can observe that the frequency upshifts are greatest near the edge of the Brillouin zone where the group velocity drops, as shown in [40,41,132]. Numerically, the non-linear energy effect for different architected materials at high optical mode leads to percentages of non-linear correction equal to 0.78%, 0.97%, 0.55% and 6.5% for the hexagonal, re-entrant hexagonal, square and triangular lattices respectively.



a)



b)

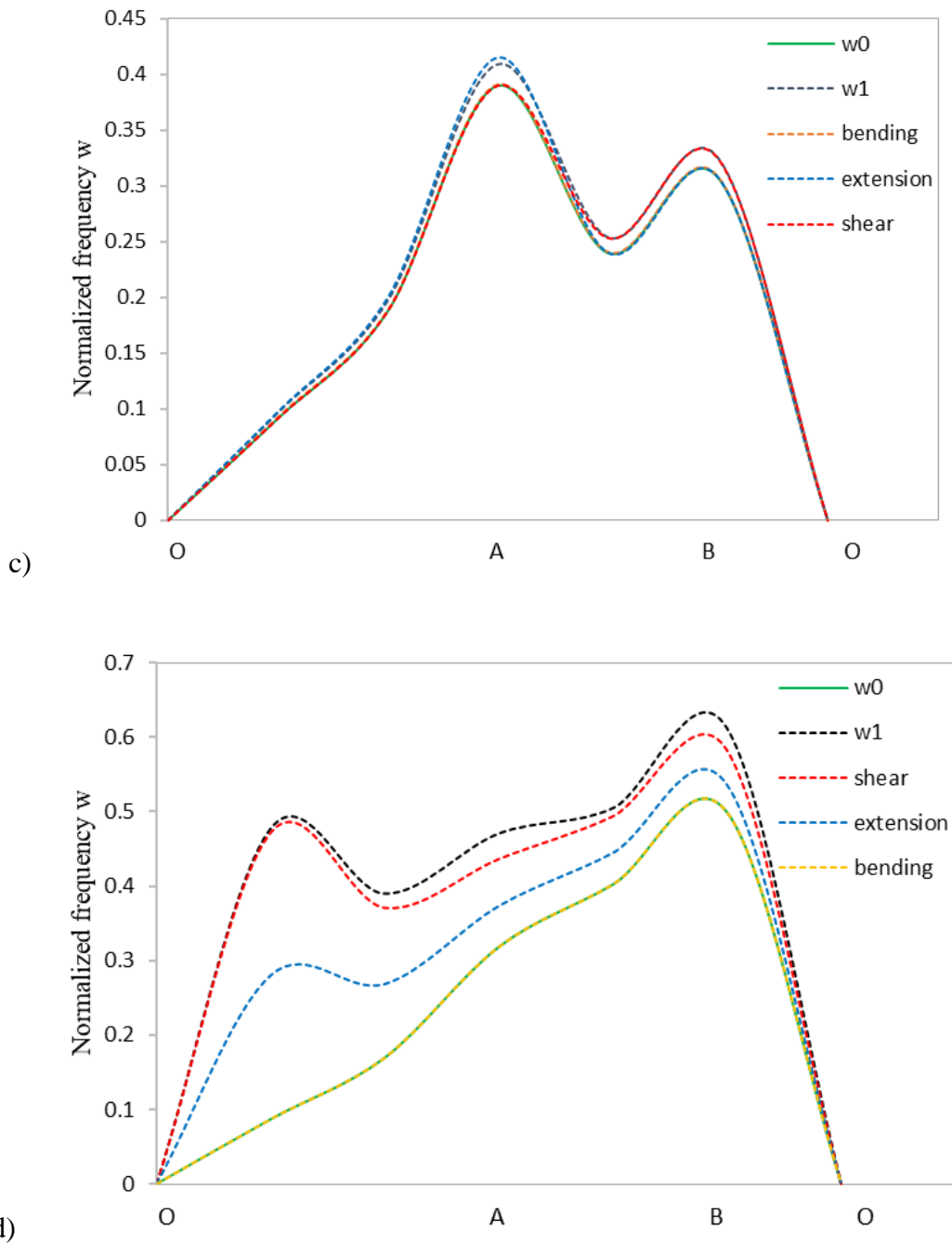


Fig.3. 6 :Dispersion diagram of an architected material for longitudinal mode frequency with hexagonal (a), re-entrant hexagonal (b), square (c) and triangular (d) unit-cell designs. Continuous green line: linear solution. Non-linear correction for the full non-linear kinematics (Black dashed lines), for the nonlinear shear mode alone (red dashed lines), for the nonlinear extension mode (blue dashed lines), for the nonlinear bending mode (orange dashed lines).

In Fig.3.6, we study the non-linear correction factor for the dispersion behavior by individuating the shear, extension, and bending energies for different architected materials for the longitudinal mode. We summarize the correction percentages of the different modes shown in Fig. 3.6 for the different studied architected materials in Table 3.2 and Table 3.3.

	Shape	Full nonlinear	Shear	Extension	Bending
	Hexagonal	63.9%,	60%	40.1 %	0.0001%
	Re-entrant hexagonal	66.1%	55.7%	54.7%	0.0002%
	Square	4.6%	0.00001%	5.9%	0.1%
	Triangular	32.3%	26.9%	14.6%	0.0001%

Table.3. 2: Percentages of difference between linear and full shear, extension and bending nonlinear energy modes for different architected unit cells at point A of the Brillouin zone

	Shape	Full nonlinear	Shear	Extension	Bending
	Hexagonal	55.1%,	54.6%	34.7 %	0.00006%
	Re-entrant hexagonal	47.7%	43.7%	34.9%	0.00003%
	Square	5.4%	5.2%	0.00005%	0.13%
	Triangular	18.4%	14.2%	6.8%	0.0002%

Table.3. 3: Percentages of difference between linear and full, shear, extension and bending nonlinear energy modes for different architected unit cells at point B of the Brillouin zone

From Table 3.2 and Table 3.3 we observe that for all considered architected materials, the shear energy has the highest effect in the non-linear correction as to energetic effects, and the dispersion diagram shows that the effect of bending on the correction mode is nearly negligible. These results are consistent with the fact that the square and triangular lattices behave in a more rigid manner compared to the bending dominated hexagonal lattice; the interpretation of previous results is that bending dominated unit cells deforms more easily and it is thus prone to a larger energy variation in comparison to the linear response. Moreover, the position of the point of study of the Brillouin zone plays an important role in energetic effects on the dispersion characteristics. The bending dominated lattices are prone to larger partial band gaps between different types of waves (extensional, shear, bending) compared to the tension dominated triangular lattice.

In Fig.3.7 and Fig.3.8 we compute the eigenvector for the initial, linear, and nonlinear deformation modes for the hexagonal and re-entrant hexagonal unit's cell based on model developed in [136].

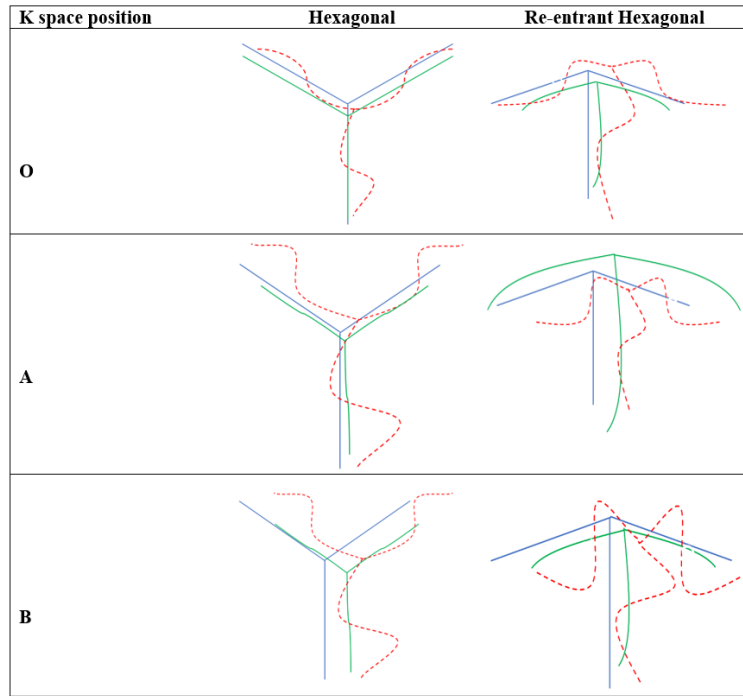


Fig.3. 7 : Eigen waves of hexagonal and re-entrant hexagonal unit cells for the shear mode. The blue line corresponds to the actual shape, the green line to the linear deformation, and the dashed red line to the non-linear deformation.

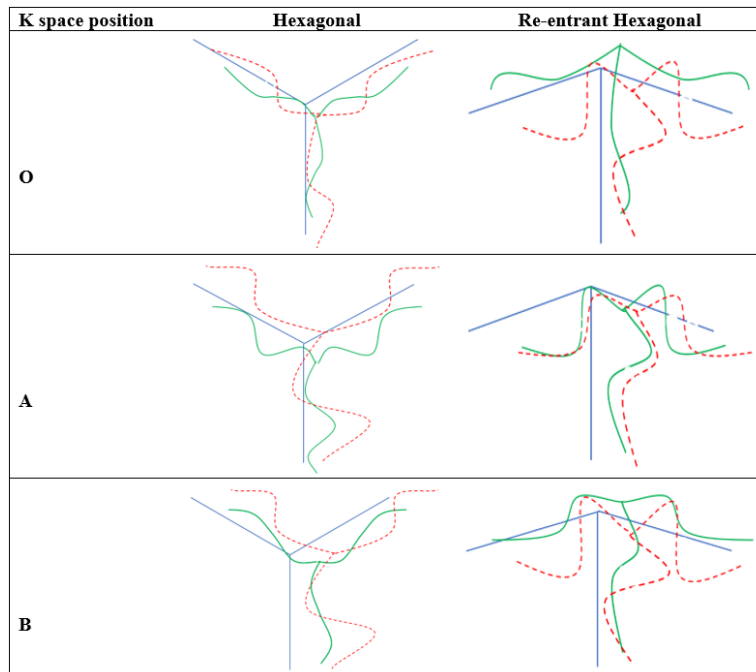


Fig.3. 8 : Eigen waves of hexagonal and re-entrant hexagonal unit cells at high optical mode. The blue line corresponds to the actual shape, the green line to the linear deformation, and the dashed red line to the non-linear deformation.

Points O, A, and B in Fig.3.7 and Fig.3.8 correspond to the Brillouin zone. The figures above show that the deformation observed at point B for the shear mode and the high optical mode for hexagonal and re-entrant hexagonal lattices is larger than the one observed at point O.

Additionally, after comparing Fig.3.7 and Fig.3.8 for linear and nonlinear modes it shows a high effect of damage in nonlinear mode however a very low effect is observed in linear mode. Similarly, according to the range of frequencies in Fig.3.7 and Fig.3.8 we observe that the unit cells of the high optical mode show a more perturbed deformed shape compared to the ones for the shear mode similarly when we compare the eigen shape at different positions of the Brillouin zone we observe that point B is most affected followed by position A then O.

Additionally, we can observe that hexagonal lattice is more affected by the nonlinear deformation than the re-entrant hexagonal lattice.

3. 5 Discussion and conclusion

The present work is devoted to the analysis of nonlinear wave propagation within repetitive lattice materials, relying on a large strain beam formulation accounting for all deformation modes of the lattice, namely extension, shear and bending. The obtained dispersion diagrams show that the geometry of the unit cell plays an important role in the magnitude of the nonlinear frequency correction in comparison to the reference linear frequency of waves. Four lattices materials have been selected to support the performed nonlinear wave propagation analysis, namely the classical hexagonal, re-entrant hexagonal, square, and triangular unit cells: in terms of results, the hexagonal unit cell shows the highest nonlinear effect for the longitudinal mode, whereas the square unit cell witnesses the lowest effect of the non-linear correction term. In decreasing order of importance of energetic contribution on the nonlinear wave correction frequency, the shear energy comes first, followed by extension energy, whereas bending has the minimal effect. Moreover, the wave amplitude enters as an additional parameter of importance, since it has a high effect on the percentage of non-linear correction. Overall, much more significant non-linear effects occur in the region of longitudinal mode for the major, lowest eigenmode, and the percentage of non-linear

correction drops as the frequency magnitude grows. Moreover, the inner architecture plays an important role in controlling the non-linear effect. Also, representing the eigenvectors associated to the different eigenmodes for the hexagonal and re-entrant hexagonal lattice we observe that hexagonal subjected to nonlinear deformation at point B of the Brillouin zone and high optical mode frequency are most affected by deformation.

Chapter 4

Propagation Analysis of Fully Nonlinear Waves in Homogenized Periodic Hexagonal and Triangular Networks in 1D and 2D

Summary:

This chapter aims to analyze the propagation of fully nonlinear waves, encompassing shear, extension, and bending deformation modes, within homogenized periodic nonlinear hexagonal and triangular networks. The wave analysis is conducted by constructing the effective strain energy density of periodic hexagonal and triangular lattices in the nonlinear regime by a continualization of the discrete lattice equations, considering all forms of energy. We incorporate into the continuous model strain gradient effects in order to account for the dispersive nature of waves.

The resulting second-order gradient nonlinear continuum exhibits two distinct propagation modes: an evanescent subsonic mode and a supersonic mode. We examine in a 1D situation the response of hexagonal and triangular lattices, considering varying levels of nonlinearity. Notably, the supersonic mode demonstrates waves propagating at higher frequencies for the hexagonal lattice in comparison to the triangular lattice, whereas the opposite behavior is observed for the subsonic mode. We further evaluate the impact of a fully nonlinear analysis in comparison to a nonlinear analysis solely based on extension energy, with regard to both supersonic and subsonic modes of wave propagation. The nonlinear wave propagation analysis is then extended to a 2D situation for the same two lattices. We compare the longitudinal and shear modes for both hexagonal and triangular lattices.

4.1 Introduction

Material structures made up of repetitive networks of structural elements, such as beams, are capable of filtering waves in certain directions and frequencies. There has been much research activity in the literature on the mechanical response of such networks as a result of their mechanical response. Nonetheless, the evaluation of the dynamic properties as well as the acoustical properties of these structures [61,62] remains a scientific challenge [25,33,63,72,73,106,107] .

Periodic lattices and structures have been the subject of numerous studies, particularly in aeronautics, due to their ability to reduce or absorb vibrations, shock, and sound in structural components [61,62] . These studies have focused on the dynamic response and wave propagation properties of materials [52,109] , structures and devices [126] that exploit spatial periodicity. Such structures have become increasingly popular in a variety of fields, including ultra-light architected materials [38,52,109] , phononic crystals [25,106], and acoustic metamaterials [25,33,63,72,73] and [48,137]. In recent years, there has been considerable interest in these structures [138], with most research focusing on the design of materials and structures with a periodic microstructure that can achieve complete sound propagation in a certain frequency range, known as the spectral band gap. This frequency band gap prohibits wave propagation within the structure, regardless of the direction of propagation.

Extensive research has been conducted on periodic networks, particularly focusing on the mechanical properties due to their spatial periodicity [1–4]. The presence of frequency bandgaps, where waves are unable to propagate through the network within a specific frequency range and quickly attenuate, has garnered significant attention. Wave bandgaps in periodic networks have been a subject of investigation, with the location and width of these bandgaps dependent on the network's topology and wave propagation direction [6–11]. While there have been numerous studies on the propagation of elastic waves in a linear framework, only a few of them have explored wave propagation in nonlinear media [12–15]. Incorporating nonlinear aspects of wave propagation becomes necessary when dealing with large deformations, presenting a considerable challenge. Material [16,17] and geometrical [18] nonlinearities are two types of nonlinearities that may arise.

Nonlinear waves in periodic structures exhibit new phenomena that differ from those observed in linear media, including amplitude-dependent wave propagation, phase velocity, and group velocity. This amplitude-dependent dispersion relation offers opportunities for passive tuning of

the dispersion band structure by controlling the amplitude of propagating waves, extending beyond dynamic and acoustic property control through design or external stimuli [113]. Consequently, the solutions of wave propagation equations become more complex compared to harmonic plane wave solutions in linear wave equations, as nonlinear periodic structures support various wave solutions depending on wave amplitude, interactions, and the type of nonlinearity. Examples of these specific solutions include solitary wave solutions for Boussinesq-type equations and shallow water waves for Burger's equation [48,114–117,137,139,140]. Previous studies on nonlinear elastic waves have primarily focused on classical Cauchy-type elasticity theory, which only considers the first-order displacement gradient. However, Cauchy-based models do not provide realistic predictions regarding medium properties such as dispersion relations, as they lack internal length parameters [141]. Experimental evidence has shown that most waves are dispersive, meaning each wavenumber travels at a different phase velocity [142,143] This discrepancy has led to the success of gradient-enriched theories in capturing dynamic behaviors overlooked by classical elasticity.

The following chapter is structured as follows: In Section 4.2, we employ the second-order gradient theory to compute the homogenized nonlinear behavior of the hexagonal and triangular lattices. This is achieved through an analytical homogenization method that is based on the strain energy of the initial network within a unit cell. Subsequently, we incorporate the effective constitutive laws into the dynamical planar equilibrium equations. We also formulate a Boussinesq-type equation that reflects the propagation of solitary strain waves within the effective medium, which is discussed in Section 4.3 along with an analysis of the instability of 2D nonlinear elastic architected materials. In Section 4.4, we investigate wave propagation in 2D nonlinear architected materials. Finally, we summarize the main findings in Section 4.5.

4.2. Discrete homogenization of nonlinear architected materials

Previous research work [22] has solely focused on the nonlinear energy associated with extension force, overlooking the impact of both shear and bending. However, our work presents a comprehensive analysis that accounts for the effects of extension, bending, and shear energy in our nonlinear energy evaluation. The inclusion of all these energy components is crucial, as we have observed in previous chapters two and three a significant influence of extension and a discrepancy between the full nonlinear energy analysis and the extension-based nonlinear energy analysis. Therefore, it is imperative to consider all the nonlinear energy contributions to obtain a more

accurate understanding of the dynamical behavior. To establish the stage, we use the general expression of internal deformation energy given as follows:

$$W = W_L + W_c \tag{4.1}$$

where W_L and W_c are the linear and non-linear cubic internal deformation energies respectively.

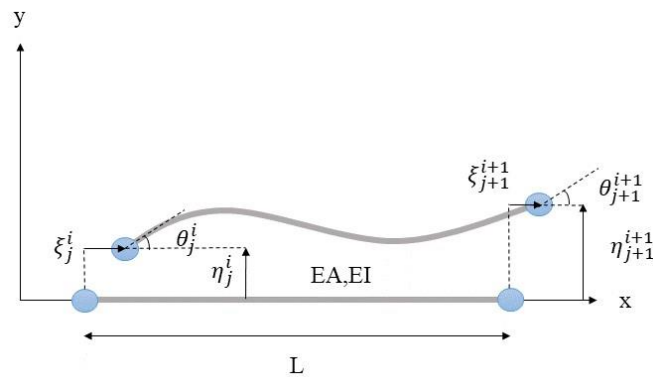


Fig.4. 1: Timoshenko beam element with the indicated of kinematic and repetitive network.

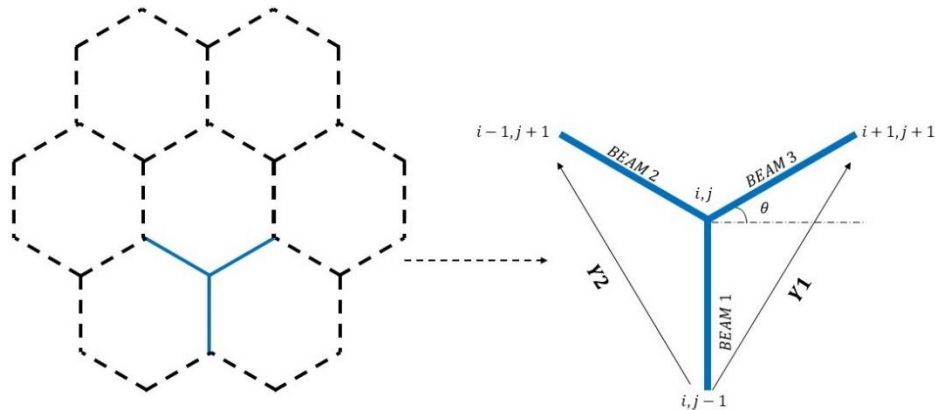


Fig.4. 2: 2D unit cell of the hexagonal lattice

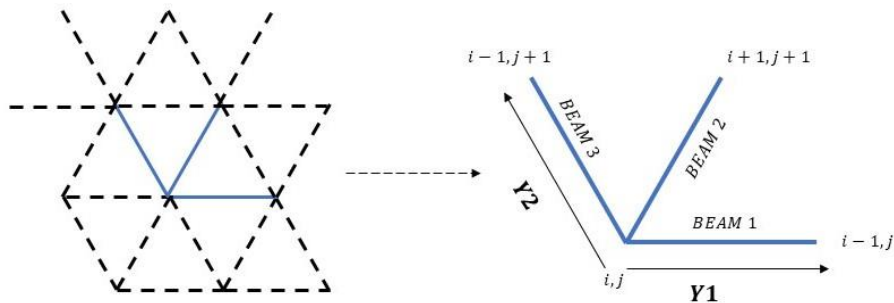


Fig.4. 3: 2D unit cell of triangular lattice

Fig.4.1 represents the beam element kinematics in a repetitive network, wherein the function η represents the displacement of the neutral axis of the beam in the y-direction and the function ξ represents the displacement in the x-direction. The function θ describes the rotation of the cross-section of the beam at its mid-plane. The expression of single beam element of Fig.4.2 and Fig.4.3 internal deformation of linear and non-linear cubic energies can be expressed in the local coordinates (ξ, η) in Fig. 4.1 as [124]:

$$W_L = \frac{1}{2} G A k_s \left[\frac{1}{L} (\eta_{j+1}^{i+1} - \eta_j^i) - \frac{1}{2} (\theta_{j+1}^{i+1} + \theta_j^i) \right]^2 + \frac{EA}{2L^2} (\xi_{j+1}^{i+1} - \xi_j^i)^2 + \frac{EI}{2L^2} (\theta_{j+1}^{i+1} - \theta_j^i)^2 \quad (4.2)$$

$$W_c = -\frac{1}{2L^2} G A k_k k_s (\theta_{j+1}^{i+1} + \theta_j^i) (\xi_{j+1}^{i+1} - \xi_j^i) (\eta_{j+1}^{i+1} - \eta_j^i) + \frac{1}{4L} G A k_k k_s (\theta_{j+1}^{i+1} + \theta_j^i)^2 (\xi_{j+1}^{i+1} - \xi_j^i) + \frac{1}{2L^3} EA (\xi_{j+1}^{i+1} - \xi_j^i)^3 \quad (4.3)$$

$$+ \frac{1}{2L^3} EA k_s (\xi_{j+1}^{i+1} - \xi_j^i) (\eta_{j+1}^{i+1} - \eta_j^i)^2 + \frac{1}{8L} \lambda A (\xi_{j+1}^{i+1} - \xi_j^i) (\theta_{j+1}^{i+1} + \theta_j^i)^2$$

wherein G , E and λ are shear, young's modulus and lame coefficients respectively, while k_k and k_s are the beam correction factors. In order to see the effect of nonlinear terms related to the third order terms displacements it will only be considered. Using different finite difference schemes Eqs. (D1), (D2), and (D3) developed in **Appendix D** in the expression of the linear and nonlinear energies of beam can be written as:

$$W_{L(i)} = \frac{1}{2} G A k_s \left(\frac{\partial \eta_{(i)}}{\partial s} + \frac{L}{2} \frac{\partial^2 \eta_{(i)}}{\partial s^2} - \frac{\partial \eta_{(i)}}{\partial s} \right)^2 + \frac{1}{2} EA \left(\frac{\partial \xi_{(i)}}{\partial s} + \frac{L}{2} \frac{\partial^2 \xi_{(i)}}{\partial s^2} \right)^2 \quad (4.4)$$

$$W_{c(i)} = -\frac{1}{L^2} G A k_k k_s \frac{\partial \eta_{(i)}}{\partial s} \left(L \frac{\partial \xi_{(i)}}{\partial s} + \frac{L^2}{2} \frac{\partial^2 \xi_{(i)}}{\partial s^2} \right) \left(L \frac{\partial \eta_{(i)}}{\partial s} + \frac{L^2}{2} \frac{\partial^2 \eta_{(i)}}{\partial s^2} \right) + \frac{1}{2L} G A k_k k_s \left(\frac{\partial \eta_{(i)}}{\partial s} \right)^2 \left(L \frac{\partial \xi_{(i)}}{\partial s} + \frac{L^2}{2} \frac{\partial^2 \xi_{(i)}}{\partial s^2} \right) \quad (4.5)$$

$$+ \frac{1}{2L^3} EA k_s \left(L \frac{\partial \xi_{(i)}}{\partial s} + \frac{L^2}{2} \frac{\partial^2 \xi_{(i)}}{\partial s^2} \right) \left(L \frac{\partial \eta_{(i)}}{\partial s} + \frac{L^2}{2} \frac{\partial^2 \eta_{(i)}}{\partial s^2} \right)^2 + \frac{\lambda A}{2L} \left(L \frac{\partial \xi_{(i)}}{\partial s} + \frac{L^2}{2} \frac{\partial^2 \xi_{(i)}}{\partial s^2} \right) \left(\frac{\partial \eta_{(i)}}{\partial s} \right)^2$$

where (i) represent the number of beams. The total energy, defined as the sum of the energies of all beams within the unit cell in the Cartesian basis, is finally calculated by dividing the energy density by the area of the elementary unit cell S for hexagonal and triangular lattices, wherein the area of hexagonal lattice is $S = 2L^2 \cos \theta (1 + \sin \theta)$ and for triangular lattice $S = \sqrt{3}L^2/4$. As a result, the decomposition of the unit cell's energy density into three contributions reflecting successively the linear component of first-order elasticity, the linear component of second-order

elasticity, and the nonlinear component related to first-order elasticity is held in full generality, such that [54]:

$$W/S = W_{linear} + W_{second\ gradient} + W_{nonlinear} \quad (4.6)$$

Then we obtain the constitutive law, which includes both classical and higher order, strain gradient terms. This is indicated by the existence of the stress and hyperstress tensors computed from the homogenized strain energy density. The first order Piola-Kirchhoff stress is given in component form as the sum of a linear term and a nonlinear contribution [54]

$$T_{ij} = \frac{\partial(W_{linear} + W_{nonlinear})}{\partial(\partial u_i / \partial x_j)} = T_{ij}^L + T_{ij}^{NL} \quad (4.7)$$

Similarly, the second order hyperstress expresses as

$$S_{ijk} = \frac{\partial W_{second\ gradient}}{\partial(\partial^2 u_{ij} / \partial x_k^2)} \quad (4.8)$$

The linear part of the constitutive law for hexagonal and triangular can be expressed as:

$$\begin{aligned} T_{xx} &= C_{11} \frac{\partial u(x, y)}{\partial x} + C_{12} \frac{\partial v(x, y)}{\partial y} \\ T_{yy} &= C_{12} \frac{\partial u(x, y)}{\partial x} + C_{22} \frac{\partial v(x, y)}{\partial y} \\ T_{xy} &= C_{33} \left(\frac{\partial u(x, y)}{\partial y} + \frac{\partial v(x, y)}{\partial x} \right) = T_{yx} \end{aligned} \quad (4.9)$$

The nonlinear part of the constitutive law for hexagonal and triangular writes:

$$\begin{aligned} T_{xx}^{NL} &= A_{11} \frac{\partial u(x, y)}{\partial x} \frac{\partial u(x, y)}{\partial x} + A_{12} \frac{\partial v(x, y)}{\partial y} \frac{\partial v(x, y)}{\partial y} \\ T_{yy}^{NL} &= A_{12} \frac{\partial u(x, y)}{\partial x} \frac{\partial u(x, y)}{\partial x} + A_{22} \frac{\partial v(x, y)}{\partial y} \frac{\partial v(x, y)}{\partial y} \\ T_{xy}^{NL} &= A_{33} \left\{ \frac{\partial u(x, y)}{\partial y} \frac{\partial u(x, y)}{\partial y} + \frac{\partial v(x, y)}{\partial x} \frac{\partial v(x, y)}{\partial x} \right\} = T_{yx}^{NL} \end{aligned} \quad (4.10)$$

wherein $[C]$ and $[A]$ are the linear effective moduli derived from the linear part of the energy density and the nonlinear effective moduli characteristic of the large deformation behavior

respectively for hexagonal and triangular lattices, as shown in Table 4.1 and Table 4.2. However, the expression of second gradient tensors are given in relations (D4) and (D5) of **Appendix D**.

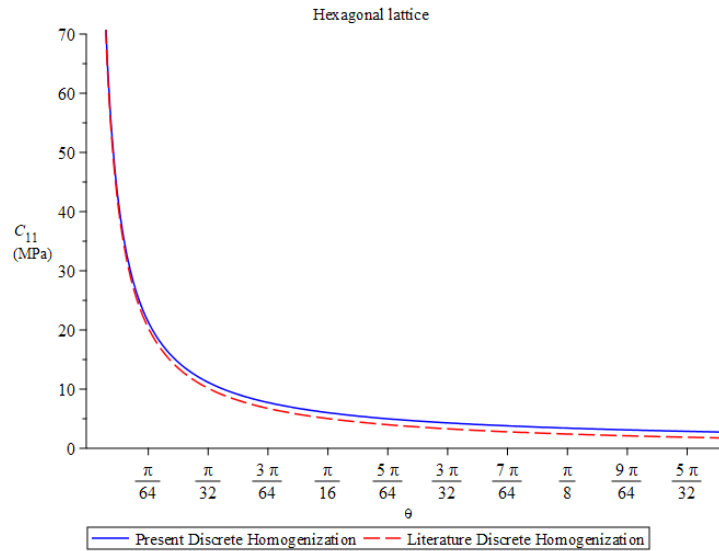


Fig.4. 4: Homogenized Cauchy modulus in extension computed from the present discrete homogenization method and the method [14] in versus the angular variable θ for the hexagonal UC.

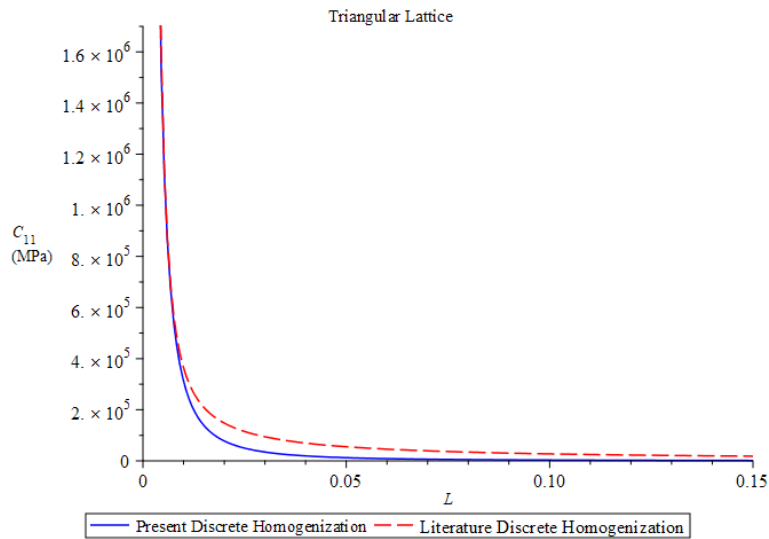


Fig.4. 5: Homogenized Cauchy modulus in extension obtained computed from the present discrete homogenization method and the method [12] in versus the length variable L for the triangular UC .

The discrete homogenization method predictions of the strain gradient moduli are compared to the predictions of the same moduli using an alternative discrete homogenization method developed

in [14], wherein the moduli are plotted versus the function angular variable θ of a hexagonal unit cell, using the method developed in [12] as function of the length L of the triangular unit cell. The values of the effective moduli parameters obtained using both approaches are in good agreement, as shown in Fig.4.4 and Fig.4.5.

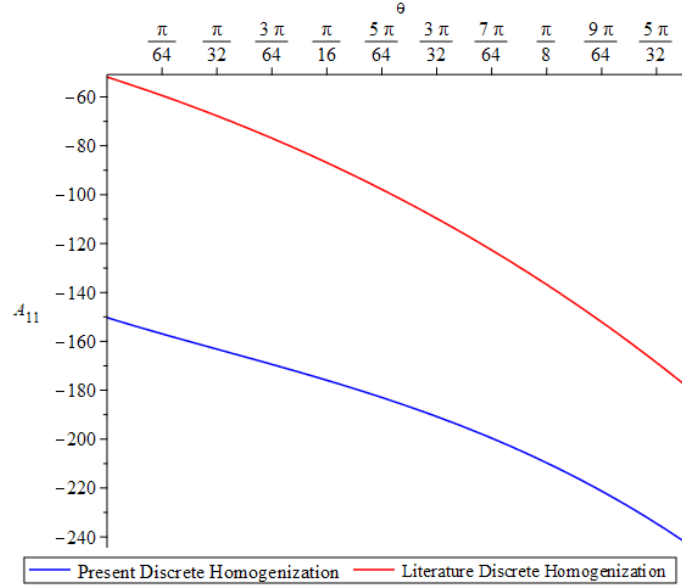


Fig.4. 6: Homogenized Cauchy modulus o A_{11} obtained computed from the present discrete homogenization method and the method [22] in versus the angular variable θ for the hexagonal UC.

Fig.4.6 illustrates a comparison between the current nonlinear discrete homogenization method and the discrete homogenization method developed in [22], specifically in relation to the angular variable θ of a hexagonal unit cell. This comparison highlights the disparity in energy observed between the previous study and the present investigation due to the presence of extension and bending energy, in addition to shear energy.

4.3. Wave propagation in 1D nonlinear architected materials

We analyze the propagation of longitudinal waves in a one-dimensional continuum micro-structured beam with numerous hexagonal and triangular unit cells repeated with periodicity along the longitudinal direction, and single unit cell in the thickness direction. The beam is subjected to a uniaxial loading state along x direction, $T_{xx} \neq 0; \partial u / \partial x \neq 0$.

From the results obtained using Eqs. (4.9), (4.10), (D4), and (D5), we derived the homogenized nonlinear wave equation:

$$E_1 \frac{\partial^2 u}{\partial x^2} + E_2 \frac{\partial^2 u}{\partial x^2} \frac{\partial u}{\partial x} - E_3 \frac{\partial^4 u}{\partial x^4} = \rho^* \frac{\partial^2 u}{\partial t^2} \quad (4.11)$$

The effective moduli E_1, E_2 and E_3 are used to describe the mechanical behavior of the composite material with a periodic microstructure. E_1 is the linear effective modulus, which is derived from the linear part of the energy density. E_2 is the nonlinear effective modulus that characterizes the large deformation behavior of the material, and E_3 is the second-order effective modulus, which characterizes the second-order gradient behavior of the material. Moreover ρ^* is the effective density defined by $\rho^* = M/A_{cell}$ with A_{cell} is the area of the periodic unit cell and M is the mass of the set of lattice beams. The expressions for E_1, E_2, E_3 and ρ^* are provided in **Appendix B**, where they are defined in terms of specific variables and parameters.

The behavior of waves propagating within a periodic lattice can be described by the equation of motion Eq. (4.11), which characterizes the quasi-static properties of the waves. It is important to note that the second-order modulus term in the equation is always negative, which indicates that the presence of a microstructure in the lattice leads to positive dispersion. This means that as the wavenumber increases, the phase velocity of the waves also increases.

A mathematical model similar to this one has been essentially developed for shallow water waves in order to describe wave propagation in fluid [144]. The wave Equation (4.11) is an example of a Bossiness'-type equation. The extensive study has been done on the general characteristics of Boussinesq and Boussinesq-type equations, including nonlinear effects in solid dynamics [129,145]. Solutions to these equations of this type have also been examined in [111,146–150].

We should point out that Eq. (4.11), which has a single elliptical wave solution that is well-known in the literature [37], can be integrated using elliptic functions. According to the degree of nonlinearity, a set of elliptic functions are explicitly stated in [51]. These functions are represented by a universal coefficient s that does not depend on the mechanical properties of the material but instead consider the form, period, and velocity of waves. A quantitative indicator of how far the nonlinearity mode differs from a linear situation is the parameter “ s ”.

The following step is to derive an explicit analytical stationary solution for the governing wave. We convert Eq. (4.11) into the ordinary differential equation for the new non-dimensional strain of the wave function, utilizing the change of variable $y_1 = x - vt$, where $v = \omega/k$ is the phase velocity, ω is the frequency and k the wavenumber [51], introducing the new function $N = \partial u / \partial y_1$:

$$\frac{\partial^2 N}{\partial y_1^2} + \alpha_1 N + \alpha_2 N^2 + \alpha_3 = 0 \quad (4.12)$$

wherein α_1, α_2 , and α_3 express as $\frac{1}{E_3}(E_1 - \rho \omega^2/k^2)$, $\frac{1}{2}(E_2/E_3)$, and integration constant.

We take into consideration the following initial conditions [51]:

$$N = -\frac{A_0}{2}, \frac{\partial N}{\partial y_1} = 0 \text{ for } y_1 = 0 \quad (4.13)$$

wherein the strain amplitude is A_0 . Exact integration in terms of elliptic functions is possible for with the initial-value problems Eqs. (4.12) and integration of (4.13) [51,142]. Many authors, however, came up with solutions that ignored the integration constant α_3 or simply set it to zero. Such conclusions could be physically deceiving even when they are mathematically valid. Here, we suggest calculating the constant c from the assumption that the strain wave field's mean value is zero:

$$\int_0^1 N \partial y_1 = 0 \quad (4.14)$$

Since the displacement cannot increase indefinitely, Eq. (4.14) physical meaning leads to the determination of constant c in Eq. (4.12). The solution to Eq. (4.13) can then be written as [22,51]:

$$N = -\frac{A_0}{2} + \frac{A_0 s^2}{2(1 - E(s)/K(s))} \operatorname{sn}^2\left(\frac{k_0}{2} y_1, s\right) \quad (4.15)$$

where s is the so-called universal constant, the elliptic function's modulus, which indicates the degree of nonlinearity ($0 \leq s \leq 1$). The duration, shape, and velocity of the waves are all considered by this parameter. In general, it can be thought of as a numerical measurement of the strength of the nonlinear effects and of how far the nonlinear motion deviates from the linear motion. For small

values of s , the nonlinearity has little impact on the constitutive law, and the structure behaves roughly linearly as a result. The nonlinearity's impact on the constitutive law grows as s increases. $K(s)$ and $E(s)$ is the complete elliptic integrals of the first and second kind such that $K(s) = \int_0^1 ((1-t^2)(1-st^2))^{-1/2} dt$ and $E(s) = \int_0^1 (1-t^2)^{-1/2} (1-st^2)^{1/2} dt$, $sn(\cdot)$ is the elliptic sine, and respectively, where k_0 is the propagation constant related to k the wave number such as $k = \pi k_0 / 2K(s)$. The following relation can be utilized for determining the strain amplitude [22]:

$$3(1 - E(s)/K(s)) = -bA_0/k_0^2 \quad (4.16)$$

When s approaches zero, which corresponds to the linear case, Eq. (4.14) has a solution that is simplified to the solution of a harmonic plane wave $N = -\frac{A_0}{2} \cos(k_0 y_1) \rightarrow u = -\frac{A_0}{2k} \sin(ky_1), k = k_0$.

When s tends to 1, the Eq. (4.15) portrays a solitary strain wave that is localized, and its non-dimensional strain is given by the equation. $N = -\frac{A_0}{2} \text{sech}^2(k_0, y_1) \rightarrow u = -\frac{A_0}{k_0} \tanh(k_0, y_1)$.

When A is less than zero, it is possible for compression solitary waves to exist, whereas for A greater than zero, dilatation solitary waves, also known as tension waves, can be observed. For the nonlinear wave Eq. (4.12) with low values of s , an asymptotic solution can be developed. The Lidstedt-Poincaré method, which is explained in detail in [151], can be used to obtain the asymptotic development, and the comparison between the asymptotic development and the exact solution is presented in [24,51], demonstrating acceptable agreement for even relatively high values of the universal constant s . In the following analysis, we will use the following non-dimensional system parameters: $k.L$ represents the dimensionless wavenumber and the length of the beam, respectively.

Fig.4.7 displays the dispersion relation for the hexagonal lattice and triangular lattice with θ below zero, for various values of the nonlinear parameter s .

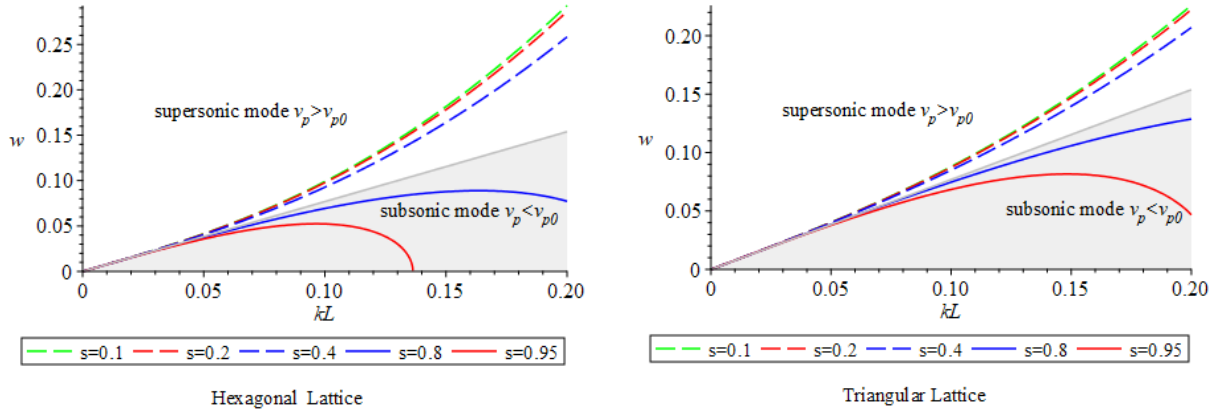


Fig.4. 7: Dispersion relation in the hexagonal and triangular lattice for various values of s

We will use in the sequel the notations v_p and v_{p0} respectively to denote the phase velocities for the nonlinear and linear effective medium. Fig.4.7 shows that for the hexagonal and triangular lattice the nonlinearity is weak, a supersonic mode appears, causing the dispersion curves to be located above the linear dispersion curve ($v = v_0$). With increasing nonlinearity, the waves transition from a supersonic to an evanescent subsonic mode between $s = 0.8$ and $s = 0.4$. As a result, the dispersion curve drops below the linear curve, and the frequency vanishes for specific values of k as explained in [23]. In a nonlinear scenario, the second-order gradient anisotropic continuum presents two propagation modes (subsonic and supersonic), whereas Cauchy only exhibit supersonic modes, with the frequency increasing as the wavenumber rises.

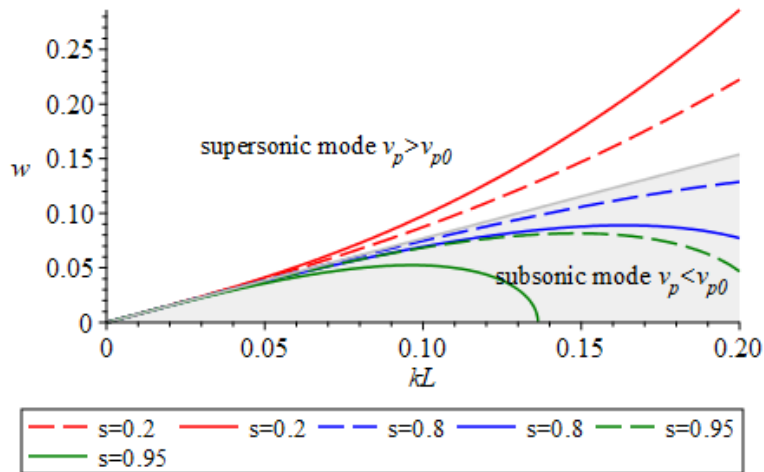


Fig.4. 8: Dispersion relation in the hexagonal (solid line) and triangular (dashed line) lattice for various values of $s = 0.2$, $s = 0.8$, and $s = 0.95$.

Fig.4.8 shows the behavior of fully nonlinear wave propagation in the inner material of hexagonal and triangular lattices at different degrees of nonlinearity. Fig.4.9 displays the response of hexagonal and triangular lattices under varying degrees of nonlinearity. For $s = 0.2$ for the supersonic mode, the triangular lattice exhibits a higher response compared to the hexagonal lattice. However, as the degree of nonlinearity increases to $s = 0.8$ and $s = 0.95$, and when reaching the supersonic mode, we reach the subsonic mode, the behavior of frequency in the hexagonal lattice becomes significantly greater compared to the triangular lattice. Fig. 4.9 depicts the results of an experimental investigation to study the effects of the full nonlinear model, and the nonlinear model based solely on extension energy on the frequency. The study aims to shed light on the differences between the two models and provide insights into each model's impact on the frequency behavior.

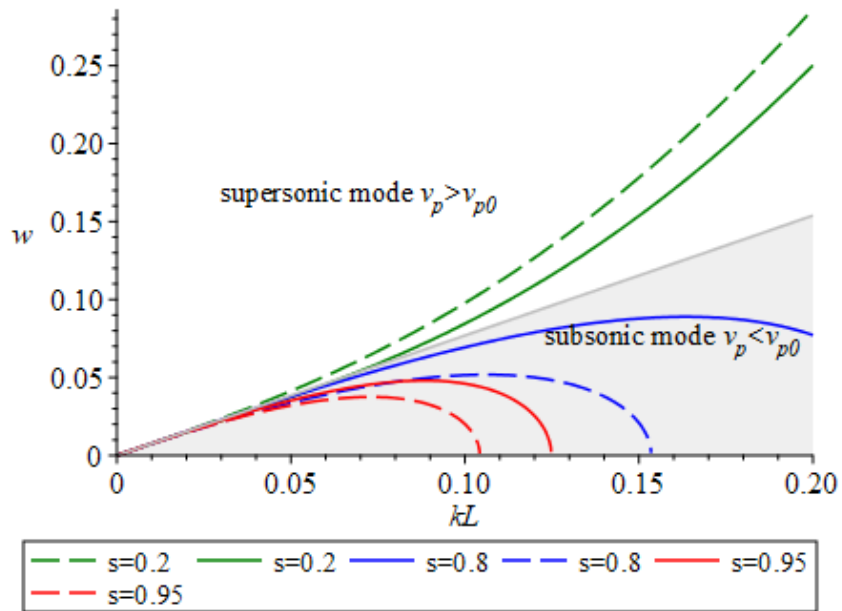


Fig.4. 9: Comparison between the dispersion relation for the hexagonal lattice for different values of s , using both the full nonlinear (dashed line) and nonlinear response based on extension energy (solid line)

Fig.4.9 illustrates the impact of the full nonlinear analysis, including the contributions from the energy of shear, extension, and bending, compared to a nonlinear analysis based solely on

extension energy, on the frequency of wave a propagation. The dashed line represents the fully nonlinear analysis, while the solid line represents the analysis based on extension energy only. As shown in the figure, the fully nonlinear analysis has a greater effect on both the supersonic and subsonic modes of wave propagation. Notably, the difference between the two analyses is more pronounced in the subsonic mode, particularly at higher degrees of nonlinearity. This observation can be attributed to the presence of both shear and bending energy, in addition to extension energy, in the fully nonlinear analysis, resulting in a greater percentage effect of the nonlinearity.

The group velocity of a wave refers to the velocity at which the energy of the wave is transported through a medium. In certain situations, such as when considering evanescent subsonic modes, the group velocity tends towards zero as the frequencies of the waves approach their higher values; this phenomenon is depicted in Fig. 4.10.

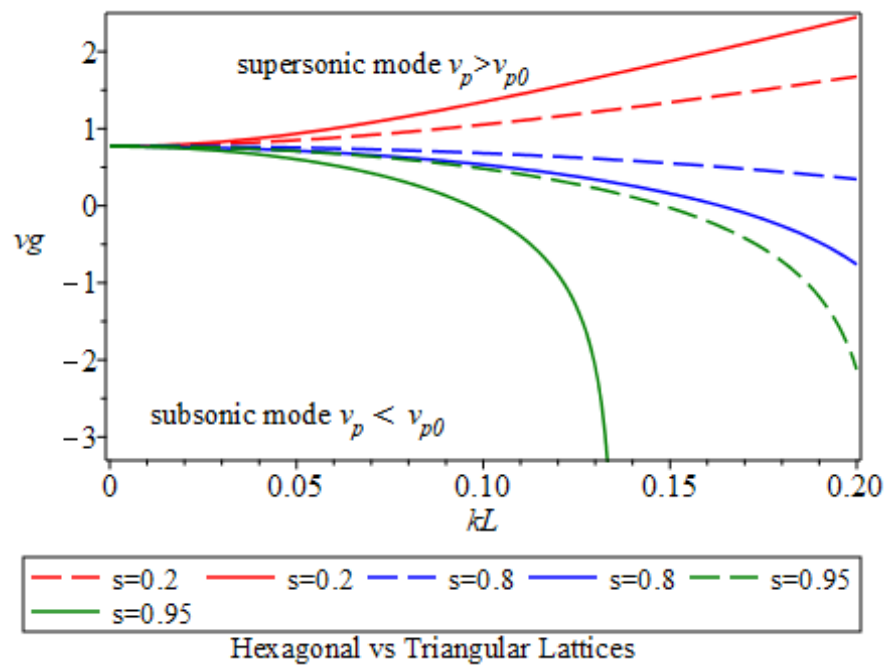


Fig.4. 10: Group velocities for the hexagonal (solid line) and triangular (dashed line) lattices for various values of the nonlinearity parameter: $s = 0.2$, $s = 0.8$, and $s = 0.95$.

Fig.4.10 illustrates the behavior of totally nonlinear energy as a result of variations in group velocity under increasing degrees of nonlinearity within the inner material of hexagonal and triangular lattices. The study aimed to investigate the unique properties of these lattice structures

and their ability to effectively transmit energy through a medium. The results show that at $s = 0.2$ in the supersonic mode, the triangular lattice demonstrates a greater reaction than the hexagonal lattice. However, as the degree of nonlinearity increased to $s = 0.8$ and $s = 0.95$, the hexagonal lattice exhibited much more effective behavior than the triangular lattice, particularly in the subsonic mode. This is likely due to the increased nonlinearity, which causes the energy to be better able to propagate through the hexagonal lattice.

4.4. Wave propagation in 2D nonlinear architected materials

The method used to provide a 2D wave propagation analysis is similar to the one-dimensional case, however at the expense of more involved technical steps and writings. Similar to the 1D situation, the constitutive law is derived from the expression of the nonlinear strain energy density in a two-dimensional Cartesian plane, with reference to the hexagonal and triangular lattices. By applying the dynamical equilibrium equation, a nonlinear wave equation in two dimensions can be obtained. The process of determining the acoustic characteristics, such as the dispersion relation and phase and group velocities, for periodic uniform two-dimensional lattices follows the same methodology as in the previous one-dimensional scenario. Expanding the solution of the one-dimensional wave equation, Eq. (4.15), to a two-dimensional context involves adopting the same non-dimensional strain N in the y direction. However, it now incorporates two distinct strain amplitudes B_1 and B_2 , as well as the variable $y_1 = x + y - vt$.

$$N = -\frac{B_1}{2} + \frac{B_1 s^2}{2(1-E(s)/K(s))} sn^2\left(\frac{k_0}{2} y_1, s\right) \quad (4.17)$$

$$M = -\frac{B_2}{2} + \frac{B_2 s^2}{2(1-E(s)/K(s))} sn^2\left(\frac{k_0}{2} y_1, s\right) \quad (4.18)$$

wherein we have introduced the two new functions $N = \frac{\partial u}{\partial y_1}$; $M = \frac{\partial v}{\partial y_1}$. Two modes of propagation exist based on Eqs. (4.17), (4.18): the longitudinal mode and the shear mode, representing different ways in which waves travel through the medium.

To investigate the characteristics of hexagonal lattices in comparison to triangular lattices in a two-dimensional (2D) setting, we will analyze the impact of the angle θ on the frequency band structure for both hexagonal and triangular lattices.

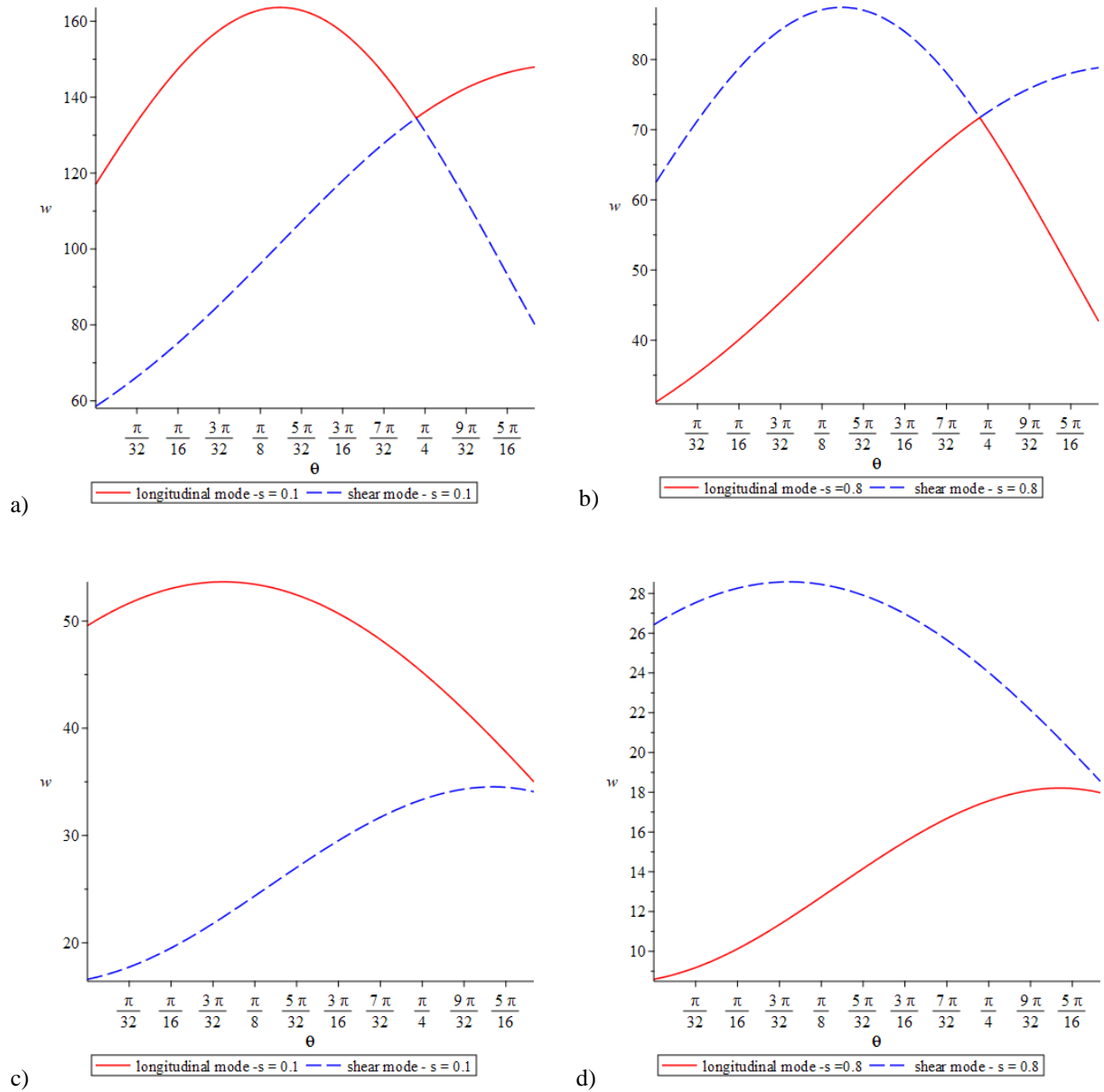


Fig.4. 11: Frequency band structure as a function of the angle θ with the direction of propagation equal to $\pi/4$: (a) and (c) correspond to hexagonal and triangular lattices with a degree of nonlinearity $s = 0.1$, (b) and (d) depict the same lattice structures, but with a degree of nonlinearity $s=0.8$.

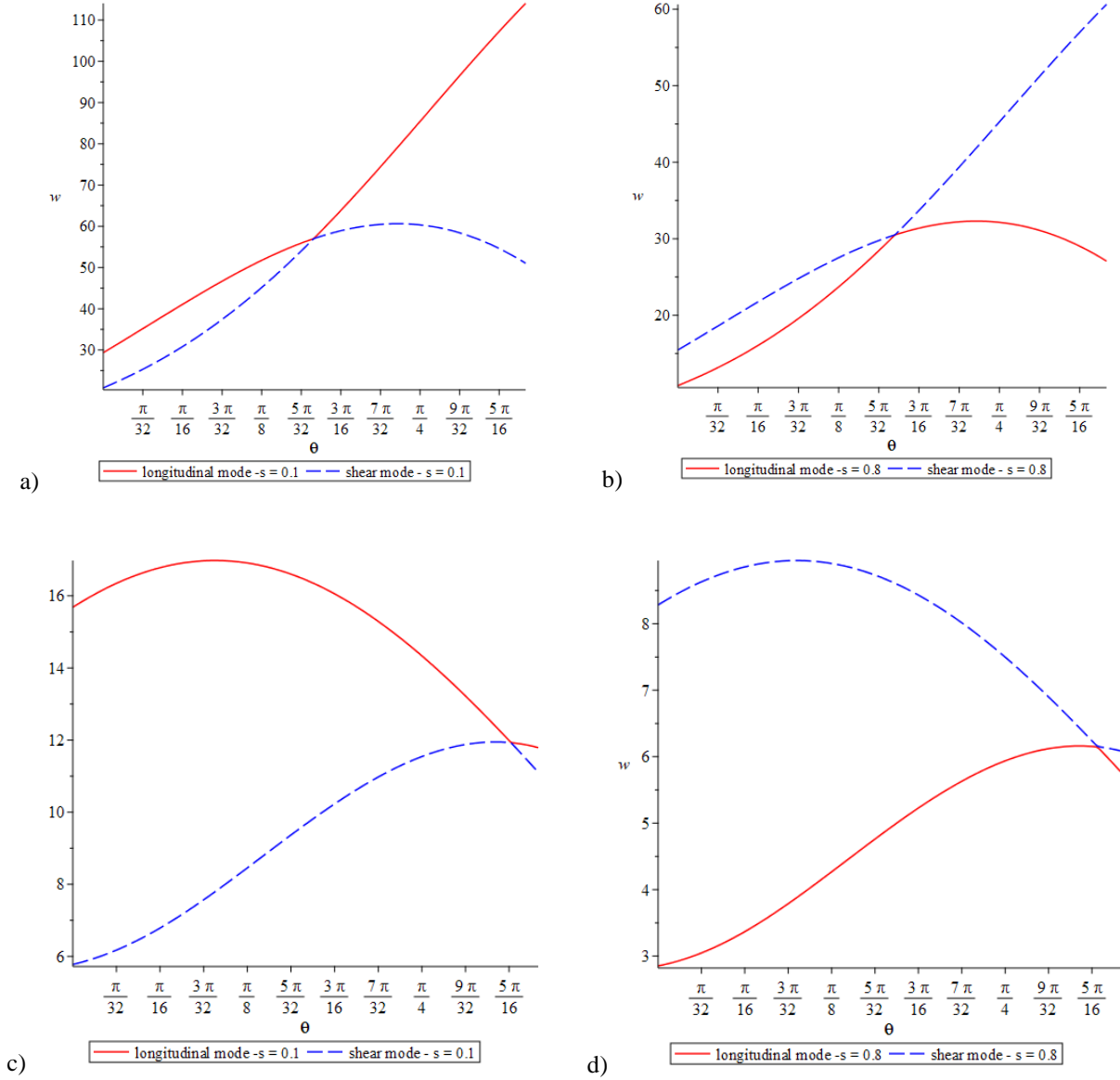


Fig.4. 12: Frequency band structure as a function of the angle θ with the direction of propagation equal to $\pi/2$: (a) and (c) correspond to hexagonal and triangular lattices with a degree of nonlinearity $s = 0.1$, (b) and (d) depict the same lattice structures, but with a degree of nonlinearity $s=0.8$.

Fig.4.11 and Fig.4.12 showcase the frequency band structure as a function of the angle θ with the direction of propagation set at $\pi/4$ and $\pi/2$, respectively. These figures examine the behavior in both hexagonal and triangular lattices. In particular, subfigures (a) and (c) correspond to the hexagonal and triangular lattices with a nonlinearity degree of $s = 0.1$. On the other hand, subfigures (b) and (d) depict the same lattice structures but with a higher nonlinearity degree of $s = 0.8$. These

figures provide a visual representation of how the frequency band structure varies in different lattice types (hexagonal and triangular) and with varying levels of nonlinearity.

Fig.4.11 and Fig.4.12 present the frequency characteristics of both hexagonal and triangular lattices. In the case of a low degree of nonlinearity, the longitudinal mode exhibits a higher frequency response compared to the shear mode for both lattice types. However, as the degree of nonlinearity increases to $s=0.8$, the shear mode surpasses the longitudinal mode in terms of frequency, with a stronger response observed in the hexagonal lattice for both scenarios.

Moreover, Fig.4.12 shows that when the direction of propagation is altered, a decrease in frequency is observed for both the hexagonal and triangular lattices.

Fig.4.11 -a and Fig.4.12-a shows a very similar shape of the diagram for the shear and longitudinal modes to those obtained in [23] for the hexagonal-shaped unit cell. The slight difference between the following results and the previous ones can be attributed to the presence of bending and shear energy in addition to extension energy in the nonlinear correction unlike works in [23] considering only extension energy in the nonlinear correction.

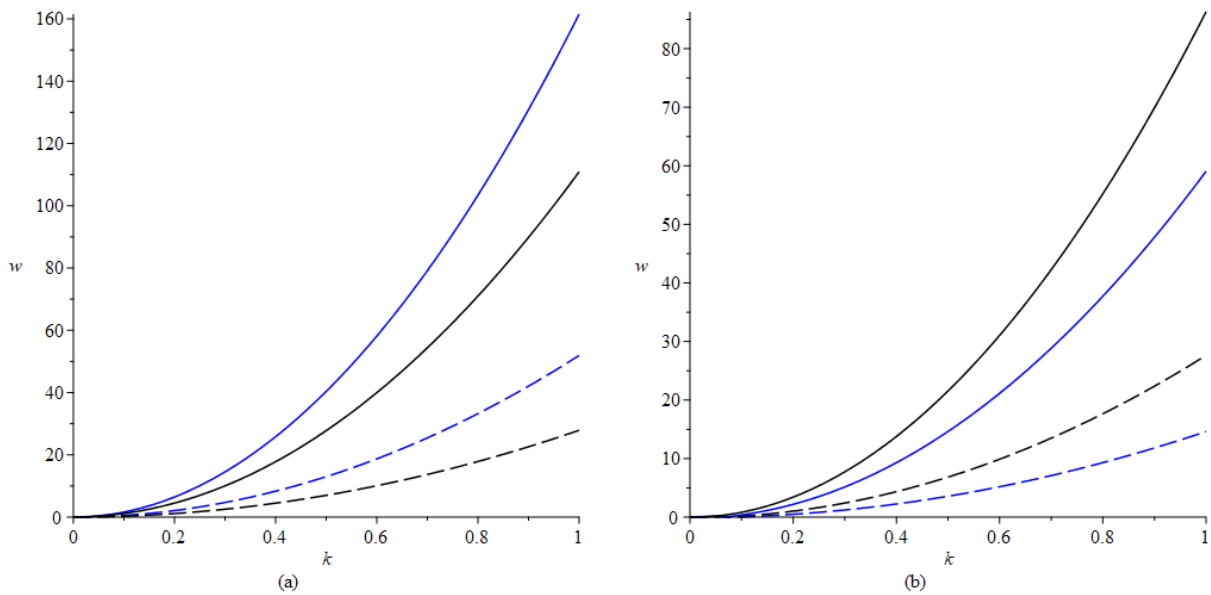
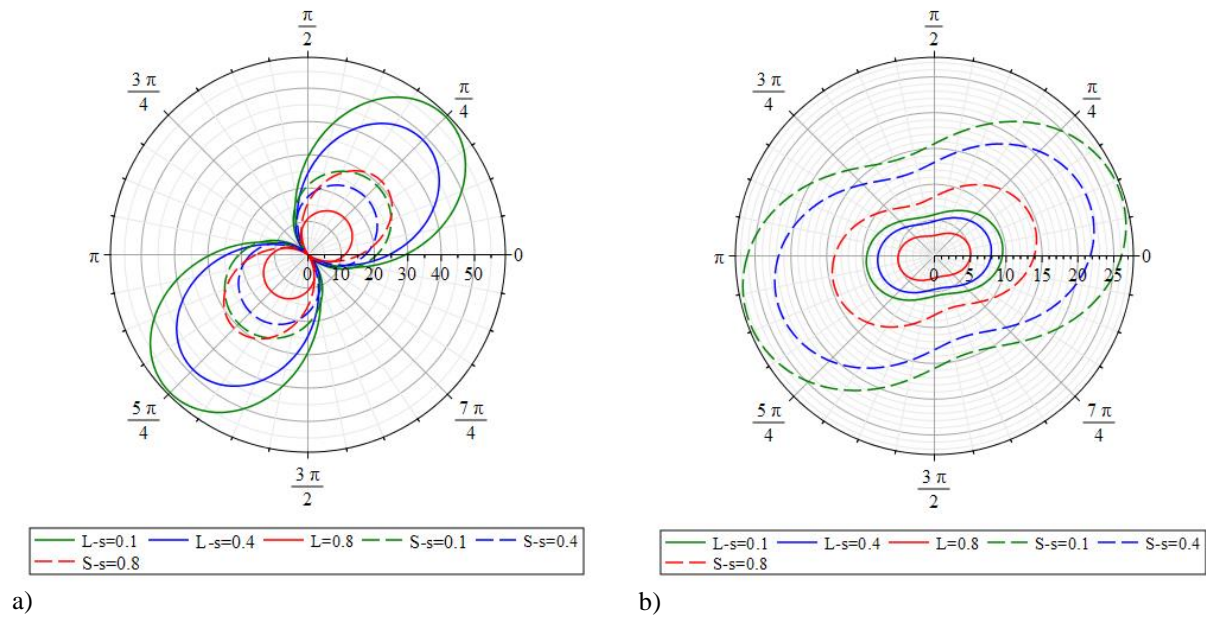
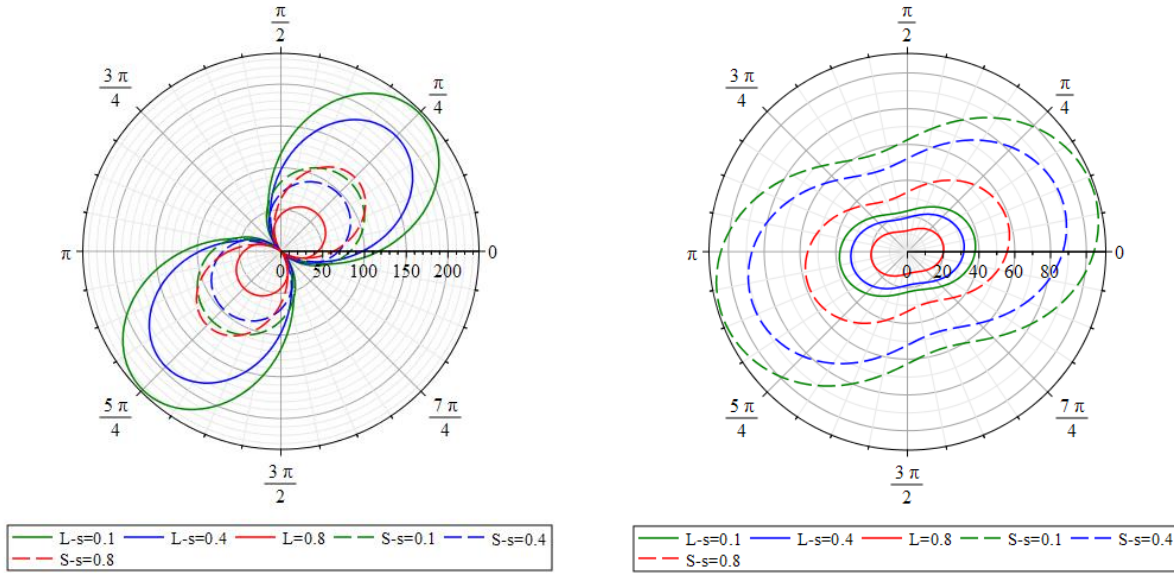


Fig.4. 13: Frequency band structure as a function of the wave number \mathbf{k} for triangular (dashed lines) and hexagonal (solid lines) lattices: blue lines correspond to longitudinal mode while black lines correspond to shear mode at degree of nonlinearity (a) $s = 0.1$ and (c) $s = 0.8$.

Fig.4.13 illustrates the relationship between the frequency band structure and the wave number k for both hexagonal and triangular lattices. The figure reveals that the longitudinal mode exhibits a higher frequency at a low degree of nonlinearity. However, as the degree of nonlinearity increases, the shear mode surpasses the longitudinal mode in terms of frequency. Furthermore, the figure demonstrates that the hexagonal lattices consistently yield higher frequencies than the triangular lattice in both cases.

In Fig.4.14, we study the properties of hexagonal and triangular lattices in a two-dimensional (2D) setting, specifically examining the impact of wave number (k) and the degree of nonlinearity. To visualize this, we present polar plots depicting the phase velocity for both hexagonal and triangular lattice configurations.





c) d)
 Fig.4. 14 : Phase velocity for both hexagonal and triangular lattices in the nonlinear effective medium, with $\theta = 0$. (a) and (b) are hexagonal and triangular lattices with $k=1$, (b) and (d) depict the same lattice structures, but with a $k= 2$.

In Fig.4.14, we can observe how the wave number (k) and the level of nonlinearity affect the frequency of waves in hexagonal and triangular lattices. When comparing hexagonal and triangular configurations at wave number $k = 1$, we find that hexagonal lattice has a higher frequency response compared to the triangular lattice. Specifically, the hexagonal lattice has a stronger impact on the longitudinal mode, while the triangular lattice is more significant in the shear mode. Interestingly, as we increase the degree of nonlinearity, a substantial change occurs in the magnitude of frequency for both the longitudinal and shear modes. This suggests that the nonlinearity parameter has a considerable influence on the behavior of waves in the lattices. Furthermore, when we increase the wave number to $k = 2$, the frequency experiences an overall increase for both hexagonal and triangular architected materials. This demonstrates that the wave behavior is dependent on the wave number, and a higher wave number leads to higher frequencies in both lattice configurations.

Overall, these observations highlight the significance of lattice geometry on the dominant mode of wave propagation. The differences in behavior between hexagonal and triangular lattices underscore the role of lattice configuration in determining how waves propagate through the material.

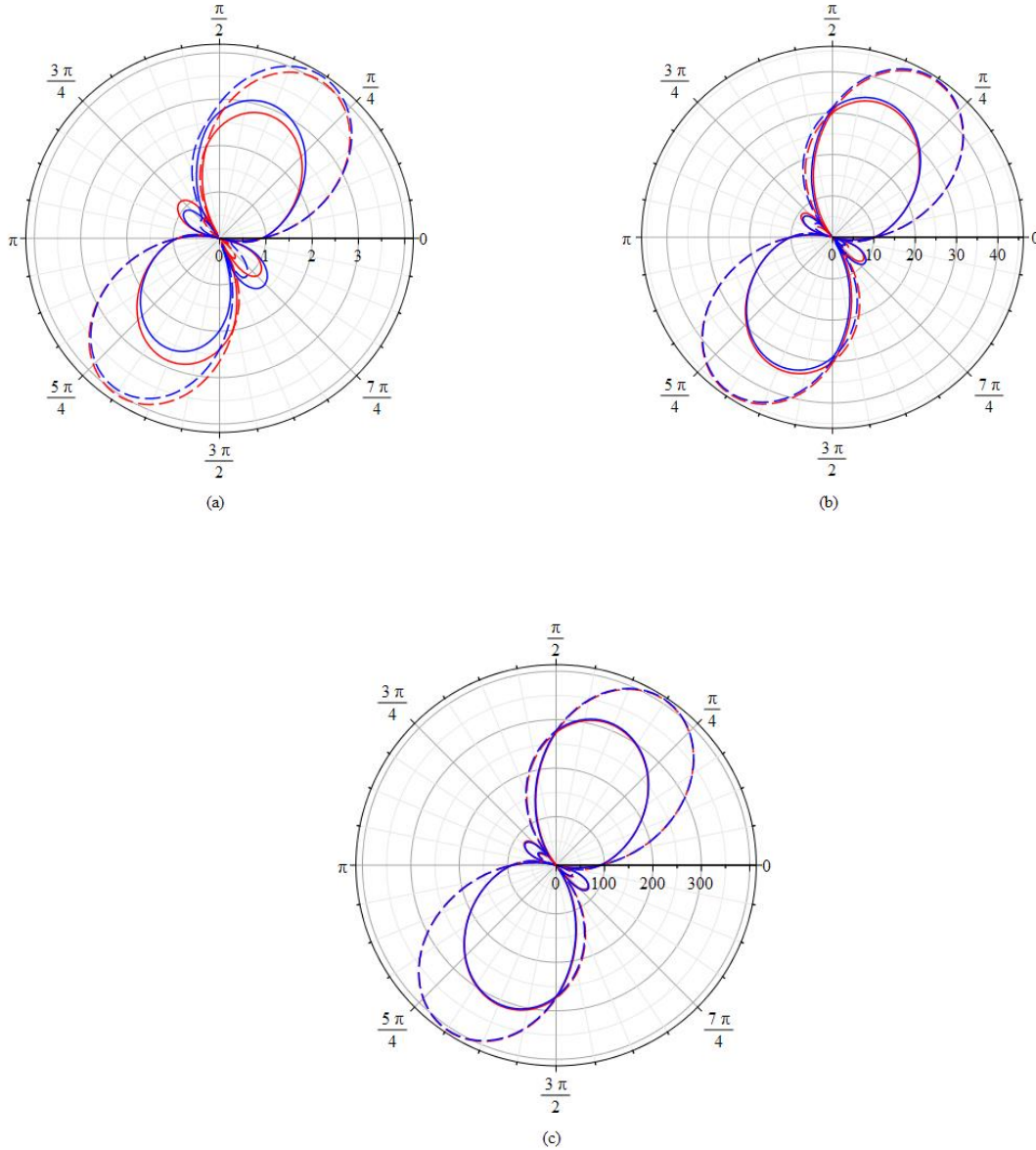


Fig.4. 15: Phase velocity for hexagonal lattice in the nonlinear effective medium with full nonlinear energy (red) and nonlinear based on shear energy (blue) at degree of nonlinearity $s = 0.8$ for both longitudinal (solid line) and shear (dashed line) modes, with $\theta = \pi/6$. (a) for wave number $k=0.3$ (b) for $k=1$, (c) for $k=3$.

Fig.4.15 illustrates the comparison between full nonlinear energy and nonlinear energy based on shear mode, examining the influence of wave number (k) at $\theta = \pi/6$. In Fig. 4.15-a, when $k = 0.3$, both the longitudinal and shear modes exhibit higher frequencies in the full nonlinear energy compared to the shear-based nonlinear energy. This indicates stronger oscillations in the full nonlinear energy. As we increase k to 1 in Fig.4.15-b, the difference between the full nonlinear

energy and the shear-based nonlinear energy decreases. When $k = 3$ in Fig.4.15-c, the difference becomes almost negligible.

These findings suggest that as the wave number increases, the nonlinearity has a lesser impact on the frequency behavior. The shape change of the phase velocity is more influenced by other factors, such as the second gradient. This indicates a transition from highly nonlinear behavior at lower wave numbers to a more linear behavior at higher wave numbers.

Fig.4.15 helps us understand the relationship between increasing wave number and the behavior of nonlinearity, as well as the impact of second gradient on the shape change of phase velocity.

4.5. Discussion and Conclusion

In this study, we thoroughly analyzed the nonlinear homogenization of hexagonal and triangular lattice materials. We derived the nonlinear wave equation based on the homogenized response of the initial repetitive network and studied the contribution of nonlinear waves. From the obtained form of the effective (continuous) strain energy density in the nonlinear regime, we conducted a nonlinear wave analysis featuring two propagation modes: a supersonic mode with an increasing frequency with wavenumber and an evanescent subsonic mode that vanishes past a certain wavenumber.

For weak nonlinearities, the nonlinear dispersion curves lie above the linear dispersion curve and they exhibit a supersonic mode. At the specific value of the nonlinearity parameter $s = 0.2$ for the supersonic mode, the hexagonal lattice displays waves propagating at a lower frequency compared to the triangular lattice. There appears a trade-off in the response, since waves propagate at a higher frequency in the hexagonal lattice as the degree of nonlinearity increases to high values ($s = 0.8$ and $s = 0.95$), entering the subsonic mode.

Moreover, we compared the behavior for the full nonlinear energy to that based on the sole shear energy and found that the fully nonlinear analysis has a greater impact on wave propagation in both the supersonic and subsonic modes. This impact is particularly significant in the subsonic mode, particularly at higher degrees of nonlinearity. This observation is due to the presence of both extension and bending energy, as well as shear energy, in the fully nonlinear analysis.

Overall, our findings provide valuable insights into the behavior of nonlinear waves in hexagonal and triangular lattice materials and highlight the importance of considering full nonlinear energy in the analysis of wave propagation.

In 2D the longitudinal mode exhibits a higher frequency response at lower levels of nonlinearity. However, as the nonlinearity degree increases, the shear mode surpasses the longitudinal mode in terms of frequency. Additionally, the hexagonal lattices consistently have higher frequencies compared to the triangular lattice. Additionally, the wave behavior is dependent on the wave number, with higher wave numbers leading to higher frequencies in both lattice configurations. As the wave number increases, the behavior of nonlinearity decreases, and the impact of the second gradient becomes dominant in shaping the phase velocity. These findings provide important insights into the frequency behavior of different lattice structures and highlight the influence of nonlinearity on their properties.

Appendix D. Deformational expressions of beam the expressions of the effective moduli and second gradient of hexagonal and triangular lattices

The different finite difference schemes developed:

$$(\eta_{j+1}^{i+1} - \eta_j^i) = a \left. \frac{\partial \eta}{\partial s} \right|_j^i + \frac{a^2}{2} \left. \frac{\partial^2 \eta}{\partial s^2} \right|_j^i \quad (D1)$$

$$(\xi_{j+1}^{i+1} - \xi_j^i) = a \left. \frac{\partial \xi}{\partial s} \right|_j^i + \frac{a^2}{2} \left. \frac{\partial^2 \xi}{\partial s^2} \right|_j^i \quad (D2)$$

$$\theta_{j+1}^{i+1} = \theta_j^i = a \left. \frac{\partial \eta}{\partial s} \right|_j^i \quad (D3)$$

The expression of Timoshenko beam coefficient $\beta = \frac{12EI}{k_s GAL^2}$

The expressions of the effective properties of 2D hexagonal and triangular lattices:

Effective Moduli	Closed form expression
C_{11}	$\frac{3E\beta \left(\cos^2 \theta + \sin \theta \cos \theta - \frac{1}{2} \right)}{(1 + \sin \theta) \cos \theta}$
C_{12}	$-\frac{9E\beta (\sin \theta - 1)}{2 \cos^3 \theta}$
C_{22}	$\frac{3E\beta \left(\cos^2 \theta + \sin \theta \cos \theta - \frac{1}{2} \right)}{(1 + \sin \theta) \cos \theta}$
C_{33}	$-\frac{3E\beta (4 \sin \theta \cos \theta - 3)}{2(1 + \sin \theta) \cos \theta}$
A_{11}	$-\frac{9\sqrt{3}A \left(\left((E + \lambda) \cos^2 \theta - \frac{3E}{2} - \frac{\lambda}{2} \right) \sin \theta - \frac{E}{2} \right)}{2L^2 \cos \theta (1 + \sin \theta)}$
A_{12}	$\frac{9\sqrt{3}A (2E \cos^2 \theta - E + \lambda)}{4L^2 (1 + \sin \theta)}$
A_{22}	$-\frac{9\sqrt{3}A \left(\left((E + \lambda) \cos^2 \theta - \frac{3E}{2} - \frac{\lambda}{2} \right) \sin \theta - \frac{E}{2} \right)}{2L^2 \cos \theta (1 + \sin \theta)}$

A_{33}

$$\left| \frac{3\sqrt{3}A \left(\left((E + \lambda) \cos \theta^2 + \frac{E}{2} - \frac{\lambda}{2} \right) \sin \theta + \frac{E}{2} + \frac{\lambda}{2} \right)}{2L^2 \cos \theta (1 + \sin \theta)} \right|$$

Table.4 1 The expressions of the effective properties of 2D hexagonal lattice

Effective Moduli	C_{11}	C_{12}	C_{22}	C_{33}	A_{11}	A_{12}	A_{21}	A_{22}	A_{33}
Closed form expression	$\frac{9E\beta}{2}$	$\frac{3\sqrt{3}E\beta}{2}$	$\frac{9E\beta}{2}$	$\frac{3E\beta}{2}$	$\frac{3AE}{8L^2}$	$\frac{3A(E + \lambda)}{8L^2}$	$\frac{3A(4E + \lambda)}{32L^2}$	$\frac{3A(E + \lambda)}{8L^2}$	$\frac{9AE\sqrt{3}}{8L^2}$

Table.4 2 The expressions of the effective properties of 2D triangular lattice

The second gradient homogenized properties for hexagonal lattice expressed as:

$$\begin{Bmatrix} S_{xxx} \\ S_{yyy} \\ S_{yyy} \\ S_{yyx} \\ S_{yxx} \\ S_{yxx} \end{Bmatrix} = \begin{bmatrix} B_{11} & B_{12} & 0 & 0 & B_{15} & 0 \\ B_{21} & B_{22} & 0 & 0 & B_{25} & 0 \\ 0 & 0 & B_{33} & B_{34} & 0 & B_{36} \\ 0 & 0 & B_{43} & B_{44} & 0 & B_{46} \\ B_{51} & B_{52} & 0 & 0 & B_{55} & 0 \\ 0 & 0 & B_{63} & B_{64} & 0 & B_{66} \end{bmatrix} \begin{Bmatrix} \frac{\partial^2 u(x, y)}{\partial x^2} \\ \frac{\partial^2 u(x, y)}{\partial y^2} \\ \frac{\partial^2 v(x, y)}{\partial y^2} \\ \frac{\partial^2 v(x, y)}{\partial x \partial y} \\ \frac{\partial^2 u(x, y)}{\partial y \partial x} \\ \frac{\partial^2 v(x, y)}{\partial x^2} \end{Bmatrix} \quad (D4)$$

wherein these elements express as:

$$B_{11} = -\frac{1}{16 \cos \theta^3} (L^2 E \beta (\beta^2 + \cos \theta^2) (\sin \theta - 1)) ; B_{12} = -\frac{3}{16 \cos \theta^3} (L^2 E \beta (\beta^2 + \cos \theta^2) (\sin \theta - 1)) ;$$

$$B_{15} = -\frac{3}{32 \cos \theta^3} (L^2 E \beta (\beta^2 + \cos \theta^2) (\sin \theta - 1)) ; B_{21} = -\frac{3}{16 \cos \theta^3} (L^2 E \beta (\beta^2 + \cos \theta^2) (\sin \theta - 1)) ;$$

$$B_{22} = -\frac{9}{16 \cos \theta^3} (L^2 E \beta (\beta^2 + \cos \theta^2) (\sin \theta - 1)) ; B_{25} = -\frac{9}{32 \cos \theta^3} (L^2 E \beta (\beta^2 + \cos \theta^2) (\sin \theta - 1)) ;$$

$$B_{33} = -\frac{9}{32 \cos \theta^3} (L^2 E \beta (\beta^2 - 2 \cos \theta^2 + 3)) (\sin \theta - 1) ; B_{34} = -\frac{9}{64 \cos \theta^3} (L^2 E \beta (\beta^2 - 2 \cos \theta^2 + 3)) (\sin \theta - 1) ;$$

$$B_{36} = -\frac{3}{32 \cos \theta^3} (L^2 E \beta (\beta^2 - 2 \cos \theta^2 + 3)) (\sin \theta - 1) ; B_{43} = -\frac{9}{64 \cos \theta^3} (L^2 E \beta (\beta^2 - 2 \cos \theta^2 + 3)) (\sin \theta - 1) ;$$

$$B_{44} = -\frac{9}{128 \cos \theta^3} (L^2 E \beta (\beta^2 - 2 \cos \theta^2 + 3)) (\sin \theta - 1) ; B_{46} = -\frac{3}{64 \cos \theta^3} (L^2 E \beta (\beta^2 - 2 \cos \theta^2 + 3)) (\sin \theta - 1) ;$$

$$B_{51} = -\frac{3}{32 \cos \theta^3} (L^2 E \beta (\beta^2 + \cos \theta^2)) (\sin \theta - 1) ; B_{52} = -\frac{9}{32 \cos \theta^3} (L^2 E \beta (\beta^2 + \cos \theta^2)) (\sin \theta - 1) ;$$

$$B_{55} = -\frac{9}{64 \cos \theta^3} (L^2 E \beta (\beta^2 + \cos \theta^2)) (\sin \theta - 1) ; B_{63} = -\frac{3}{32 \cos \theta^3} (L^2 E \beta (\beta^2 - 2 \cos \theta^2 + 3)) (\sin \theta - 1) ;$$

$$B_{64} = -\frac{3}{64 \cos \theta^3} (L^2 E \beta (\beta^2 - 2 \cos \theta^2 + 3)) (\sin \theta - 1) ; B_{66} = -\frac{1}{32 \cos \theta^3} (L^2 E \beta (\beta^2 - 2 \cos \theta^2 + 3)) (\sin \theta - 1) ;$$

The second gradient homogenized properties for triangular lattice expressed as:

$$\begin{Bmatrix} S_{xxx} \\ S_{xyy} \\ S_{yyy} \\ S_{xyx} \\ S_{yxx} \\ S_{yxx} \end{Bmatrix} = \begin{bmatrix} B_{11} & B_{12} & B_{13} & B_{14} & B_{15} & B_{16} \\ B_{21} & B_{22} & 0 & 0 & B_{25} & B_{26} \\ B_{31} & 0 & B_{33} & B_{34} & 0 & B_{36} \\ B_{41} & 0 & B_{43} & B_{44} & 0 & B_{46} \\ B_{51} & B_{52} & 0 & 0 & B_{55} & B_{56} \\ B_{61} & B_{62} & B_{63} & B_{64} & B_{65} & B_{66} \end{bmatrix} \begin{Bmatrix} \frac{\partial^2 u(x, y)}{\partial x^2} \\ \frac{\partial^2 u(x, y)}{\partial y^2} \\ \frac{\partial^2 v(x, y)}{\partial x^2} \\ \frac{\partial^2 v(x, y)}{\partial y^2} \\ \frac{\partial^2 v(x, y)}{\partial x \partial y} \\ \frac{\partial^2 u(x, y)}{\partial y \partial x} \\ \frac{\partial^2 v(x, y)}{\partial x^2} \end{Bmatrix} \quad (D5)$$

wherein these elements express as:

$$B_{11} = \frac{1}{64} (125 L^2 E \beta (\beta^2 + 1)) ; B_{12} = \frac{1}{64} (75 L^2 E \beta (\beta^2 + 1)) ; B_{13} = \frac{1}{128} (15 \sqrt{3} L^2 E \beta (\beta^2 + 1))$$

$$B_{14} = \frac{1}{128} (15 \sqrt{3} L^2 E \beta (\beta^2 + 1)) ; B_{15} = \frac{1}{128} (75 L^2 E \beta (\beta^2 + 1)) ; B_{16} = \frac{1}{64} (25 \sqrt{3} L^2 E \beta (\beta^2 + 1))$$

$$B_{21} = \frac{1}{64} (75L^2 E \beta (\beta^2 + 1)); B_{22} = \frac{1}{64} (45L^2 E \beta (\beta^2 + 1)); B_{25} = \frac{1}{128} (45L^2 E \beta (\beta^2 + 1))$$

$$B_{26} = \frac{1}{64} (15\sqrt{3}L^2 E \beta (\beta^2 + 1));$$

$$B_{31} = \frac{1}{64} (15\sqrt{3}L^2 E \beta (\beta^2 + 1)); B_{33} = \frac{1}{64} (9L^2 E \beta (\beta^2 + 1)); B_{34} = \frac{1}{128} (9L^2 E \beta (\beta^2 + 1))$$

$$B_{36} = \frac{1}{64} (15L^2 E \beta (\beta^2 + 1));$$

$$B_{41} = \frac{1}{128} (15\sqrt{3}L^2 E \beta (\beta^2 + 1)); B_{43} = \frac{1}{128} (9L^2 E \beta (\beta^2 + 1)); B_{44} = \frac{1}{128} (9L^2 E \beta (\beta^2 + 1));$$

$$B_{46} = \frac{1}{128} (15L^2 E \beta (\beta^2 + 1));$$

$$B_{51} = \frac{1}{128} (75L^2 E \beta (\beta^2 + 1)); B_{52} = \frac{1}{128} (45L^2 E \beta (\beta^2 + 1)); B_{55} = + \frac{1}{256} (45L^2 E \beta (\beta^2 + 1));$$

$$B_{56} = \frac{1}{128} (15\sqrt{3}L^2 E \beta (\beta^2 + 1));$$

$$B_{61} = \frac{1}{64} (25\sqrt{3}L^2 E \beta (\beta^2 + 1)); B_{62} = \frac{1}{64} (15\sqrt{3}L^2 E \beta (\beta^2 + 1)); B_{63} = \frac{1}{64} (15L^2 E \beta (\beta^2 + 1));$$

$$B_{64} = \frac{1}{128} (15L^2 E \beta (\beta^2 + 1)); B_{65} = \frac{1}{128} (15\sqrt{3}L^2 E \beta (\beta^2 + 1)); B_{66} = \frac{1}{64} (25L^2 E \beta (\beta^2 + 1));$$

Chapter 5

General conclusion and perspectives

This thesis focuses on studying the behavior of Timoshenko beams used as structural elements of architected materials, specifically looking at their nonlinearity and how it affects their stiffness. We start by examining the shape function of these beams and then proceed to develop a nonlinear stiffness matrix for the lattice unit cell. The purpose is to compare this matrix with the linear stiffness matrix and to understand the differences between them. Next, we investigate how the nonlinear kinematics of Timoshenko beam elements influence the propagation of waves in materials with specific architectures. We analyze how these nonlinear effects impact various wave propagation characteristics. We also aim to determine the relative contributions of linear, full nonlinear, and each nonlinear energy mode to the attributes of nonlinear wave dispersion. Finally, we study the propagation of fully nonlinear waves, considering shear, extension, and bending deformation modes, within homogenized periodic networks that have a hexagonal or triangular structure. By examining the nonlinear dynamical response of these networks, we gain insights into the behavior of fully nonlinear waves and their interactions within such architected materials.

In conclusion, this thesis has provided significant scientific insights into the nonlinear kinematics and wave propagation characteristics of architected materials, specifically focusing on Timoshenko beams and lattice structures. Through comprehensive analyses conducted across the different chapters, several key findings have emerged.

Chapter 2 specifically explored the nonlinear kinematics of Timoshenko beams, considering the interactions between shear, bending, and extension energies. The application of the Hamilton principle enabled the determination of nonlinear beam shape functions, as well as the mass matrix and nonlinear stiffness matrices. Importantly, the consideration of full nonlinear kinematics

highlighted the crucial role played by the nonlinear stiffness matrix, resulting in increased material stiffness due to the coupling effects among shear, bending, and extension modes.

Moving on to Chapter 3, the analysis centered on nonlinear wave propagation within repetitive lattice materials. The study revealed that the geometry of the unit cell significantly influenced the magnitude of nonlinear frequency correction compared to the reference linear frequency. Different lattice materials, including hexagonal, re-entrant hexagonal, square, and triangular unit cells, were examined. Notably, the hexagonal unit cell exhibited the highest nonlinear effect on the longitudinal mode, while the square unit cell displayed the lowest non-linear correction term. The energetic contributions to nonlinear wave correction frequency ranked shear energy as the most important, followed by extension energy, while bending had minimal impact. Additionally, the wave amplitude played a crucial role in the percentage of nonlinear correction. The occurrence of significant nonlinear effects was observed in the longitudinal mode for the major, lowest eigenmode, with the nonlinear correction decreasing as the frequency magnitude increased. Moreover, the internal architecture of the lattice played a significant role in controlling the nonlinear effect.

Chapter 4 focused on the comprehensive analysis of nonlinear homogenization in hexagonal and triangular lattice materials. The derived nonlinear wave equation enabled the study of two propagation modes: supersonic and subsonic. The analysis showcased the influence of the degree of nonlinearity and unit cell geometry on the frequency behavior of the lattice materials. Additionally, the investigation compared the impact of the full nonlinear energy analysis with that of solely considering shear energy, underscoring the greater influence of the fully nonlinear analysis, particularly in the subsonic mode and at higher degrees of nonlinearity.

Overall, this thesis has provided valuable scientific insights into the nonlinear kinematics of Timoshenko beams and the wave propagation characteristics of lattice materials. The findings highlight the importance of considering the full nonlinear kinematics, the unit cell geometry, and the contributions of different energy modes in understanding and analyzing the dynamical behavior of architected materials.

Perspectives

Theoretical and numerical developments in this study open up numerous perspectives for further exploration. However, in this section, we will only provide a brief outline of what we consider to be the most important perspectives based on our own opinion.

- To study the applicability of the non-linear kinematics and wave propagation models analyzed to engineering scenarios such as mechanical engineering, aerospace, biomechanics, and wave propagation control. This involves carrying out experimental studies or case studies to validate the theoretical results and understand their practical implications in the applications concerned by the aforementioned fields.
- To explore the influence of additional factors on the non-linear behavior of the systems studied. This may involve considering the non-linearity of materials, geometrical variations, temperature effects, or dynamic loading conditions to further improve the understanding of system response.
- Investigate the possibility of incorporating advanced computational methods or machine learning techniques to improve the accuracy and efficiency of the analysis. This could involve the development of new numerical algorithms or the use of data-driven approaches to capture complex non-linear behavior more efficiently.
- Investigate the dynamic stability and failure mechanisms of the systems studied under non-linear conditions. This may involve analyzing post-deformation behavior, identifying critical failure modes, or exploring strategies to improve system resilience and durability.
- To explore the possibilities of optimizing the design and performance of the systems analyzed based on the information obtained. This could involve developing optimization algorithms or design guidelines to achieve desired properties such as increased stiffness, improved energy dissipation, or adapted wave propagation characteristics.
- To study the behavior of analyzed systems under dynamic or extreme loading conditions. This may involve studying the response to impact, explosion, earthquake, or other transient events in order to understand non-linear behavior and develop strategies to mitigate potential risks.
- Extend the analysis to three-dimensional systems or complex geometries to explore non-linear behavior in more realistic scenarios. This involves developing new mathematical

models, calculation methods, or experimental devices to capture the full complexity of the response of three-dimensional structures.

- Investigate the potential of multi-scale analysis to bridge the gap between the microscopic and macroscopic behavior of the systems under study. This involves exploring how different length scales and material heterogeneities influence the non-linear response and developing effective homogenization techniques.
- Exploring interdisciplinary applications of the results by collaborating with researchers in other fields such as biomechanics, acoustics, and materials design. This could lead to innovative solutions in areas such as bio-engineering, noise control and the development of advanced materials.

Résumé de la thèse en français

Introduction

Tout au long de l'histoire, l'humanité a fait d'importantes découvertes dans le domaine des matériaux et des techniques de fabrication, ce qui a eu des répercussions sur la société. Les avancées technologiques récentes, telles que la fabrication additive et la manipulation de la matière au niveau atomique, ont créé de nouvelles possibilités de conception et de production de matériaux dotés de propriétés mécaniques exceptionnelles et d'autres propriétés multiphysiques. Les ingénieurs dans le domaine de la science des matériaux ont adopté un nouveau paradigme en considérant l'architecture interne du matériau comme un facteur supplémentaire, appelé "architecture interne du matériau". Cette approche [1] vise à créer des matériaux à la fois fonctionnels et visuellement attrayants, rappelant l'élégance de structures telles que la Tour Eiffel. Un matériau architecturé est un matériau qui combine de manière synergique plusieurs matériaux de base plus simples. Cette combinaison implique souvent un arrangement hiérarchique de différentes échelles, conduisant à l'émergence de nouvelles caractéristiques de performance. L'architecture interne des matériaux architecturés offre une vaste gamme d'options de conception, permettant la création de matériaux aux propriétés diverses et personnalisées. Les attributs de performance de ces matériaux peuvent être visualisés et condensés dans des diagrammes d'Ashby, comme le montre la Fig.R1, tels que le module, la résistance et la densité.

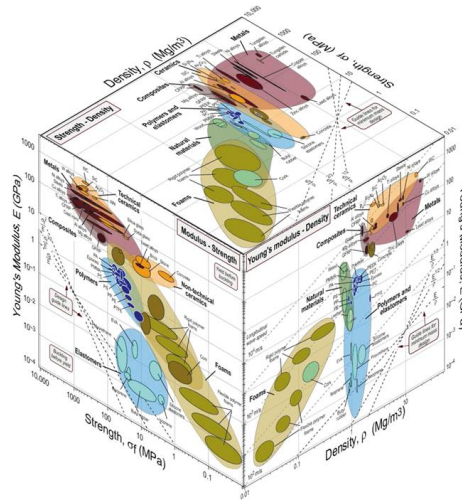


Fig.R. 1 : Caractérisation de l'interaction entre la résistance, le module et la densité dans diverses classes de matériaux : Diagramme de performance d'Ashby en 3D pour les matériaux d'ingénierie [5]

Les matériaux architecturés sont généralement caractérisés par une cellule unitaire avec un arrangement périodique, ce qui permet une fabrication et une modélisation pratiques. Des exemples de matériaux cellulaires avec des architectures régulières sont présentés à la Fig.R.2, bien que la microstructure réelle puisse ne pas être parfaitement périodique.

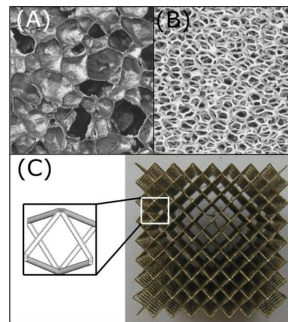


Fig.R. 2: Illustration de différents types de matériaux cellulaires : (A) mousse à cellules fermées, (B) mousse à cellules ouvertes, (C) matériau cellulaire régulier (cellule unitaire cubique centrée sur le corps BCC) [6].

La conception des matériaux est souvent intégrée à la mécanique des structures, mais cette méthodologie repose sur l'heuristique, l'expérience et l'intuition du concepteur. Les métamatériaux constituent une classe distincte de matériaux qui possèdent des attributs mécaniques que l'on ne

trouve généralement pas dans les matériaux naturels. Les métamatériaux ont la capacité d'ajuster les propriétés effectives du matériau au niveau de la cellule unitaire en modifiant la topologie interne, plutôt que de s'appuyer uniquement sur des changements de composition chimique. Le coefficient de Poisson est une mesure des propriétés des matériaux, et les matériaux auxétiques présentent des caractéristiques statiques et dynamiques exceptionnelles, telles qu'une résistance élevée aux chocs et aux impacts, l'atténuation des vibrations et la manipulation des ondes sonores. Le lien entre les matériaux architecturés et la non-linéarité est lié à la manière dont les conditions de chargement affectent la réponse mécanique de la structure. Les grandes déformations, la non-linéarité des matériaux, les non-linéarités géométriques et les conditions aux limites peuvent entraîner un comportement non linéaire. Dans l'analyse structurelle, deux types importants de non-linéarité sont la non-linéarité matérielle et la non-linéarité géométrique [8,9]. La non-linéarité géométrique se produit lorsque la déformation d'une structure est suffisamment importante pour entraîner des changements significatifs dans sa géométrie. Une porosité interne élevée associée à la présence d'éléments élancés peut entraîner des rotations et des déplacements internes importants qui ne sont pas nécessairement associés à des déformations ou des moments de flexion importants. Les structures soumises à de fortes charges, où la déformation est supérieure au seuil standard de 5 %, peuvent présenter des non-linéarités. Ces non-linéarités comprennent les problèmes de contact, où la relation force-déplacement ou déformation-déformation est essentiellement non linéaire. Des modèles de matériaux peuvent être utilisés pour décrire un tel comportement, tels que des modèles non linéaires élastiques, élastoplastiques, viscoélastiques ou viscoplastiques. Le comportement idéal d'un matériau élastique et entièrement plastique est illustré à la Fig.R.3, où la pente initiale de la région élastique diminue fortement jusqu'à zéro, ce qui permet au matériau de se déformer indéfiniment sans subir d'augmentation supplémentaire de la contrainte. Cependant, jusqu'à la contrainte maximale du matériau, presque tous les matériaux réels présentent un certain écrouissage.

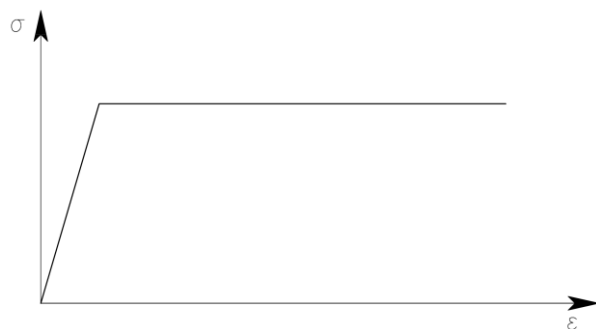


Fig.R. 3 : Exploration de la non-linéarité des matériaux à l'aide d'un comportement élastique et parfaitement plastique [13]

La non-linéarité géométrique est liée aux grandes déformations ou aux changements dans la géométrie d'une structure, tandis que la non-linéarité matérielle est liée à la réponse du matériau lui-même. Pour un examen approfondi et réaliste des structures et des matériaux, les deux types de non-linéarité doivent être pris en compte.

Les méthodes d'homogénéisation remplacent les structures hétérogènes par des milieux de substitution équivalents aux propriétés efficaces, en évitant les coûts numériques élevés. Ces méthodes impliquent l'identification d'une cellule unitaire, sa traduction pour générer la structure entière, et l'homogénéisation à la cellule unitaire de référence entourant la microstructure. Il existe deux types de méthodes d'homogénéisation : l'homogénéisation continue, traditionnellement utilisée pour les composites, et la continualisation ou les techniques d'homogénéisation discrète, qui utilisent des modèles condensés et discrets pour les éléments structurels. L'homogénéisation discrète (DH) convient aux matériaux en treillis de faible densité, car elle offre une efficacité de calcul et des formules mathématiques simples pour les modules homogénéisés. Les méthodes d'homogénéisation continue remplacent les équations de mouvement discrètes par des équations différentielles continues afin de déterminer les propriétés effectives statiques et dynamiques des treillis périodiques à un niveau continu. La formulation lagrangienne, introduite il y a deux décennies, fournit une approche alternative pour décrire la statique ou la dynamique des treillis. Le développement de méthodes de calcul efficaces pour incorporer la non-linéarité matérielle et géométrique dans l'homogénéisation discrète est un sujet d'intérêt [22–24].

Au cours des deux dernières décennies, des recherches importantes ont été consacrées à l'analyse de la propagation des ondes dans les réseaux périodiques, en particulier en termes d'atténuation des ondes et de bandes interdites. Les propriétés de propagation des ondes dans les réseaux périodiques dépendent de l'architecture interne, notamment des propriétés géométriques et matérielles. Les configurations des cellules unitaires peuvent restreindre la propagation des ondes dans une gamme de fréquences spécifique, créant ainsi des bandes interdites. Le théorème de Bloch peut déterminer les caractéristiques de propagation des ondes des structures périodiques, ce qui permet d'étudier la propagation des ondes à l'intérieur d'une seule cellule unitaire. Les études de sensibilité à haute paramétrie sont cruciales pour comprendre la structure de bande des matériaux d'architecture [33].

Cependant, seul un nombre limité d'auteurs a étudié la propagation des ondes dans les milieux non linéaires. La propagation d'ondes non linéaires dans des structures périodiques conduit à une relation de dispersion dépendant de l'amplitude, qui permet un réglage passif de la structure de la bande de dispersion. Les solutions aux équations de propagation des ondes dans les structures périodiques non linéaires sont plus complexes que les solutions au plan harmonique des équations d'ondes linéaires [37–41]. Des études sur l'impact de la précontrainte ou de la pré-déformation sur la propagation des ondes dans les milieux homogènes anisotropes ont également été menées, mais l'étude de l'influence des déformations élastiques finies sur la propagation des ondes reste un défi important. Des études antérieures ont analysé les propriétés effectives incrémentielles de milieux homogènes précontraints soumis à de grandes déformations, en imposant des restrictions sur l'énergie de déformation pour s'assurer que les ondes élastiques peuvent au sein de la structure.

Travail de thèse

Cette thèse vise à formuler une théorie non linéaire de Timoshenko pour les matériaux périodiques en réseau de type Cauchy en utilisant un modèle de la mécanique des poutres au niveau du réseau périodique. Les matrices de rigidité non linéaire et linéaire pour une poutre de Timoshenko sont calculées, et les équations différentielles et les conditions aux limites associées sont obtenues. Les fonctions de forme sont extraites, ce qui permet d'obtenir les matrices de masse, de rigidité linéaire et de rigidité non linéaire. Nous obtenons l'expression de l'énergie de déformation non linéaire à partir de l'intégration de la densité d'énergie de déformation sur la longueur de la poutre :

$$\begin{aligned}
 U = & \int_0^L \left[\underbrace{\frac{1}{2} k_s GA (u_{z,x} - \phi)^2 + \frac{(\lambda + 2G)}{2} (u_{x,x})^2 A + \frac{EI}{2} (\phi_x)^2}_{\text{linear}} \right] dx + \underbrace{\int_0^L \frac{EA}{8} \phi^2 dx}_{\text{linear term related to non-linear theory}} \\
 & + \int_0^L \left[\underbrace{\frac{G}{2} \left(\phi^2 (u_{x,x})^2 - 2\phi u_{x,x} u_{z,x} + 2\phi^2 u_{x,x} \right) A (k_k k_s) + \frac{1}{8} EA (u_{x,x})^4 + \frac{1}{8} k_s EA (u_{z,x})^4}_{\text{non-linear}} \right. \\
 & \left. + \frac{EA}{4} k_s (u_{z,x})^2 u_{x,x}^2 + \frac{EA}{2} (u_{x,x})^3 + \frac{EA}{2} k_s u_{x,x} (u_{z,x})^2 + \frac{\lambda A}{2} u_{x,x} \phi^2 + \frac{\lambda A}{4} u_{x,x}^2 \phi^2 \right. \\
 & \left. + \frac{\lambda A}{4} (u_{z,x})^2 \phi^2 \right] dx
 \end{aligned}$$

Après avoir effectué plusieurs calculs et utilisé l'équation d'équilibre de l'énergie d'expression non linéaire, nous obtenons l'expression de la forme non linéaire de la poutre de Timoshenko. Nous

calculons ensuite les matrices de masse, de rigidité linéaire et non linéaire, où ces fonctions de forme sont utilisées pour calculer les matrices de bourrage non linéaire. La matrice de rigidité non linéaire augmente considérablement la rigidité du matériau en raison des couplages entre le cisaillement, la flexion et l'extension.

Dans le deuxième chapitre, nous analysons les caractéristiques de dispersion des ondes au sein de matériaux architecturés bidimensionnels, en considérant à la fois les régimes linéaires et non linéaires. Nous examinons comment les modes de déformation par cisaillement, extension et flexion dans les cellules unitaires carrées, triangulaires, hexagonales et hexagonales rentrantes influencent la déformation interne du matériau. Notre étude comprend une analyse dynamique menée à haute et basse fréquence, ainsi que pour deux amplitudes d'ondes différentes. En utilisant la méthode de perturbation de Linstedt-Poincaré, nous évaluons la correction non linéaire du diagramme de dispersion, puis nous étudions le facteur de correction non linéaire du comportement de dispersion en individualisant les énergies de cisaillement, d'extension et de flexion pour différents matériaux architecturés pour le mode longitudinal.

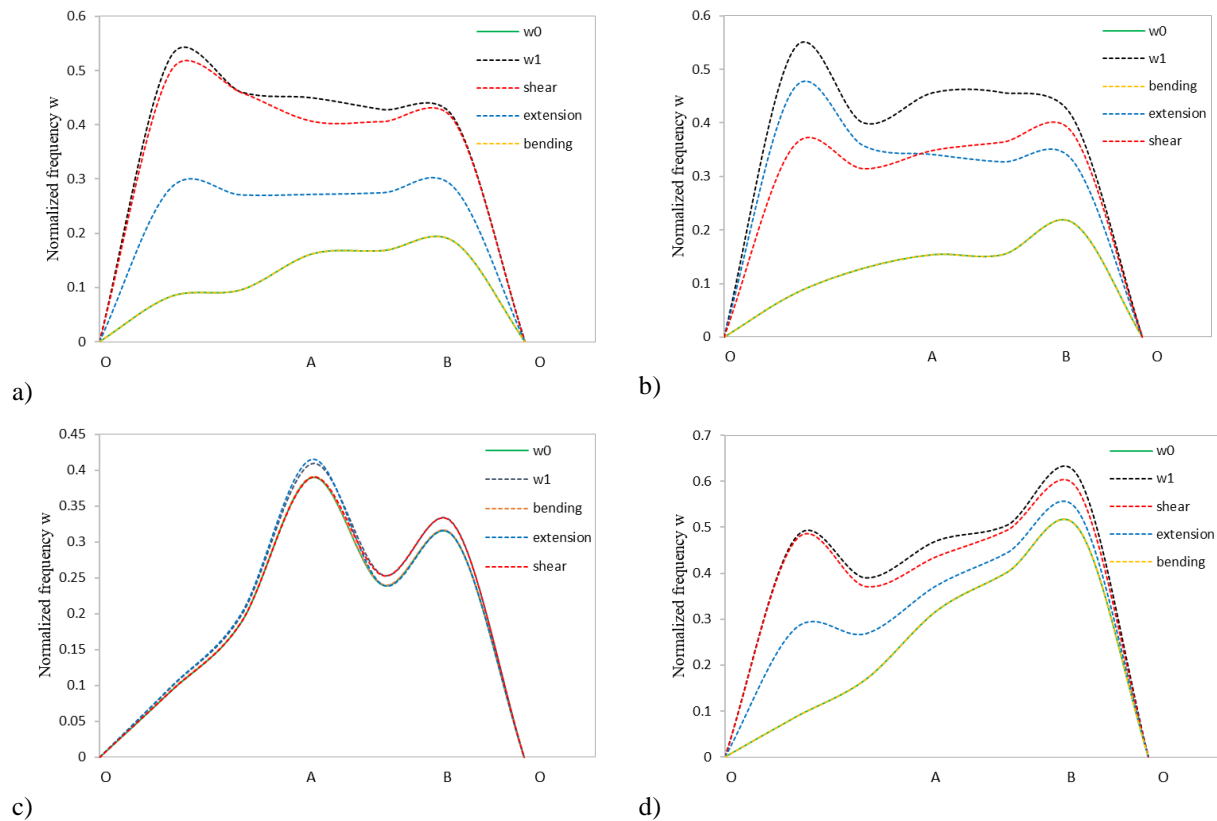


Fig.R. 4: Diagramme de dispersion d'un matériau architecturé pour la fréquence du mode longitudinal avec des cellules unitaires hexagonales (a), hexagonales rentrantes (b), carrées (c) et triangulaires (d). Ligne verte continue : solution linéaire. Correction non linéaire pour la cinématique non linéaire complète (lignes pointillées noires), pour le mode de cisaillement non linéaire seul (lignes pointillées rouges), pour le mode d'extension non linéaire (lignes pointillées bleues), pour le mode de flexion non linéaire (lignes pointillées orange).

Dans la Fig.R.4, nous étudions le facteur de correction non linéaire pour le comportement de dispersion en individualisant les énergies de cisaillement, d'extension et de flexion pour différents matériaux architecturés pour le mode longitudinal. Nous observons que pour tous les matériaux architecturés considérés, l'énergie de cisaillement a l'effet le plus élevé dans la correction non linéaire en ce qui concerne les effets énergétiques, et le diagramme de dispersion montre que l'effet de la flexion sur le mode de correction est presque négligeable. Ces résultats sont cohérents avec le fait que les treillis carrés et triangulaires se comportent de manière plus rigide que le treillis hexagonal dominé par la flexion. L'interprétation des résultats précédents est que les cellules unitaires dominées par la flexion se déforment plus facilement et sont donc sujettes à une plus grande variation d'énergie par rapport à la réponse linéaire. En outre, la position du point d'étude de la zone de Brillouin joue un rôle important dans les effets énergétiques sur les caractéristiques de dispersion. Les treillis dominés par la flexion sont sujets à des écarts de bande partiels plus importants entre les différents types d'ondes (extension, cisaillement, flexion) par rapport au treillis triangulaire dominé par la tension.

Dans le chapitre 4, nous analysons la propagation d'ondes entièrement non linéaires, englobant les modes de déformation par cisaillement, extension et flexion, à l'intérieur de réseaux hexagonaux et triangulaires périodiques non linéaires homogénéisés. L'analyse des ondes est effectuée en construisant la densité d'énergie de déformation effective des réseaux hexagonaux et triangulaires périodiques dans le régime non linéaire par une continualisation des équations discrètes du réseau, en tenant compte de toutes les formes d'énergie. Nous incorporons dans le modèle continu les effets de gradient de déformation afin de tenir compte de la nature dispersive des ondes. Le continuum non linéaire à gradient du deuxième ordre qui en résulte présente deux modes de propagation distincts : un mode subsonique évanescent et un mode supersonique. Nous examinons dans une situation 1D la réponse des treillis hexagonaux et triangulaires, en considérant différents

niveaux de non-linéarité. Dans la Fig.R.5, nous étudions le comportement de la propagation d'ondes entièrement non linéaires dans le matériau interne des treillis hexagonaux et triangulaires à différents degrés de non-linéarité.

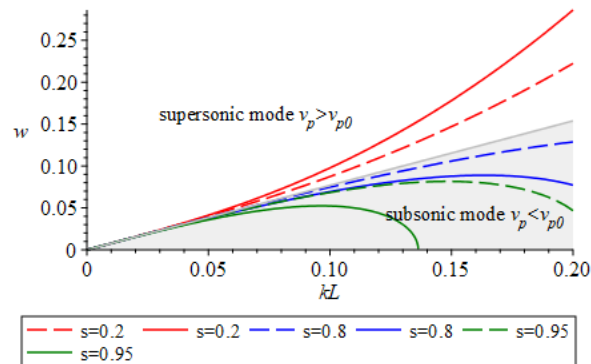


Fig.R. 5: Relation de dispersion dans le réseau hexagonal (ligne continue) et triangulaire (ligne pointillée) pour différentes valeurs de $s = 0,2$, $s = 0,8$ et $s = 0,95$

La Fig.R.5 montre la réponse des treillis hexagonaux et triangulaires à différents degrés de non-linéarité. Pour une valeur $s = 0,2$ et pour le mode supersonique, le treillis hexagonal présente une réponse plus élevée que le treillis triangulaire. Cependant, lorsque le degré de non-linéarité augmente jusqu'à $s = 0,8$ et $s = 0,95$, et lorsque nous atteignons le mode supersonique, nous atteignons le mode subsonique, le comportement de la fréquence dans le treillis hexagonal devient significativement plus important par rapport au treillis triangulaire. L'analyse non linéaire de la propagation des ondes est ensuite étendue à une situation 2D pour les deux mêmes treillis. Nous comparons les modes longitudinaux et de cisaillement pour les treillis hexagonaux et triangulaires.

En conclusion, nous examinons le comportement des poutres de Timoshenko et leur non-linéarité, en nous concentrant sur leur rigidité. Elle examine la fonction de forme de ces poutres et développe une matrice de rigidité non linéaire à comparer à la matrice de rigidité linéaire. L'étude examine comment la cinématique non linéaire des éléments de la poutre de Timoshenko influence la propagation des ondes dans des matériaux d'architectures spécifiques. L'analyse examine également les contributions des modes d'énergie linéaires et non linéaires complets et de chaque mode non linéaire à la dispersion non linéaire des ondes.

En outre, nous examinons la propagation d'ondes entièrement non linéaires dans des réseaux périodiques homogénéisés avec une structure hexagonale ou triangulaire. L'analyse révèle que la géométrie de la cellule unitaire influence de manière significative l'ampleur de la correction de la fréquence non linéaire par rapport à la fréquence linéaire de référence. La cellule unitaire hexagonale a présenté l'effet non linéaire le plus élevé sur le mode longitudinal, tandis que la cellule unitaire carrée a exhibé le terme de correction non linéaire le plus faible. L'énergie de cisaillement était la contribution énergétique la plus importante à la fréquence de correction non linéaire des ondes, suivie par l'énergie d'extension. L'amplitude de la vague a également joué un rôle crucial dans le pourcentage de correction non linéaire. Le chapitre 4 s'est concentré sur l'analyse complète de l'homogénéisation non linéaire dans les matériaux à treillis hexagonal et triangulaire. L'équation d'onde non linéaire dérivée a permis d'étudier deux modes de propagation : supersonique et subsonique. L'étude a comparé l'impact de l'analyse de l'énergie non linéaire complète avec la prise en compte de l'énergie de cisaillement, en soulignant l'influence plus importante de l'analyse non linéaire complète en mode subsonique et à des degrés de non-linéarité plus élevés. En conclusion, cette recherche fournit des informations scientifiques précieuses sur la cinématique non linéaire et les caractéristiques de propagation des ondes des matériaux architecturés, en particulier les poutres de Timoshenko et les structures en treillis.

Perspectives

Les développements théoriques et numériques de cette thèse ouvrent de nombreuses perspectives à explorer. Cependant, dans cette section, nous ne donnerons qu'un bref aperçu de ce que nous considérons comme les perspectives les plus importantes, selon notre propre opinion.

1. Étudier l'applicabilité des modèles de cinématique non linéaire et de propagation des ondes analysés à des scénarios d'ingénierie tels que la construction mécanique, l'aérospatial, la biomécanique, le contrôle de la propagation des ondes. Cela implique la réalisation d'études expérimentales ou d'études de cas pour valider les résultats théoriques et comprendre leurs implications pratiques dans les applications concernées par les domaines précités.
2. Explorer l'influence de facteurs supplémentaires sur le comportement non linéaire des systèmes étudiés. Il peut s'agir de prendre en compte la non-linéarité des matériaux, les

variations géométriques, les effets de la température ou les conditions de charge dynamique afin d'améliorer encore la compréhension de la réponse des systèmes.

3. Étudier la possibilité d'intégrer des méthodes informatiques avancées ou des techniques d'apprentissage automatique pour améliorer la précision et l'efficacité de l'analyse. Cela pourrait impliquer le développement de nouveaux algorithmes numériques ou l'utilisation d'approches basées sur les données pour saisir plus efficacement le comportement non linéaire complexe.
4. Étudier la stabilité dynamique et les mécanismes de défaillance des systèmes étudiés dans des conditions non linéaires. Il peut s'agir d'analyser le comportement après déformation, d'identifier les modes de défaillance critiques ou d'explorer des stratégies visant à améliorer la résilience et la durabilité du système.
5. Explorer les possibilités d'optimisation de la conception et des performances des systèmes analysés sur la base des informations obtenues. Il pourrait s'agir de développer des algorithmes d'optimisation ou des lignes directrices de conception pour obtenir les propriétés souhaitées telles qu'une rigidité accrue, une meilleure dissipation de l'énergie ou des caractéristiques de propagation des ondes adaptées.
6. Étudier le comportement des systèmes analysés dans des conditions de charge dynamique ou extrême. Il peut s'agir d'étudier la réponse à un impact, à une explosion, à un séisme ou à d'autres événements transitoires afin de comprendre le comportement non linéaire et d'élaborer des stratégies pour atténuer les risques potentiels.
7. Étendre l'analyse à des systèmes tridimensionnels ou à des géométries complexes pour explorer le comportement non linéaire dans des scénarios plus réalistes. Cela implique le développement de nouveaux modèles mathématiques, de méthodes de calcul ou de dispositifs expérimentaux pour saisir toute la complexité de la réponse de structures tridimensionnelles.
8. Étudier le potentiel de l'analyse multi-échelle pour combler le fossé entre le comportement microscopique et macroscopique des systèmes étudiés. Cela implique l'exploration de la manière dont les différentes échelles de longueur et les hétérogénéités des matériaux influencent la réponse non linéaire et le développement de techniques d'homogénéisation efficaces.

9. Explorer les applications interdisciplinaires des résultats en collaborant avec des chercheurs d'autres domaines tels que la biomécanique, l'acoustique ou la conception de matériaux. Cela pourrait déboucher sur des solutions innovantes dans des domaines tels que la bio-ingénierie, le contrôle du bruit ou le développement de matériaux avancés.

References

- [1] M.F. Ashby, Y.J.M. Bréchet, Designing hybrid materials, *Acta Mater.* 51 (2003) 5801–5821. [https://doi.org/10.1016/S1359-6454\(03\)00441-5](https://doi.org/10.1016/S1359-6454(03)00441-5).
- [2] H. Loyrette, *Gustave Eiffel*, Rizzoli International Publications, New York, 1885.
- [3] J. Harriss, *The Tallest Tower*, Unlimited Publishing LLC, 2004.
- [4] M.J. Kirkby, *The fractal geometry of nature*. Benoit B. Mandelbrot. W. H. Freeman and co., San Francisco, 1982. No. of pages: 460. Price: £22.75 (hardback), *Earth Surf. Process. Landforms.* 8 (1983) 406–406. <https://doi.org/10.1002/esp.3290080415>.
- [5] J.R. Greer, V.S. Deshpande, Three-dimensional architected materials and structures: Design, fabrication, and mechanical behavior, *MRS Bull.* 44 (2019) 750–757. <https://doi.org/10.1557/mrs.2019.232>.
- [6] M. Benedetti, A. du Plessis, R.O. Ritchie, M. Dallago, S.M.J. Razavi, F. Berto, Architected cellular materials: A review on their mechanical properties towards fatigue-tolerant design and fabrication, *Mater. Sci. Eng. R Reports.* 144 (2021) 100606. <https://doi.org/10.1016/j.mser.2021.100606>.
- [7] N. Karathanasopoulos, F. Dos Reis, H. Reda, J.F. Ganghoffer, Computing the effective bulk and normal to shear properties of common two-dimensional architected materials, *Comput. Mater. Sci.* 154 (2018) 284–294. <https://doi.org/10.1016/j.commatsci.2018.07.044>.
- [8] K.K. Riyas Moideen, U.K. Dewangan, Effect of Material Nonlinearity on Deflection of Beams and Frames, *Indian J. Sci. Technol.* 9 (2016). <https://doi.org/10.17485/ijst/2016/v9i28/92375>.
- [9] P. Wriggers, Nonlinear finite element methods, *Nonlinear Finite Elem. Methods.* (2008) 1–559. <https://doi.org/10.1007/978-3-540-71001-1>.
- [10] D. Nolan, C. Lally, Coupled finite element-agent-based models for the simulation of vascular growth and remodeling, *Numer. Methods Adv. Simul. Biomech. Biol. Process.* (2018) 283–300. <https://doi.org/10.1016/B978-0-12-811718-7.00016-2>.
- [11] D. Nolan, C. Lally, Coupled finite element-agent-based models for the simulation of vascular growth and remodeling, Elsevier Ltd, 2018. <https://doi.org/10.1016/B978-0-12-811718-7.00016-2>.
- [12] K. Elnady, Nonlinear constitutive models for lattice materials by discrete homogenization methods at large strains . Application to biomembranes and textiles Khaled Elnady To cite this version : HAL Id : tel-01751488 soutenance et mis à disposition de l ’ ensemble d, (2018).
- [13] H.G. Payer, H. Matthies, Nonlinear finite element analysis of ship and offshore structures, *Comput. Struct.* 26 (1987) 325–337. [https://doi.org/10.1016/0045-7949\(87\)90262-8](https://doi.org/10.1016/0045-7949(87)90262-8).
- [14] N. Mawassy, J.F. Ganghoffer, H. Reda, S.E. Alavi, H. Lakiss, Analysis of surface effects based on first and second strain gradient mechanics, *Mech. Mater.* 175 (2022) 104462. <https://doi.org/10.1016/j.mechmat.2022.104462>.
- [15] J. Ganghoffer, A. Wazne, H. Reda, Frontiers in homogenization methods towards generalized continua for architected materials, *Mech. Res. Commun.* 130 (2023) 104114. <https://doi.org/10.1016/j.mechrescom.2023.104114>.
- [16] F. Dos Reis, J.F. Ganghoffer, Equivalent mechanical properties of auxetic lattices from discrete

- homogenization, *Comput. Mater. Sci.* 51 (2012) 314–321.
<https://doi.org/10.1016/j.commatsci.2011.07.014>.
- [17] Z.P. Bažant, M. Christensen, Analogy between micropolar continuum and grid frameworks under initial stress, *Int. J. Solids Struct.* 8 (1972) 327–346. [https://doi.org/10.1016/0020-7683\(72\)90093-5](https://doi.org/10.1016/0020-7683(72)90093-5).
- [18] A. Bacigalupo, L. Gambarotta, Identification of non-local continua for lattice-like materials, *Int. J. Eng. Sci.* 159 (2021). <https://doi.org/10.1016/j.ijengsci.2020.103430>.
- [19] H. Askes, A. V. Metrikine, Higher-order continua derived from discrete media: Continualisation aspects and boundary conditions, *Int. J. Solids Struct.* 42 (2005) 187–202.
<https://doi.org/10.1016/j.ijsolstr.2004.04.005>.
- [20] R.S. Kumar, D.L. McDowell, Generalized continuum modeling of 2-D periodic cellular solids, *Int. J. Solids Struct.* 41 (2004) 7399–7422. <https://doi.org/10.1016/j.ijsolstr.2004.06.038>.
- [21] A. V. Metrikine, H. Askes, One-dimensional dynamically consistent gradient elasticity models derived from a discrete microstructure: Part 1: Generic formulation, *Eur. J. Mech. A/Solids.* 21 (2002) 555–572. [https://doi.org/10.1016/S0997-7538\(02\)01218-4](https://doi.org/10.1016/S0997-7538(02)01218-4).
- [22] H. Reda, Y. Rahali, J.F. Ganghoffer, H. Lakiss, Wave propagation analysis in 2D nonlinear hexagonal periodic networks based on second order gradient nonlinear constitutive models, *Int. J. Non. Linear. Mech.* 87 (2016) 85–96. <https://doi.org/10.1016/j.ijnonlinmec.2016.10.002>.
- [23] H. Reda, Y. Rahali, J.F. Ganghoffer, H. Lakiss, Wave propagation analysis in 2D nonlinear hexagonal periodic networks based on second order gradient nonlinear constitutive models, *Int. J. Non. Linear. Mech.* 87 (2016) 85–96. <https://doi.org/10.1016/j.ijnonlinmec.2016.10.002>.
- [24] H. Reda, Y. Rahali, J.F. Ganghoffer, H. Lakiss, Nonlinear dynamical analysis of 3D textiles based on second order gradient homogenized media, *Compos. Struct.* 154 (2016) 538–555.
<https://doi.org/10.1016/j.compstruct.2016.07.053>.
- [25] R.S. Langley, The response of two-dimensional periodic structures to impulsive point loading, 1997. <https://doi.org/10.1006/jsvi.1996.0744>.
- [26] J.H. Lee, J.P. Singer, E.L. Thomas, Micro-/nanostructured mechanical metamaterials, *Adv. Mater.* 24 (2012) 4782–4810. <https://doi.org/10.1002/adma.201201644>.
- [27] N. Karathanasopoulos, H. Reda, J. Francois Ganghoffer, Designing two-dimensional metamaterials of controlled static and dynamic properties, *Comput. Mater. Sci.* 138 (2017) 323–332.
<https://doi.org/10.1016/j.commatsci.2017.06.035>.
- [28] A.S. Phani, J. Woodhouse, N. Fleck, A.S. Phani, J. Woodhouse, N.F. Wave, A.S. Phani, J. Woodhouse, N.A. Fleck, Wave propagation in two-dimensional periodic lattices To cite this version : HAL Id : hal-02273392, 119 (2019).
- [29] M.I. Hussein, M.J. Leamy, M. Ruzzene, Dynamics of phononic materials and structures: Historical origins, recent progress, and future outlook, *Appl. Mech. Rev.* 66 (2014).
<https://doi.org/10.1115/1.4026911>.
- [30] D.J. Mead, Wave propagation in continuous periodic structures: Research contributions from Southampton, 1964-1995, *J. Sound Vib.* 190 (1996) 495–524.
<https://doi.org/10.1006/jsvi.1996.0076>.
- [31] K.F. Tee, A. Spadoni, F. Scarpa, M. Ruzzene, Wave propagation in auxetic tetrachiral

- honeycombs, *J. Vib. Acoust. Trans. ASME*. 132 (2010) 0310071–0310078.
<https://doi.org/10.1115/1.4000785>.
- [32] M.I. Hussein, Theory of damped Bloch waves in elastic media, *Phys. Rev. B - Condens. Matter Mater. Phys.* 80 (2009). <https://doi.org/10.1103/PhysRevB.80.212301>.
- [33] S. Gonella, M. Ruzzene, Analysis of in-plane wave propagation in hexagonal and re-entrant lattices, *J. Sound Vib.* 312 (2008) 125–139. <https://doi.org/10.1016/j.jsv.2007.10.033>.
- [34] M. Lepidi, A. Bacigalupo, Parametric design of the band structure for lattice materials, *Meccanica*. 53 (2018) 613–628. <https://doi.org/10.1007/s11012-017-0644-y>.
- [35] M. Lepidi, A. Bacigalupo, Multi-parametric sensitivity analysis of the band structure for tetrachiral acoustic metamaterials, *Int. J. Solids Struct.* 136–137 (2018) 186–202.
<https://doi.org/10.1016/j.ijsolstr.2017.12.014>.
- [36] A. Bacigalupo, M. Lepidi, G. Gnecco, F. Vadalà, L. Gambarotta, Optimal design of the band structure for beam lattice metamaterials, *Front. Mater.* 6 (2019).
<https://doi.org/10.3389/fmats.2019.00002>.
- [37] P.L. Bhatnagar, *Nonlinear waves in one-dimensional dispersive systems.*, Oxford, 1979.
<https://doi.org/10.1112/blms/14.3.267>.
- [38] R.W. Ogden, D.G. Roxburgh, The effect of pre-stress on the vibration and stability of elastic plates, *Int. J. Eng. Sci.* 31 (1993) 1611–1639. [https://doi.org/10.1016/0020-7225\(93\)90079-A](https://doi.org/10.1016/0020-7225(93)90079-A).
- [39] A. V Porubov, *Amplification of Nonlinear Strain Waves in Solids*, WORLD SCIENTIFIC, 2003.
<https://doi.org/10.1142/5238>.
- [40] H. Reda, N. Karathanasopoulos, J.F. Ganghoffer, H. Lakiss, Wave propagation characteristics of periodic structures accounting for the effect of their higher order inner material kinematics, *J. Sound Vib.* 431 (2018) 265–275. <https://doi.org/10.1016/j.jsv.2018.06.006>.
- [41] N. Karathanasopoulos, H. Reda, J.F. Ganghoffer, The role of non-slender inner structural designs on the linear and non-linear wave propagation attributes of periodic, two-dimensional architected materials, *J. Sound Vib.* 455 (2019) 312–323. <https://doi.org/10.1016/j.jsv.2019.05.011>.
- [42] W.J. Parnell, Effective wave propagation in a pre-stressed nonlinear elastic composite bar, *Proc. 5th Eur. Conf. Const. Model. Rubber, ECCMR 2007.* (2008) 361–366.
- [43] C. Daraio, V.F. Nesterenko, E.B. Herbold, S. Jin, Tunability of solitary wave properties in one-dimensional strongly nonlinear phononic crystals, *Phys. Rev. E - Stat. Nonlinear, Soft Matter Phys.* 73 (2006). <https://doi.org/10.1103/PhysRevE.73.026610>.
- [44] S. SEN, J. HONG, J. BANG, E. AVALOS, R. DONEY, Solitary waves in the granular chain, *Phys. Rep.* 462 (2008) 21–66. <https://doi.org/10.1016/j.physrep.2007.10.007>.
- [45] A.F. Vakakis, M.E. King, A.J. Pearlstein, Forced localization in a periodic chain of non-linear oscillators, *Int. J. Non. Linear. Mech.* 29 (1994) 429–447. [https://doi.org/10.1016/0020-7462\(94\)90013-2](https://doi.org/10.1016/0020-7462(94)90013-2).
- [46] A.F. and M.E.K. Vakakis, Nonlinear wave transmission in a monocoupled elastic periodic system., *J. Acoust. Soc. Am.* (1995).
- [47] I. Paper, NON-LINEAR NORMAL MODES (NNM s) AND THEIR APPLICATIONS IN VIBRATION THEORY : AN OVERVIEW, *Mech. Syst. Signal Process.* 11 (1997) 3–22.

- [48] A.F. Vakakis, M.E. King, Resonant oscillations of a weakly coupled, nonlinear layered system, *Acta Mech.* 128 (1998) 59–80. <https://doi.org/10.1007/BF01463160>.
- [49] Y. Starosvetsky, A.F. Vakakis, Traveling waves and localized modes in one-dimensional homogeneous granular chains with no precompression, *Phys. Rev. E - Stat. Nonlinear, Soft Matter Phys.* 82 (2010). <https://doi.org/10.1103/PhysRevE.82.026603>.
- [50] B. PL, *Nonlinear Waves in One-Dimensional Dispersive Systems*, Clarendon Press, Oxford, 1979.
- [51] I. V. Andrianov, V. V. Danishevs'kyy, O.I. Ryzhkov, D. Weichert, Dynamic homogenization and wave propagation in a nonlinear 1D composite material, *Wave Motion.* 50 (2013) 271–281. <https://doi.org/10.1016/j.wavemoti.2012.08.013>.
- [52] H. Reda, Y. Rahali, J.F. Ganghoffer, H. Lakiss, Wave propagation in 3D viscoelastic auxetic and textile materials by homogenized continuum micropolar models, *Compos. Struct.* 141 (2016) 328–345. <https://doi.org/10.1016/j.compstruct.2016.01.071>.
- [53] H. Reda, K. Elnady, J.F. Ganghoffer, H. Lakiss, Wave propagation in pre-deformed periodic network materials based on large strains homogenization, *Compos. Struct.* 184 (2018) 860–871. <https://doi.org/10.1016/j.compstruct.2017.10.054>.
- [54] H. Reda, Y. Rahali, J.F. Ganghoffer, H. Lakiss, Nonlinear dynamical analysis of 3D textiles based on second order gradient homogenized media, *Compos. Struct.* 154 (2016) 538–555. <https://doi.org/10.1016/j.compstruct.2016.07.053>.
- [55] S. Tadjono, A. Han, D.-K. Nguyen, S. Kiryu, B.S. Gan, Exact Shape Functions for Timoshenko Beam Element, *IOSR J. Comput. Eng.* 19 (2017) 12–20. <https://doi.org/10.9790/0661-1903041220>.
- [56] A. Bazoune, Y.A. Khulief, N.G. Stephen, Shape functions of three-dimensional Timoshenko beam element, *J. Sound Vib.* 259 (2003) 473–480. <https://doi.org/10.1006/jsvi.2002.5122>.
- [57] S.E. Alavi, M. Sadighi, M.D. Pazhooh, J.F. Ganghoffer, Development of size-dependent consistent couple stress theory of Timoshenko beams, *Appl. Math. Model.* 79 (2020) 685–712. <https://doi.org/10.1016/j.apm.2019.10.058>.
- [58] N. Li, Z. Li, L. Xie, A fiber-section model based Timoshenko beam element using shear-bending interdependent shape function, *Earthq. Eng. Eng. Vib.* 12 (2013) 421–432. <https://doi.org/10.1007/s11803-013-0183-z>.
- [59] S.K. Parashar, U. Von Wagner, P. Hagedorn, A modified Timoshenko beam theory for nonlinear shear-induced flexural vibrations of piezoceramic continua, *Nonlinear Dyn.* 37 (2004) 181–205. <https://doi.org/10.1023/B:NODY.0000044678.78930.cb>.
- [60] P.R. Heyliger, J.N. Reddy, A higher order beam finite element for bending and vibration problems, *J. Sound Vib.* 126 (1988) 309–326. [https://doi.org/10.1016/0022-460X\(88\)90244-1](https://doi.org/10.1016/0022-460X(88)90244-1).
- [61] D.J. Mead, Free wave propagation in periodically supported, infinite beams, *J. Sound Vib.* 11 (1970) 181–197. [https://doi.org/10.1016/S0022-460X\(70\)80062-1](https://doi.org/10.1016/S0022-460X(70)80062-1).
- [62] D.J. Mead, A general theory of harmonic wave propagation in linear periodic systems with multiple coupling, *J. Sound Vib.* 27 (1973) 235–260. [https://doi.org/10.1016/0022-460X\(73\)90064-3](https://doi.org/10.1016/0022-460X(73)90064-3).
- [63] D.J. Mead, N.S. Bardell, Free vibration of a thin cylindrical shell with periodic circumferential stiffeners, *J. Sound Vib.* 115 (1987) 499–520. [https://doi.org/10.1016/0022-460X\(87\)90293-8](https://doi.org/10.1016/0022-460X(87)90293-8).

- [64] F. Dos Reis, J.F. Ganghoffer, Construction of micropolar continua from the asymptotic homogenization of beam lattices, *Comput. Struct.* 112–113 (2012) 354–363. <https://doi.org/10.1016/j.compstruc.2012.08.006>.
- [65] H. Reda, S.E. Alavi, M. Nasimsobhan, J.F. Ganghoffer, Homogenization towards chiral Cosserat continua and applications to enhanced Timoshenko beam theories, *Mech. Mater.* 155 (2021) 103728. <https://doi.org/10.1016/j.mechmat.2020.103728>.
- [66] J.F. Ganghoffer, H. Reda, A variational approach of homogenization of heterogeneous materials towards second gradient continua, *Mech. Mater.* 158 (2021) 103743. <https://doi.org/10.1016/j.mechmat.2021.103743>.
- [67] M. Janus-Michalska, Hyperelastic behavior of cellular structures based on micromechanical modeling at small strain, *Arch. Mech.* 63 (2011) 3–23. <https://doi.org/10.24423/aom.464>.
- [68] M. Janus-Michalska, R. Pęcherski, Macroscopic properties of open-cell foams based on micromechanical modelling, *Tech. Mech.* 23 (2003) 234–244.
- [69] S. Mechanics, Effective Models Describing Elastic Behaviour, *Arch. Metall. Mater.* 50 (2005) 595–608.
- [70] A. Vigliotti, V.S. Deshpande, D. Pasini, Non linear constitutive models for lattice materials, *J. Mech. Phys. Solids.* 64 (2014) 44–60. <https://doi.org/10.1016/j.jmps.2013.10.015>.
- [71] P. Wang, F. Casadei, S. Shan, J.C. Weaver, K. Bertoldi, Harnessing buckling to design tunable locally resonant acoustic metamaterials, *Phys. Rev. Lett.* 113 (2014). <https://doi.org/10.1103/PhysRevLett.113.014301>.
- [72] A.S. Phani, J. Woodhouse, N.A. Fleck, Wave propagation in two-dimensional periodic lattices, *J. Acoust. Soc. Am.* 119 (2006) 1995–2005. <https://doi.org/10.1121/1.2179748>.
- [73] D.J. Mead, Y. Yaman, The harmonic response of rectangular sandwich plates with multiple stiffening: A flexural wave analysis, *J. Sound Vib.* 145 (1991) 409–428. [https://doi.org/10.1016/0022-460X\(91\)90111-V](https://doi.org/10.1016/0022-460X(91)90111-V).
- [74] V. V. Zozulya, Couple stress theory of curved rods. 2-D, high order, Timoshenko's and Euler-Bernoulli models, *Curved Layer. Struct.* 4 (2017) 119–133. <https://doi.org/10.1515/cls-2017-0009>.
- [75] Z. Friedman, J.B. Kosmatka, An improved two-node timoshenko beam finite element, *Comput. Struct.* 47 (1993) 473–481. [https://doi.org/10.1016/0045-7949\(93\)90243-7](https://doi.org/10.1016/0045-7949(93)90243-7).
- [76] T. Yu, H. Hu, J. Zhang, T.Q. Bui, Isogeometric analysis of size-dependent effects for functionally graded microbeams by a non-classical quasi-3D theory, *Thin-Walled Struct.* 138 (2019) 1–14. <https://doi.org/10.1016/j.tws.2018.12.006>.
- [77] R.D. Mindlin, H.F. Tiersten, Effects of couple-stresses in linear elasticity, *Arch. Ration. Mech. Anal.* 11 (1962) 415–448. <https://doi.org/10.1007/BF00253946>.
- [78] W.T. Koiter, Couples-stress in the theory of elasticity, *Proc. K. Ned. Akad. Wet.* 67 (1964) 17–44.
- [79] A.C. Eringen, Linear theory of micropolar viscoelasticity, 1967. [https://doi.org/10.1016/0020-7225\(67\)90004-3](https://doi.org/10.1016/0020-7225(67)90004-3).
- [80] A.C. Pereira, F.L. Fertonani, G.D.O. Neto, L.T. Kubota, H. Yamanaka, Reagentless biosensor for isocitrate using one step modified Pt-Ir microelectrode, *Talanta.* 53 (2001) 801–806. [https://doi.org/10.1016/S0039-9140\(00\)00566-X](https://doi.org/10.1016/S0039-9140(00)00566-X).

- [81] I. Goda, M. Assidi, S. Belouettar, J.F. Ganghoffer, A micropolar anisotropic constitutive model of cancellous bone from discrete homogenization, *J. Mech. Behav. Biomed. Mater.* 16 (2012) 87–108. <https://doi.org/10.1016/j.jmbbm.2012.07.012>.
- [82] I. Goda, M. Assidi, J.F. Ganghoffer, A 3D elastic micropolar model of vertebral trabecular bone from lattice homogenization of the bone microstructure, *Biomech. Model. Mechanobiol.* 13 (2014) 53–83. <https://doi.org/10.1007/s10237-013-0486-z>.
- [83] I. City, *Experimental Study of Micropolar, Bone.* (1975) 2–9.
- [84] M. Asghari, M.H. Kahrobaian, M. Rahaeifard, M.T. Ahmadian, Investigation of the size effects in Timoshenko beams based on the couple stress theory, *Arch. Appl. Mech.* 81 (2011) 863–874. <https://doi.org/10.1007/s00419-010-0452-5>.
- [85] G. Alotta, G. Failla, M. Zingales, Finite element method for a nonlocal Timoshenko beam model, *Finite Elem. Anal. Des.* 89 (2014) 77–92. <https://doi.org/10.1016/j.finel.2014.05.011>.
- [86] A.M. Dehrouyeh-Semnani, A. Bahrami, On size-dependent Timoshenko beam element based on modified couple stress theory, *Int. J. Eng. Sci.* 107 (2016) 134–148. <https://doi.org/10.1016/j.ijengsci.2016.07.006>.
- [87] F. Yang, A.C.M. Chong, D.C.C. Lam, P. Tong, Couple stress based strain gradient theory for elasticity, *Int. J. Solids Struct.* 39 (2002) 2731–2743. [https://doi.org/10.1016/S0020-7683\(02\)00152-X](https://doi.org/10.1016/S0020-7683(02)00152-X).
- [88] H.M. Ma, X.L. Gao, J.N. Reddy, A microstructure-dependent Timoshenko beam model based on a modified couple stress theory, *J. Mech. Phys. Solids.* 56 (2008) 3379–3391. <https://doi.org/10.1016/j.jmps.2008.09.007>.
- [89] M.H. Kahrobaian, M. Asghari, M.T. Ahmadian, A Timoshenko beam element based on the modified couple stress theory, *Int. J. Mech. Sci.* 79 (2014) 75–83. <https://doi.org/10.1016/j.ijmecsci.2013.11.014>.
- [90] B. Reinaldo Goncalves, A. Karttunen, J. Romanoff, J.N. Reddy, Buckling and free vibration of shear-flexible sandwich beams using a couple-stress-based finite element, *Compos. Struct.* 165 (2017) 233–241. <https://doi.org/10.1016/j.compstruct.2017.01.033>.
- [91] A.T. Karttunen, J. Romanoff, J.N. Reddy, Exact microstructure-dependent Timoshenko beam element, *Int. J. Mech. Sci.* 111–112 (2016) 35–42. <https://doi.org/10.1016/j.ijmecsci.2016.03.023>.
- [92] B.R. Goncalves, A.T. Karttunen, J. Romanoff, A nonlinear couple stress model for periodic sandwich beams, *Compos. Struct.* 212 (2019) 586–597. <https://doi.org/10.1016/j.compstruct.2019.01.034>.
- [93] M. Levinson, A new rectangular beam theory, *J. Sound Vib.* 74 (1981) 81–87. [https://doi.org/10.1016/0022-460X\(81\)90493-4](https://doi.org/10.1016/0022-460X(81)90493-4).
- [94] W.B. Bickford, Consistent Higher Order Beam Theory., in: *Dev. Theor. Appl. Mech., CONFERENCE ON THEORETICAL AND APPLIED MECHANICS., ARIZONA STATE UNIV./USA, 1982: pp. 137–150.* <http://pascal-francis.inist.fr/vibad/index.php?action=getRecordDetail&idt=PASCAL83X0184967>.
- [95] J. Petrolito, Stiffness analysis of beams using a higher-order theory, *Comput. Struct.* 55 (1995) 33–39. [https://doi.org/10.1016/0045-7949\(94\)00505-W](https://doi.org/10.1016/0045-7949(94)00505-W).
- [96] J.N. Reddy, C.M. Wang, K.H. Lee, Relationships between bending solutions of classical and shear

- deformation beam theories, *Int. J. Solids Struct.* 34 (1997) 3373–3384.
[https://doi.org/10.1016/S0020-7683\(96\)00211-9](https://doi.org/10.1016/S0020-7683(96)00211-9).
- [97] M. di S. Tessler, A., Refinement of Timoshenko Beam Theory for Composite and Sandwich Beams Using Zigzag Kinematics, *Natl. Aeronaut. Sp. Adm.* (2007) 45.
<http://ntrs.nasa.gov/search.jsp?R=20070035078>.
- [98] M. T K, J. P D, A Simple Higher Order Theory for Bending Analysis of Steel Beams, *Int. J. Civ. Eng.* 2 (2015) 29–36. <https://doi.org/10.14445/23488352/ijce-v2i4p106>.
- [99] R.D.Z. William McGuire, Richard H. Gallagher, *Matrix Structural Structural Analysis*, 1999.
<https://doi.org/10.1080/01422419908228843>.
- [100] E. Ramm, *Finite element procedures in engineering analysis*, K-J. Bathe, Prentice-Hall, 1982. No. of pages: 735, *Int. J. Numer. Anal. Methods Geomech.* 7 (1983) 500–500.
<https://doi.org/10.1002/nag.1610070412>.
- [101] P. Nanakorn, L.N. Vu, A 2D field-consistent beam element for large displacement analysis using the total Lagrangian formulation, *Finite Elem. Anal. Des.* 42 (2006) 1240–1247.
<https://doi.org/10.1016/j.finel.2006.06.002>.
- [102] M. Santana, R.A.M. Silveira, U. Federal, D.O. Preto, *Sistema Computacional Gráfico Interativo para Problemas de Instabilidade em Sistema Computacional Gráfico Interativo para Problemas de Instabilidade em Pórticos Planos*, (2014).
- [103] G.C. Oliveira, W.T. Matias Silva, Análise Não-Linear De Arcos Utilizando O Elemento De Viga Unificado Bernoulli-Timoshenko E a Formulação Co-Rotacional, *REEC - Rev. Eletrônica Eng. Civ.* 13 (2017) 1–16. <https://doi.org/10.5216/reec.v13i2.43393>.
- [104] M.A.C. Rodrigues, R.B. Burgos, L.F. Martha, A unified approach to the timoshenko geometric stiffness matrix considering higher-order terms in the strain tensor, *Lat. Am. J. Solids Struct.* 16 (2019) 1–22. <https://doi.org/10.1590/1679-78255273>.
- [105] R.S. Langley, N.S. Bardell, H.M. Ruivo, The response of two-dimensional periodic structures to harmonic point loading: A theoretical and experimental study of a beam grillage, *J. Sound Vib.* 207 (1997) 521–535. <https://doi.org/10.1006/jsvi.1997.1154>.
- [106] S. Gonella, M. Ruzzene, Homogenization and equivalent in-plane properties of two-dimensional periodic lattices, *Int. J. Solids Struct.* 45 (2008) 2897–2915.
<https://doi.org/10.1016/j.ijsolstr.2008.01.002>.
- [107] A. Bacigalupo, L. Gambarotta, Homogenization of periodic hexa- and tetrachiral cellular solids, *Compos. Struct.* 116 (2014) 461–476. <https://doi.org/10.1016/j.compstruct.2014.05.033>.
- [108] H. Reda, Y. Rahali, J.F. Ganghoffer, H. Lakiss, Wave propagation in 3D viscoelastic auxetic and textile materials by homogenized continuum micropolar models, *Compos. Struct.* 141 (2016) 328–345. <https://doi.org/10.1016/j.compstruct.2016.01.071>.
- [109] H. Reda, Y. Rahali, J.F. Ganghoffer, H. Lakiss, Analysis of dispersive waves in repetitive lattices based on homogenized second-gradient continuum models, *Compos. Struct.* 152 (2016) 712–728.
<https://doi.org/10.1016/j.compstruct.2016.05.080>.
- [110] R.T. Beyer, *Nonlinear Acoustics*, in: *Phys. Acoust.*, Academic Press, San Diego, 1965: pp. 231–264. <https://doi.org/10.1016/B978-0-12-395662-0.50014-X>.
- [111] A. V. Porubov, *Amplification of nonlinear strain waves in solids*, 2003.

<https://doi.org/https://doi.org/10.1142/5238>.

- [112] T. Hayat, S. Zaib, S. Asghar, K. Bhattacharyya, S.A. Shehzad, *Nonlinear theory of Elasticity Applied Mathematics and Mechanics*, 2013.
- [113] K.L. Manktelow, M.J. Leamy, M. Ruzzene, Topology design and optimization of nonlinear periodic materials, *J. Mech. Phys. Solids*. 61 (2013) 2433–2453. <https://doi.org/10.1016/j.jmps.2013.07.009>.
- [114] C. Daraio, V.F. Nesterenko, E.B. Herbold, S. Jin, Tunability of solitary wave properties in one-dimensional strongly nonlinear phononic crystals, *Phys. Rev. E - Stat. Nonlinear, Soft Matter Phys.* 73 (2006) 1–10. <https://doi.org/10.1103/PhysRevE.73.026610>.
- [115] S. Sen, J. Hong, J. Bang, E. Avalos, R. Doney, Solitary waves in the granular chain, *Phys. Rep.* 462 (2008) 21–66. <https://doi.org/10.1016/j.physrep.2007.10.007>.
- [116] A.F. Vakakis, M.E. King, A.J. Pearlstein, Forced localization in a periodic chain of non-linear oscillators, *Int. J. Non. Linear. Mech.* 29 (1994) 429–447. [https://doi.org/10.1016/0020-7462\(94\)90013-2](https://doi.org/10.1016/0020-7462(94)90013-2).
- [117] A.F. Vakakis, M.E. King, Nonlinear wave transmission in a monocoupled elastic periodic system, *J. Acoust. Soc. Am.* 98 (1995) 1534–1546. <https://doi.org/10.1121/1.413419>.
- [118] Y. Starosvetsky, A.F. Vakakis, Traveling waves and localized modes in one-dimensional homogeneous granular chains with no precompression, *Phys. Rev. E - Stat. Nonlinear, Soft Matter Phys.* 82 (2010) 1–14. <https://doi.org/10.1103/PhysRevE.82.026603>.
- [119] H. Reda, Y. Rahali, J.F. Ganghoffer, H. Lakiss, Nonlinear dynamical analysis of 3D textiles based on second order gradient homogenized media, *Compos. Struct.* 154 (2016) 538–555. <https://doi.org/10.1016/j.compstruct.2016.07.053>.
- [120] H. Reda, K. El Nady, J.F. Ganghoffer, H. Lakiss, Nonlinear wave propagation analysis in hyperelastic 1D microstructured materials constructed by homogenization, *Mech. Res. Commun.* 84 (2017) 136–141. <https://doi.org/10.1016/j.mechrescom.2017.06.011>.
- [121] V. V. Zozulya, Couple stress theory of curved rods. 2-D, high order, Timoshenko's and Euler-Bernoulli models, *Curved Layer. Struct.* 4 (2017) 119–133. <https://doi.org/10.1515/cls-2017-0009>.
- [122] Z. Friedman, J.B. Kosmatka, An improved two-node timoshenko beam finite element, *Comput. Struct.* 47 (1993) 473–481. [https://doi.org/10.1016/0045-7949\(93\)90243-7](https://doi.org/10.1016/0045-7949(93)90243-7).
- [123] A. Wazne, H. Reda, J.-F. Ganghoffer, H. Lakiss, Analysis of nonlinear wave propagation within architected materials consisting of fully nonlinear Timoshenko beam structural elements, *Wave Motion*. (2023).
- [124] A. Wazne, H. Reda, J. Ganghoffer, H. Lakiss, Nonlinear wave propagation analysis in architected materials with consideration of extension, shear and bending effects, *Mech. Res. Commun.* 104044 (2023). <https://doi.org/https://doi.org/10.1016/j.mechrescom.2023.104044>.
- [125] R. LANGLEY, the Response of Two-Dimensional Periodic Structures To Point Harmonic Forcing, *J. Sound Vib.* 197 (1996) 447–469.
- [126] P.L. Bhatnagar, *Nonlinear waves in one-dimensional dispersive systems.*, illustrate, Clarendon Press, 1979. <https://doi.org/10.1112/blms/14.3.267>.
- [127] W.J. Parnell, Effective wave propagation in a pre-stressed nonlinear elastic composite bar, in: *Proc. 5th Eur. Conf. Const. Model. Rubber, ECCMR 2007*, 2008: pp. 361–366.

- [128] K.L. Manktelow, M.J. Leamy, M. Ruzzene, Topology design and optimization of nonlinear periodic materials, *J. Mech. Phys. Solids*. 61 (2013) 2433–2453. <https://doi.org/10.1016/j.jmps.2013.07.009>.
- [129] C.I. Christov, G.A. Maugin, A. V. Porubov, On Boussinesq's paradigm in nonlinear wave propagation, *Comptes Rendus - Mec.* 335 (2007) 521–535. <https://doi.org/10.1016/j.crme.2007.08.006>.
- [130] N. Sugimoto, T. Kakutani, "Generalized Burgers" equation' for nonlinear viscoelastic waves, *Wave Motion*. 7 (1985) 447–458. [https://doi.org/10.1016/0165-2125\(85\)90019-8](https://doi.org/10.1016/0165-2125(85)90019-8).
- [131] V. V. Zhakhovsky, M.M. Budzevich, N.A. Inogamov, I.I. Oleynik, C.T. White, Two-zone elastic-plastic single shock waves in solids, *Phys. Rev. Lett.* 107 (2011) 1–4. <https://doi.org/10.1103/PhysRevLett.107.135502>.
- [132] K. Manktelow, Dispersion analysis of nonlinear periodic structures, (2013). <http://smartech.gatech.edu/handle/1853/51936>.
- [133] R.K. Narisetti, M. Ruzzene, M.J. Leamy, A perturbation approach for analyzing dispersion and group velocities in two-dimensional nonlinear periodic lattices, *J. Vib. Acoust. Trans. ASME*. 133 (2011) 1–12. <https://doi.org/10.1115/1.4004661>.
- [134] R.K. Narisetti, M.J. Leamy, M. Ruzzene, A perturbation approach for predicting wave propagation in one-dimensional nonlinear periodic structures, *J. Vib. Acoust. Trans. ASME*. 132 (2010) 0310011–03100111. <https://doi.org/10.1115/1.4000775>.
- [135] H. Reda, N. Karathanasopoulos, J.F. Ganghoffer, H. Lakiss, Wave propagation characteristics of periodic structures accounting for the effect of their higher order inner material kinematics, *J. Sound Vib.* 431 (2018) 265–275. <https://doi.org/10.1016/j.jsv.2018.06.006>.
- [136] H. Reda, J.F. Ganghoffer, H. Lakiss, Micropolar dissipative models for the analysis of 2D dispersive waves in periodic lattices, *J. Sound Vib.* 392 (2017) 325–345. <https://doi.org/10.1016/j.jsv.2016.12.007>.
- [137] A.F. Vakakis, Non-linear normal modes (NNMs) and their applications in vibration theory: An overview, *Mech. Syst. Signal Process.* 11 (1997) 3–22. <https://doi.org/10.1006/mssp.1996.9999>.
- [138] K.F. Graff, *Wave motion in elastic solids*, Courier Corporation, 2012.
- [139] S. Sen, J. Hong, J. Bang, E. Avalos, R. Doney, Solitary waves in the granular chain, *Phys. Rep.* 462 (2008) 21–66. <https://doi.org/10.1016/j.physrep.2007.10.007>.
- [140] Z.K. Peng, Z.Q. Lang, Detecting the position of non-linear component in periodic structures from the system responses to dual sinusoidal excitations, *Int. J. Non. Linear. Mech.* 42 (2007) 1074–1083. <https://doi.org/10.1016/j.ijnonlinmec.2007.06.002>.
- [141] H.G. Hopkins, *Wave Motion in Elastic Solids*, *Phys. Bull.* 27 (1976) 30–30. <https://doi.org/10.1088/0031-9112/27/1/032>.
- [142] V.I. Erofejev, *Wave Processes in Solids with Microstructure*, 2003. <https://doi.org/https://doi.org/10.1142/5157>.
- [143] K. Jakata, A.G. Every, Determination of the dispersive elastic constants of the cubic crystals Ge, Si, GaAs, and InSb, *Phys. Rev. B - Condens. Matter Mater. Phys.* 77 (2008). <https://doi.org/10.1103/PhysRevB.77.174301>.
- [144] J. Boussinesq, *Théorie des ondes et des remous qui se propagent le long d'un canal rectangulaire*

horizontal, en communiquant au liquide contenu dans ce canal des vitesses sensiblement pareilles de la surface au fond, *J. Mathématiques Pures Appliquées 2e Série*. 17 (1872) 55–108.

- [145] J. Engelbrecht, A. Salupere, K. Tamm, Waves in microstructured solids and the Boussinesq paradigm, *Wave Motion*. 48 (2011) 717–726. <https://doi.org/10.1016/j.wavemoti.2011.04.001>.
- [146] A.M. Samonov, Strain Solitons in Solids; How to Construct Them, *Strain Solitons Solids; How to Constr. Them*. (2001). <https://doi.org/10.1201/9781420026139>.
- [147] I. V. Andrianov, V. V. Danishevs'kyi, O.I. Ryzhkov, D. Weichert, Numerical study of formation of solitary strain waves in a nonlinear elastic layered composite material, *Wave Motion*. 51 (2014) 405–417. <https://doi.org/10.1016/j.wavemoti.2013.10.003>.
- [148] C. Cattani, J. Rushchitsky, Wavelet and Wave Analysis as Applied to Materials with Micro or Nanostructure, *Ser. Adv. Math. Appl. Sci*. 74 (2007). <https://doi.org/10.1142/9789812709769>.
- [149] J. Engelbrecht, *Nonlinear wave dynamics: Complexity and simplicity*, 1997. [https://doi.org/10.1016/s0898-1221\(97\)90255-8](https://doi.org/10.1016/s0898-1221(97)90255-8).
- [150] J. Engelbrecht, A. Berezovski, A. Salupere, Nonlinear deformation waves in solids and dispersion, *Wave Motion*. 44 (2007) 493–500. <https://doi.org/10.1016/j.wavemoti.2007.02.006>.
- [151] A.H. Nayfeh, *Perturbation Methods*, 2000. <https://doi.org/10.1002/9783527617609>.